This is to certify that the
dissertation entitled

CREATION OF AFFINITY MEMBRANES CONTAINING FUNCTIONALIZED POLYMER BRUSHES FOR HIGH CAPACITY PURIFICATION OF HISTIDINE-TAGGED PROTEINS

presented by

Parul Jain

has been accepted towards fulfillment
of the requirements for the

Ph.D. degree in Chemisty

Major Professor's Signature

09/11/09

Date

CREATION OF AFFINITY MEMBRANES CONTAINING FUNCTIONALIZED POLYMER BRUSHES FOR HIGH-CAPACITY PURIFICATION OF HISTIDINE-TAGGED PROTEINS

By

Parul Jain

A DISSERTATION

Submitted to
Michigan State University
in partial fulfillment of the requirements
for the degree of

DOCTOR OF PHILOSOPHY

Chemistry

2009

ABSTRACT

CREATION OF AFFINITY MEMBRANES CONTAINING FUNCTIONALIZED POLYMER BRUSHES FOR HIGH-CAPACITY PURIFICATION OF HISTIDINE-TAGGED PROTEINS

By

Parul Jain

Porous membrane absorbers are attractive for rapid protein purification, but their binding capacity is low relative to nanoporous beads. Modification of membranes with functionalized polymer brushes, however, can greatly enhance capacity. Porous alumina membranes containing poly(2-hydroxyethyl methacrylate) (poly(HEMA)) brushes derivatized with nitrilotriacetate-Ni^{2+} (NTA-Ni^{2+}) complexes facilitate purification of polyhistidine-tagged ubiquitin (HisU) in less than 30 min. These materials have a binding capacity of 120 mg HisU/cm^3 of membrane, and the purity of the eluted HisU is >99%, even when the feed contains 10% bovine serum.

Unfortunately, the submicron pore size in commercial alumina membranes limits their use to simple solutions because complex mixtures such as cell extracts often plug the small pores. Polymeric membranes, on the other hand, can have larger pore diameters (1-10 μm) that allow lower pressure drops and purification of more complex solutions. Nylon membranes containing poly(HEMA)-NTA-Ni^{2+} brushes can isolate polyhistidine tagged (His-tagged) cellular retinaldehyde binding protein (CRALBP) from a cell extract with purities at least as good as those obtained with commercial Ni^{2+} columns. Unfortunately, these membranes have a low protein binding capacity (25 mg

protein/cm^3 of membrane), perhaps because the organic solvents employed in brush synthesis and derivatization partially damage the membrane structure.

A newly created aqueous procedure for growth of polymer brushes inside polymeric membranes avoids contact of polymer membranes with organic solvents. This method includes layer-by-layer adsorption of macroinitiators and subsequent aqueous ATRP from these immobilized initiators. However, the formation of protein-binding brushes still requires conversion of poly(HEMA) hydroxyl groups to carboxylic acid moieties, which involves the use of organic solvents that may damage the membrane. A new surface-initiated aqueous ATRP of an acidic monomer, 2-(methacryloyloxy)ethyl succinate (MES), overcomes this problem and provides a rapid, one-step route to polyacid brushes. ATRP from initiators immobilized on Au-coated Si wafers yields poly(MES) films with an ellipsometric thickness of 120 nm in less than 15 min. FTIR spectroscopy and ellipsometry studies show that poly(MES) brushes and their derivatives bind the equivalent of many monolayers of BSA as well as lysozyme.

Finally, modification of nylon membranes with poly(MES)-NTA-Ni^{2+} allows for high-capacity purification of His-tagged proteins directly from a cell lysate. These membranes show remarkable HisU, BSA, and lysozyme binding capacities of 85, 80 ± 2 and 118 ± 8 mg protein per cm^3 of membrane, respectively. Most importantly, the poly(MES)-NTA-Ni^{2+}-modified membranes allow isolation of His-tagged CRALBP directly from a cell extract in less than 15 min with purities comparable to commercial affinity columns. Thus, porous nylon membranes modified by poly(MES)-NTA-Ni^{2+} brushes are attractive candidates for rapid, high-capacity purification of His-tagged proteins.

I dedicate this dissertation to my parents, Ashok Jain and Sangeeta Jain, my husband, Sameer Patel and my siblings, Mayura Jain and Kamesh Jain, for their love and support.

ACKNOWLEDGMENTS

I would like to express my sincere thanks to my dissertation advisor, Dr. Merlin Bruening, for his insightful guidance and continuous support. He is a great mentor and an excellent scientist. He gave me the freedom to explore on my own and at the same time provided the guidance to recover when my steps faltered. I have learned a lot of useful presentation and scientific skills from him. I could not thank him enough for his patience and understanding.

I am deeply grateful to my second supervisor, Dr. Gregory Baker, for the discussions that helped me sort out the technical details of my work. I am also thankful to him for carefully reading and commenting on countless revisions of the manuscripts.

I also thank my committee members, Dr. James Geiger and Dr. Gary Blanchard for their kind help and great suggestions. Thanks to Dr. Geiger and his students, Dr. Xiaofei Jia and Remie Touma, for kindly providing the cell extracts needed for this study.

My deepest thanks to Dr. Jinhua Dai for being a great mentor to me. I would also like to thank current and past Bruening research group members.

I acknowledge the help of several people for training me on different instruments. Thanks to Dr. Kathy Severin for the guidance on transmission FTIR and ICP, Dr. Ruth Smith for training on ATR-IR, Dr. Dan Holmes for help with NMR and Dr. Baokang Bi for training on SEM. Thanks to Per Askeland for help with XPS studies.

Dr. S.K. Jain, my mentor in undergraduate studies, is one of the best teachers I had. I am indebted to him for his continuous encouragement, guidance and for always believing in me.

Most importantly, none of this would have been possible without the love and patience of my family. I am fortunate to have a family who has been a constant source of love, concern, support and strength all these years. I owe the maximum gratitude to my parents, Ashok Jain and Sangeeta Jain, for their unwavering faith and confidence in me and for making me the person I am today. Thanks to my husband, Sameer, for his love, support, understanding and constant encouragement. He believed in me more than I did and never let me settle down for less. Without him, I could not have done what I was able to do. Thanks to my sister, Mayura Jain and my brother, Kamesh Jain, for their immense love and concern. I owe my success to my family.

TABLE OF CONTENTS

LIST OF FIGURES

LIST OF SCHEMES

LIST OF ABBREVIATIONS

AA	Acrylic acid
AGT	O^6-alkylguanine-DNA-alkyltransferase
AIBN	2,2′-Azobis(2-methylpropionitrile)
Aminobutyl NTA	N_ω, N_α–*bis*(carboxymethyl)-L-lysine hydrate
ATR	Attenuated total reflectance
ATRP	Atom-transfer radical polymerization
BIEA	2-(2-Bromoisobutyryloxy)ethyl acrylate
Bpy	2,2'-Bipyridyl
BSA	Bovine serum albumin
CDI	1,1′-carbonyldiimidazole
CRALBP	Cellular retinaldehyde binding protein
DMAEMA	2-(Dimethylamino)ethyl methacrylate
DMAP	4-Dimethylaminopyridine
DMF	Dimethylformamide
dnNbpy	4,4′-Dinonyl-2,2′-bipyridyl
EDC	1-[3-(Dimethylamino)propyl]-3-ethylcarbodiimide hydrochloride
EDTA	Ethylenediamine tetraacetic acid
en	Ethylenediamine
FESEM	Field-emission scanning electron microscopy
FITC	Fluorescein isothiocyanate
FTIR	Fourier transform infrared
GPC	Gel permeation chromatography

HEMA	2-Hydroxyethyl methacrylate
His-tag	Polyhistidine tag
HisU	His-tagged ubiquitin
HMTETA	1,1,4,7,10,10-Hexamethyltriethylenetetramine
IMAC	Immobilized metal-affinity chromatography
MAA	Methacrylic acid
MALDI	Matrix-assisted laser desorption/ionization
MALDI-MS	Matrix-assisted laser desorption/ionization mass spectrometry
Me_4Cyclam	1,4,8,11-Tetraaza-1,4,8,11-tetramethylcyclotetradecane
MEHQ	Monomethyl ether hydroquinone
MES	2-(Methacryloyloxy)ethyl succinate
Me_6TREN	Tris[2-(dimethylamino)ethyl]amine
MPA	3-Mercaptopropionic acid
MUD	11-Mercapto-1-undecanol
NHS	N-Hydroxysuccinimide
NTA	Nitrilotriacetate
OT-CEC	Open-tubular capillary electrochromatography
PDADMAC	Poly(diallyldimethylammonium chloride)
PDMS	Poly(dimethyl siloxane)
PEG	Polyethylene glycol
PES	Polyethersulfone
PGA	Penicillin G acylase
PMI	Polycationic macroinitiator

Poly(CBMA)	Poly(carboxybetaine methacrylate)
Poly(GMA)	Poly(glycidyl methacrylate)
Poly(MAA)	Poly(methacrylic acid)
Poly(MPC)	Poly(2-methacryloyloxyethylphosphorylcholine)
Poly(TMAEMA)	Poly(2-(trimethylammonium iodide)ethyl methacrylate)
PSS	Poly(styrene sulfonate)
PTFE	Polytetrafluoroethylene
PVDF	Polyvinylidine fluoride
SAM	Self-assembled monolayer
SDS-PAGE	Sodium dodecyl sulfate-polyacrylamide gel electrophoresis
THF	Tetrahydrofuran

This chapter is adapted from our recently published work in Annual Review of Analytical Chemistry (Jain, P., Baker, G.L., Bruening, M.L. *Annual Review of Analytical Chemistry* **2009**, *2*, 387-408).

Chapter 1

Introduction and background

This dissertation describes the growth of polymer brushes on and in porous supports to form high-capacity membrane absorbers capable of purifying proteins modified with polyhistidine tags (His-tags). The research builds on previous studies of the synthesis and application of polymer brushes towards protein immobilization, so to put this work in perspective, I first define polymer brushes and then describe different approaches for the synthesis of polymer brushes (Section 1.1). Subsequent sections discuss the applications of polymer brush-modified surfaces for protein immobilization and isolation. Specifically, I describe the use of polymer brush-modified flat surfaces, beads, and monoliths towards protein immobilization and purification followed by the application of polymer brush-modified substrates as protein microarrays (Section 1.2.1.). Sections 1.2.2. and 1.2.3. present polymer-brush based capture of proteins for analysis by mass spectrometry, capillary chromatography, and electrochromatography. Subsequently I describe selective protein purification in polymer brush-modified membranes via affinity and ion-exchange interactions (Section 1.2.4.). Finally, I present an outline of the dissertation.

1.1. Polymer brushes

1.1.1. Definition of polymer brushes

Polymer brushes are assemblies of polymeric molecules tethered to a substrate such that the graft density is high enough to force the polymer chains to extend away from the surface.[1] The end of the polymer chain is usually held on the surface by physisorption or covalent bonding, whereas the bulk of the chain extends into the solution

or air interface as shown in **Scheme 1.1.**[2] In an appropriate solvent, brushes can be swollen and highly extended for rapid capture and purification of proteins or other analytes.[3-5] Highly swollen, hydrophilic brushes are also useful for minimizing non-specific adsorption of proteins,[6-8] and the functional groups in such brushes can be readily tailored for specific separations.

1.1.2. Synthesis of polymer brushes

Initially, polymer brushes were formed by physical adsorption of block copolymers.[9,10] In this case, one block has affinity for the surface, while the other block extends into the solvent. However, because such systems are often unstable, recently developed synthetic techniques use covalent attachment of polymers to substrates to provide more robust brushes. Covalent grafting generally occurs using either "grafting to"[11] or "grafting from"[12-14] techniques. In the "grafting to" method, end-functionalized polymer chains bind to a substrate via chemical reaction between active groups on the surface and active end groups in the polymer chains (**Scheme 1.1.A.**).[11] This method results in relatively low grafting densities because steric hindrance prevents incoming polymer chains from diffusing through previously deposited chains to reactive surface sites. In contrast, in the "grafting from" strategy, the polymer chains grow directly from surface-tethered initiators **(Scheme 1.1.B.)**.[12-14] The "grafting from" approach yields a high density of chains because small monomers can readily reach growing chains or initiators on the surface. Initiator immobilization on the surface is a vital step in the "grafting from" method and affords some control over brush density.[15,16] Typical initiator-attachment strategies include reaction of surface hydroxyl/amino groups with acid chlorides or acid bromides (**Scheme 1.2.(a)**),[17,18] modification of Au surfaces using

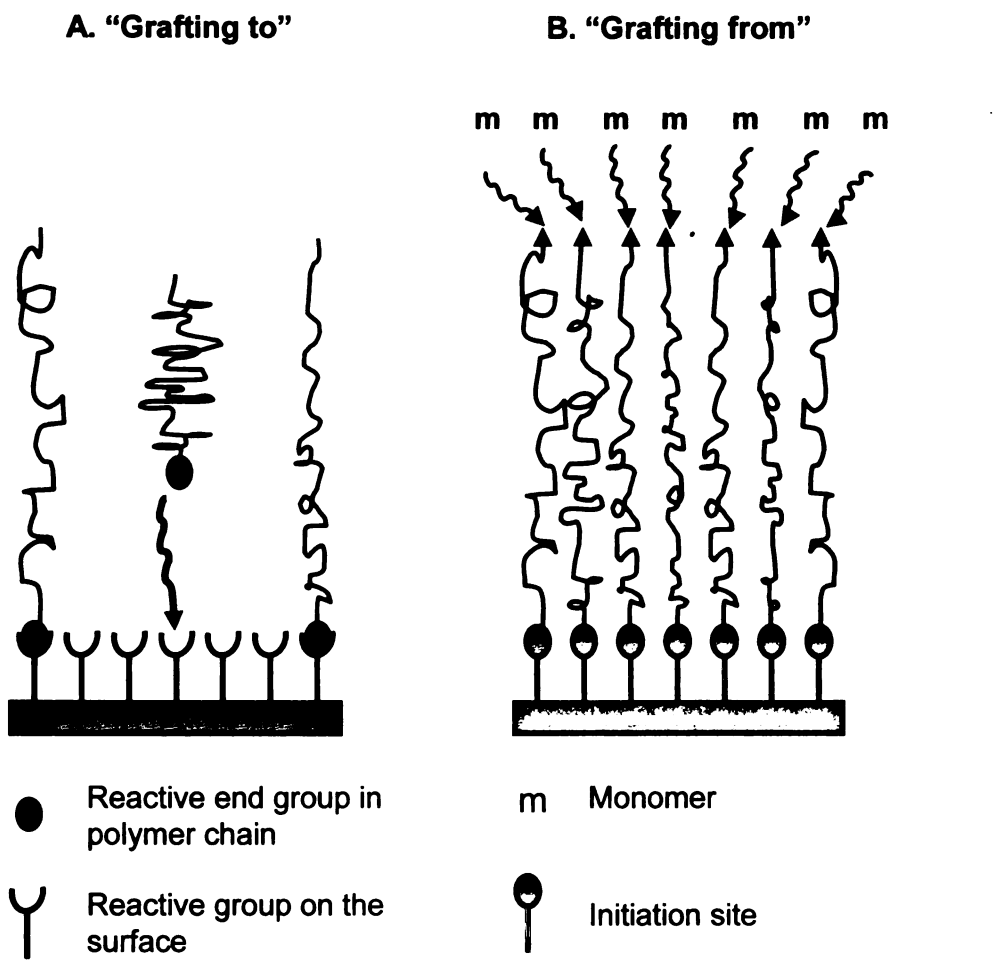

Scheme 1.1. Schematic representation of different approaches to polymer brush synthesis. **(A)** "Grafting to" method in which active groups on the surface and reactive end groups in the polymer chains react to form a covalent bond. **(B)** "Grafting from" method in which the polymer chains grow from surface-tethered initiators.

thiols or disulfides (**Scheme 1.2.(b)**),[18,19] reaction of alumina or silica with silanes (**Scheme 1.2.(c)**),[18,20] and adsorption of polyelectrolyte macroinitiators (**Scheme 1.3.**).[21,22] A number of recent review articles provide an extensive discussion of the synthesis of polymer brushes.[23-25]

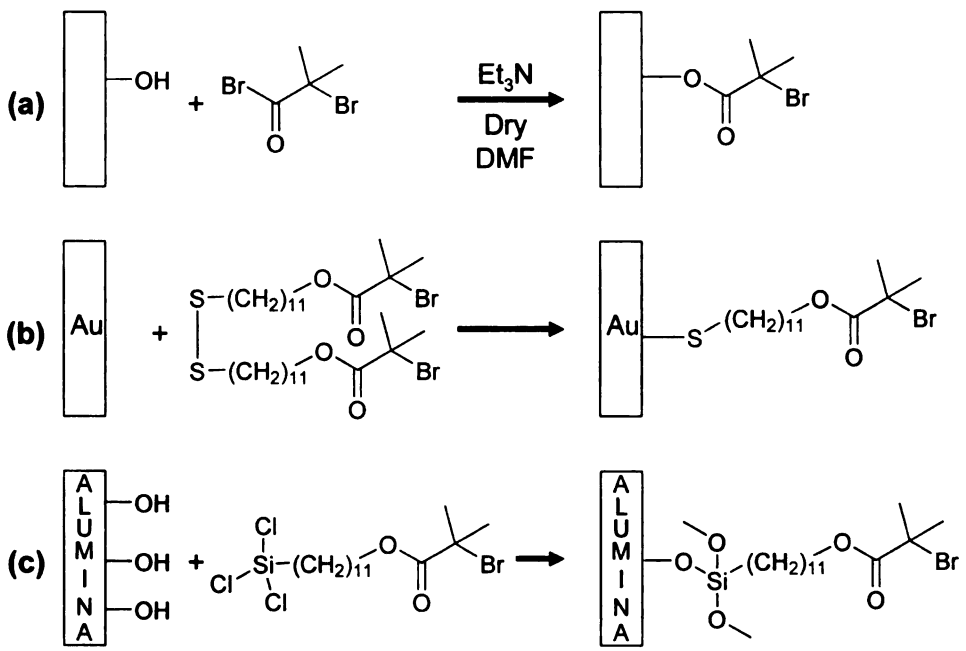

Scheme 1.2. Possible methods for attaching initiators to **(a)** hydroxylated surfaces, **(b)** Au, and **(c)** alumina.

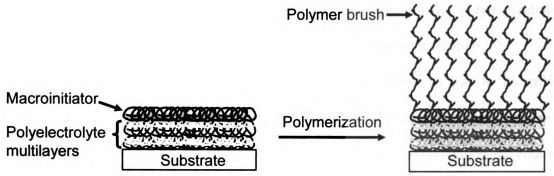

Example of macroinitiator:

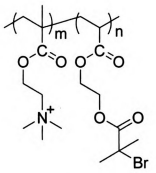

Poly (2-(trimethylamino)ethyl methacrylate-co-
2-(2-bromoisobutyryloxy)ethyl acrylate)

Scheme 1.3. Growth of polymer brushes via ATRP from macroinitiator deposited on a surface using layer-by-layer adsorption.

The "grafting from" approach has been used to modify various surfaces with almost all of the known polymerization techniques including cationic,[26] anionic,[27] radical,[28] ring-opening metathesis,[29,30] photochemical,[31,32] and electrochemical[33] polymerization. However, controlled radical polymerization techniques such as atom-transfer radical polymerization (ATRP),[34-36] reversible addition-fragmentation transfer,[37,38] and nitroxide-mediated polymerization[39] have emerged as some of the most powerful synthetic methods for brush formation because they afford controlled polymer

growth and relatively low polydispersity. Additionally, surface-initiated polymerization with these techniques frequently results in minimal polymerization in solution.

ATRP is especially attractive for controlled polymerizations due to its mild reaction conditions (room temperature in many cases), use of readily available catalysts, initiators and monomers, and tolerance to impurities.[40-42] This polymerization technique proceeds as described in **Scheme 1.4.** Radical generation in ATRP involves an initiator (an organic halide) undergoing a reversible redox process catalyzed by a transition metal complex,[43] and R· is the reactive radical that initiates the polymerization. The controlled nature of ATRP is due to the reversible activation-deactivation reaction between the growing polymer chains and a copper halide-ligand species (k_{act} and k_{deact} are the rate constants for activation and deactivation reactions respectively). The ligand forms a complex with the cuprous and cupric salts and helps to solubilize them in the organic reaction system. Fast deactivation by reaction with the $CuBr_2$(ligand) complex leads to a low concentration of propagating radicals, thereby minimizing chain termination and radical transfer reactions. A successful ATRP requires (a) fast and quantitative activation of initiator so that all the propagating species begin growth at the same time and (b) rapid reversible deactivation of growing radicals to minimize termination of living polymers. The combination of these steps ensures a narrow molecular weight distribution because all the propagating chains grow at the same time and for the same duration of time.[43]

The use of controlled polymerization is particularly important for creating films in complex geometries such as the pores of membranes, where the brushes can serve as high-capacity, selective adsorbents. In the synthesis of such materials, uncontrolled polymerization or formation of polymer in solution can rapidly plug pores to prevent

flow. Surface-initiated ATRP in membrane pores minimizes polymerization in solution and allows for control over the polymer brush thickness through variation of polymerization time. Husson and coworkers used ATRP to grow poly(poly(ethylene glycol)methacrylate) brushes **(Figure 1.1.(i))** inside regenerated-cellulose ultrafiltration membranes.[44] At a constant pressure, the water flux through the membrane decreased monotonically with increasing polymerization time because growth of the brushes decreased the pore diameters. This study also showed that the molecular weight cutoff of the membrane decreases with increasing polymerization time, further confirming that ATRP provides control over the diameter of the pores in the membrane. Yusof and Ulbricht studied the effects of photo-grafting conditions and monomer concentration on polymer brush growth inside membrane pores.[45] They found that the density of polymer chains in the membrane correlates with the density of the entrapped photo-initiator, benzophenone.

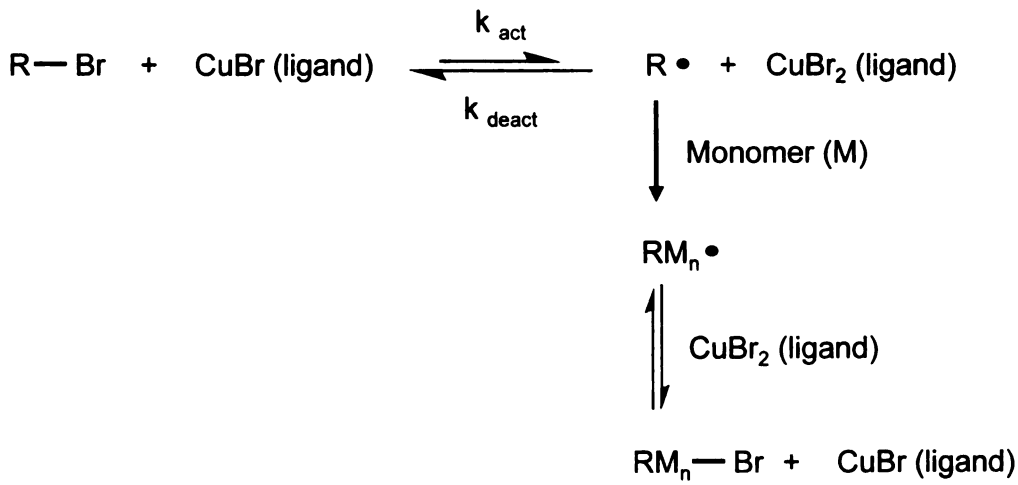

Scheme 1.4. Mechanism of ATRP. (Redrawn from Odian, G. *Principles of Polymerization*; 2004, Fourth ed.; Wiley-Interscience, pp 316.).

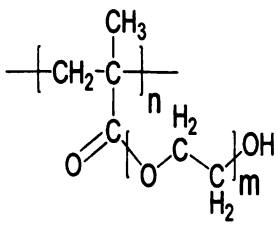

(i) Poly(poly(ethylene glycol)methacrylate)

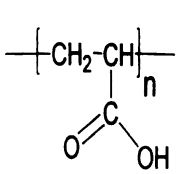

(ii) Poly(acrylic acid)

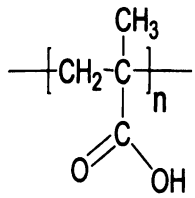

(iii) Poly(methacrylic acid)

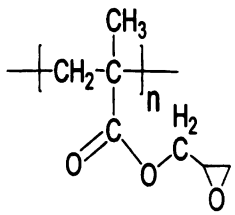

(iv) Poly(glycidyl methacrylate)

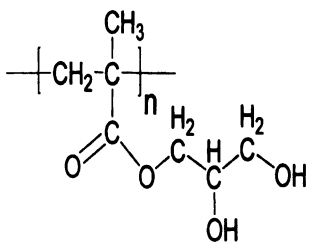

(v) Poly(glycerol monomethacrylate)

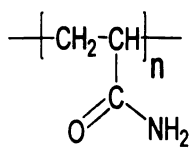

(vi) Poly(acrylamide)

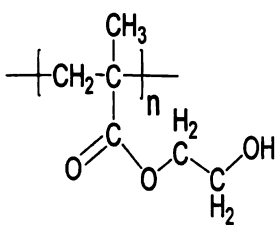

(vii) Poly(hydroxyethyl methacrylate)

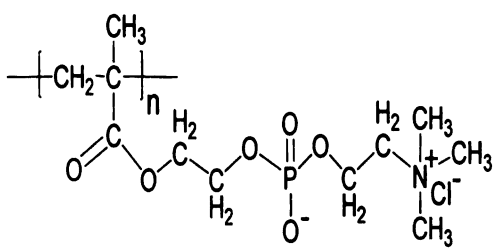

(viii) Poly(2-methacryloyloxyethyl phosphorylcholine)

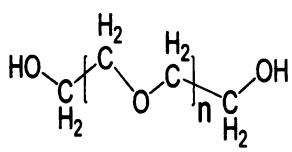

(ix) Poly(ethylene glycol)

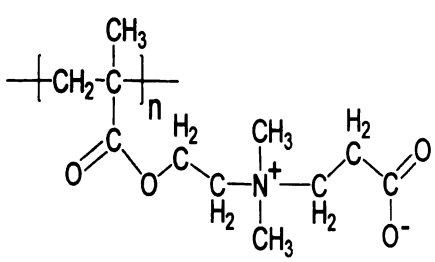

(x) Poly(carboxybetaine methacrylate)

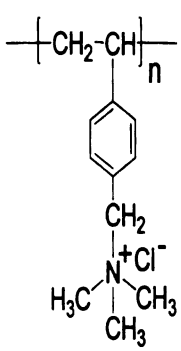

(xi) Poly(vinylbenzyl trimethylammonium chloride)

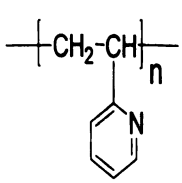

(xii) Poly(2-vinylpyridine)

Figure 1.1. Structures of the polymers included in this chapter.

1.2. Applications of polymer brushes

In recent years, polymer brush-modified surfaces were examined for applications in various fields of science and technology. This section describes recent developments in the use of polymer brush-modified flat surfaces, beads and monoliths for protein immobilization and purification. Subsequently, I discuss the applications of polymer brushes in protein microarrays, for enzyme immobilization, in mass spectrometry, and in chromatography and electrochromatography.

1.2.1. Protein immobilization and purification with polymer brush-modified substrates

1.2.1.-a. Advantages of using polymer brushes for protein immobilization and purification

Polymer brushes are attractive for protein immobilization and purification because swollen brushes can potentially bind the equivalent of many monolayers of protein. Increases in binding capacity may enhance the efficiency or sensitivity of analytical devices such as membrane absorbers, protein microarrays, and modified matrix-assisted laser desorption/ionization (MALDI) plates used for protein capture prior to analysis. Several methods for immobilizing proteins in brushes have been reported, including covalent binding, electrostatic adsorption (ion exchange), and binding to metal-ion complexes.[20,46,47] Brushes containing carboxylic acid and epoxide groups are particularly common because they can be readily derivatized.[48,49] Poly(acrylic acid) (Poly(AA) **Figure 1.1.(ii)**) brushes are especially attractive for protein immobilization because in aqueous solution these films swell to four times their initial thickness to facilitate binding of large biomolecules.[46,49,50]

1.2.1-b. Protein immobilization on brush-modified flat surfaces

Due to the ease in handling and characterization, polymer brush-modified flat surfaces such as silicon and gold-coated silicon wafers have been extensively used for studying protein immobilization. Dai and coworkers modified Au-coated Si with poly(AA) brushes and their derivatives and immobilized lysozyme in these films via ion-exchange **(Scheme 1.5.A.)** and metal-ion affinity interactions **(Scheme 1.5.B.).**[50] Both methods give high protein-binding capacities. Remarkably, about 80 monolayers (16.2 μg/cm^2) of lysozyme adsorb on a 55 nm thick poly(AA) film on Au via electrostatic adsorption. Functionalization of the poly(AA) brushes with nitrilotriacetate (NTA)-Cu^{2+} complexes yields films capable of adsorbing large amounts of protein via metal-ion affinity interactions. A 55 nm poly(AA) film modified with NTA-Cu^{2+} binds 5.8 μg/cm^2 of bovine serum albumin (BSA), 7.7 μg/cm^2 of myoglobin and 9.6 μg/cm^2 of anti-Immunoglobulin G. This corresponds to around 20 monolayers of protein in these films. Recently, Cullen, *et al.* used poly(AA)-NTA-Cu^{2+} brushes to immobilize Ribonuclease A at a capacity of 11 μg Ribonuclease A per cm^2 of film, which is 30 monolayers of the immobilized enzyme.[49]

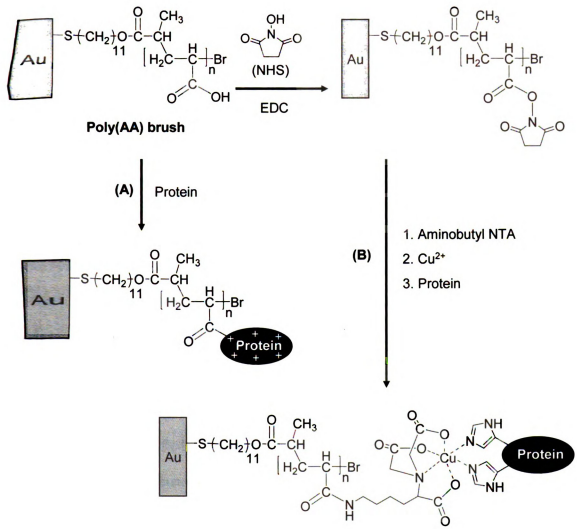

Scheme 1.5. Protein immobilization on poly(AA) brush-modified films via **(A)** ion-exchange interactions and **(B)** metal-ion affinity interactions. For metal-ion affinity binding, polymer brushes were activated with *N*-hydroxysuccinimide (NHS) in the presence of 1-[3-(dimethylamino)propyl]-3-ethylcarbodiimide hydrochloride (EDC). The NHS-activated poly(AA) brushes were derivatized with NTA-Cu^{2+} complexes. Redrawn from Dai, J. H.; Bao, Z. Y.; Sun, L.; Hong, S. U.; Baker, G. L.; Bruening, M. L. *Langmuir* **2006**, *22*, 4274-4281.

1.2.1-c. Protein immobilization and purification using brush-modified beads

Beads are attractive substrates for protein purification because of their high surface area. Several groups used beads modified with polymer brushes to purify proteins directly from egg white via ion-exchange.[51-53] As an example, Bayramoğlu and coworkers used poly(methacrylic acid) (poly(MAA), **Figure 1.1.(iii)**)-grafted chitosan beads for purification of lysozyme from 50% diluted egg white at pH 6.0.[52] The chitosan-*g*-poly(MAA) beads showed a lysozyme binding capacity of ~66 mg lysozyme/g of beads. Single-step purification of lysozyme from egg white with these beads resulted in 94% pure lysozyme as determined by high-performance liquid chromatography. The high purity is achieved because lysozyme has a net positive charge at pH 6.0, whereas most other proteins in egg white are negatively charged at this pH.

Recently, a number of groups demonstrated the immobilization of proteins on magnetic beads modified with polymer brushes **(Figure 1.2.)**.[54,55] Because these beads can be collected or focused using a modest magnetic field, they are attractive for use in drug delivery, immunoassays, protein and enzyme immobilization, and in the separation, isolation, and analysis of biomolecules. Huang and coworkers immobilized BSA in poly(glycidyl methacrylate-*co*-glycerol monomethacrylate) brushes grafted to magnetic microspheres.[54] The epoxide groups in poly(glycidyl methacrylate) (poly(GMA), **Figure 1.1.(iv)**), units can covalently bind proteins, whereas the hydrophilic poly(glycerol monomethacrylate) **(Figure 1.1.(v))** units enable the microspheres to disperse efficiently in aqueous solution. These materials have a binding capacity of ~27 mg BSA per g of beads. The poly(glycidyl methacrylate-*co*-glycerol monomethacrylate) brushes can also immobilize penicillin G acylase (PGA), and the activity of this enzyme depends on the

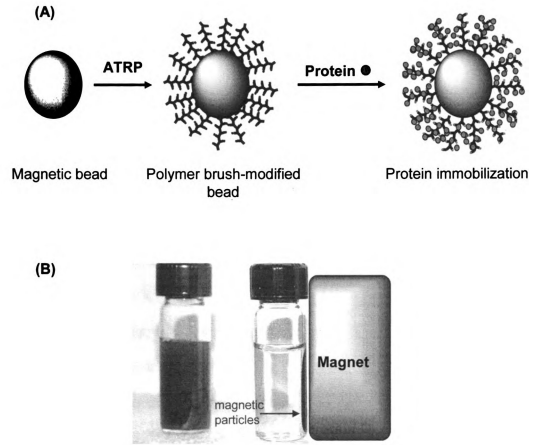

Figure 1.2. **(A)** Schematic representation of protein immobilization on polymer brush-modified magnetic beads. **(B)** Image of 100-nm diameter silica-coated magnetic beads with (right) and without (left) collection by a magnet.

ratio of the constituent monomers.[56] The maximum PGA activity (753 U per g of beads) occurs when the weight ratio of GMA to glycerol monomethacrylate used to form the brushes is 60/40. Enzyme activity decreases when more of the hydrophilic monomer, glycerol monomethacrylate, is present because the enzyme substrate, penicillin, must diffuse through the hydrophilic polymer to the enzyme. With >60% of the hydrophobic polymer, GMA, the activity of the beads also decreases because the brushes collapse in water and bind little enzyme. Compared to its free form, microsphere-immobilized PGA

is less sensitive to changes in temperature and pH. The activity of the immobilized enzyme decreased by 8.5% when the temperature was changed from 45 °C to 55 °C, while for the free enzyme under the same conditions, the enzyme activity decreased by 80%. Approximately 64% of the enzyme activity was retained after ten cycles of repeated use.

1.2.1-d. Protein immobilization and purification using brush-modified monoliths

Polymer brush-modified silica monoliths have also been used for purification of proteins using ion-exchange,[57,58] size exclusion,[28,59,60] and hydrophobic-interaction chromatography.[61-63] Kikuchi *et al.* reviewed the use of polymer brush-modified stationary phases for applications in different areas of chromatography.[62] Importantly, controlled, surface-initiated radical polymerization enables fine control over the thickness of polymer brushes so modification of porous stationary phases with brushes affords control over pore size.[28,59] Huang and Wirth modified nanoporous silica gel with poly(acrylamide) **(Figure 1.1.(vi))** brushes and used this gel for a size-exclusion-based chromatographic separation of proteins.[28] The thickness of the poly(acrylamide) brushes was 10 nm, which was much smaller than the average pore size of the silica gel (86 nm). Thus the polymer film reduced the pore size of the silica gel but did not plug the pores. Using a column of the modified gel, thyroglobulin (mol. wt. 66430 Da), ovalbumin (44000 Da), and ribonuclease (13700 Da) were separated in order of decreasing molecular weight.

In the case of smaller proteins, however, strong interactions between analytes and polymer chains limit the use of polymer brushes in size-exclusion chromatographic columns.[64] Yoshikawa, *et al.* studied the interactions of proteins with poly(2-

hydroxyethyl methacrylate) (poly(HEMA), **Figure 1.1.(vii)**) modified silica as well as the effects of the poly(HEMA) on size-exclusion chromatography.[60] Their findings suggest that the interactions of poly(HEMA) brushes with proteins are minimal on the outermost surface but more prominent inside the brushes. Thus, for large proteins that cannot penetrate the brushes, the separation is dominated by size-exclusion. However, for smaller proteins, which can enter the brushes, both size and adsorption affect the separation. The ability to use both size-exclusion and adsorption may allow some separations that are not possible with size-exclusion alone.

1.2.1.-e. Polymer brush modified substrates as protein microarrays

In the last decade, microarrays of antibodies and enzymes have emerged as important tools for rapid, parallel analyses of a wide range of analytes.[46,65] In the immobilization of proteins in arrays, however, unwanted non-specific adsorption often lowers the signal-to-background ratio and also generates false-positive identifications.[66] Thus an efficient array substrate should demonstrate specificity towards the desired protein in appropriate areas and at the same time show minimal non-specific interactions.

Recent studies suggest that surfaces modified with polymer brushes are more efficient substrates for protein microarrays than nonpolymeric self-assembled monolayers (SAMs) containing the same functional groups.[67,68] Brushes are advantageous over monolayers for several reasons. First, as shown in section 1.2.1-b., brushes have a high protein-binding capacity that can enhance the sensitivity of protein arrays. A second asset of protein arrays formed with polymer brushes is that the three-dimensional structure of swollen brushes should allow ready access to binding sites. In the case of non-polymeric self-assembled monolayers, immobilized antibodies/enzymes lie flat on

the surface and are not highly accessible to the antigen/substrate molecules. For instance, silicon wafers modified with copolymer brushes containing poly(2-methacryloyloxyethyl phosphorylcholine) (poly(MPC)) **(Figure 1.1.(viii))** and poly(GMA) can immobilize 4 times more antibody F_{ab}' fragments than a SAM containing epoxy groups.[67] Moreover, the antibody fragments immobilized on the polymer brushes show ~6 times higher activities than antibodies attached to epoxysilane films. This increased activity suggests that the antibody fragments immobilized in polymer brushes are more accessible to antigens than the antibodies immobilized on the monolayers.

Hydrophilic polymer brushes are especially attractive substrates for antibody arrays because water-swollen films typically show low non-specific protein adsorption. Poly(ethylene glycol) (PEG) **(Figure 1.1.(ix))** [6,7] brushes are especially recognized as biocompatible materials that resist protein adsorption, but poly(AA),[50] poly(HEMA),[60,69] and poly(carboxybetaine methacrylate) (poly(CBMA), **Figure 1.1.(x))** [8] brushes also exhibit low non-specific interactions and can be functionalized to allow binding of proteins. Zhang and coworkers modified gold films with poly(CBMA) brushes using surface-initiated ATRP and showed that these brushes prevent the non-specific adsorption of fibrinogen, lysozyme and human chorionic gonadotropin (hCG).[8] Immobilization of anti-hCG on N-hydroxysuccinimide (NHS)-modified poly(CBMA) brushes (**Scheme 1.6.**) results in specific binding of hCG while maintaining resistance to non-specific protein binding.

Similarly, Tugulu, *et al.* utilized glass slides modified with poly(HEMA), poly(oligo(ethylene glycol)methacrylate), or poly(MPC), for synthesizing nonfouling films for protein microarrays. The presence of the polymer brushes prevents non-specific

protein binding and at the same time, immobilization of O^6-benzylguanine onto the brushes results in chemoselective immobilization of O^6-alkylguanine-DNA-alkyltransferase (AGT) fusion proteins **(Scheme 1.7.)**.[69]

Wang *et al.* developed a chitosan-*g*-methyl-PEG-coated poly(dimethyl siloxane) (PDMS) microchip to minimize non-specific protein adsorption.[70] The methyl-PEG units provide hydrophilic domains and minimize non-specific adsorption of biomolecules. A fluorescence image of the polymer-coated microfluidic channels was acquired after exposure to fluorescein isothiocyanate (FITC)-labeled bovine serum albumin (BSA) for a period of 24 h. The image shows no detectable fluorescence, indicating effective suppression of BSA adsorption on this microchip.[70] On the other hand, a PDMS microchip without polymer modification showed bright fluorescence after exposure to FITC-BSA for 24 h.

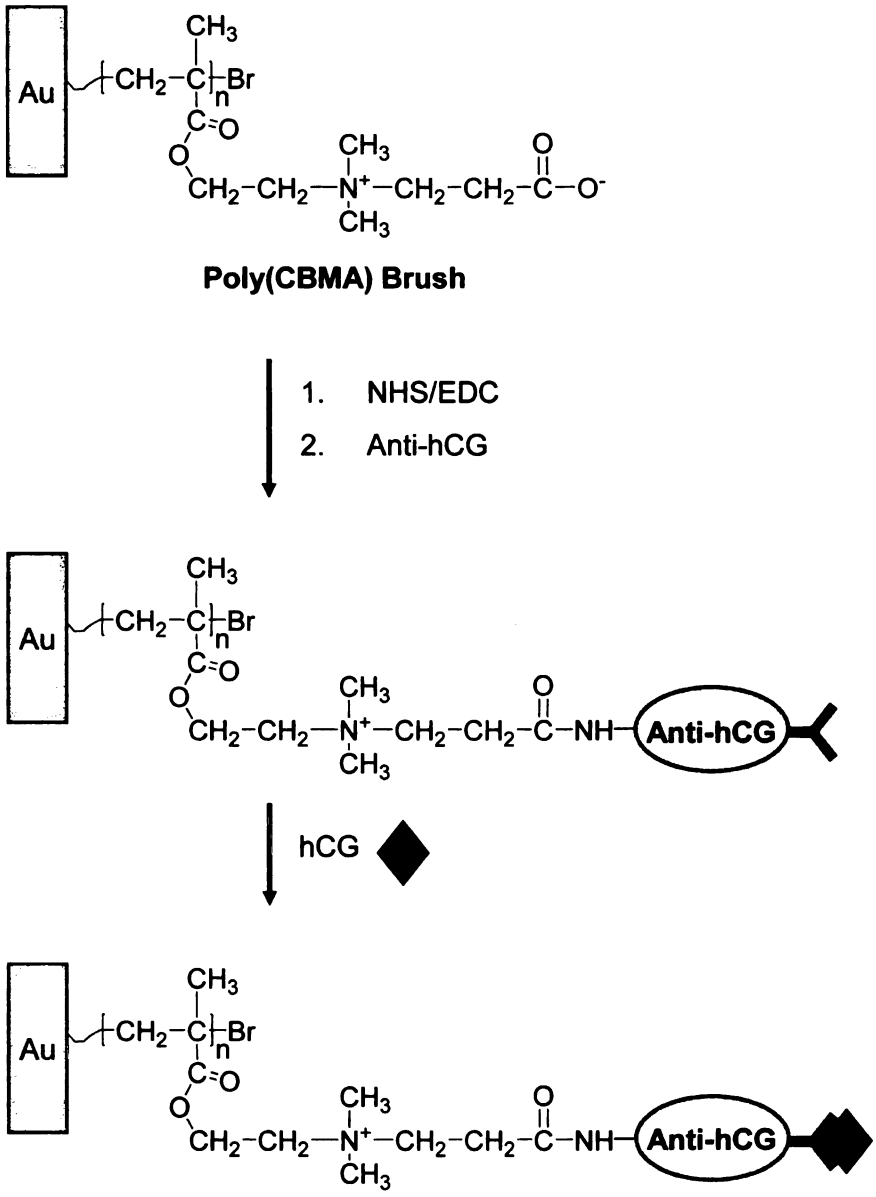

Scheme 1.6. A schematic illustration of anti-human chorionic gonadotropin (anti-hCG) immobilization on N-hydroxysuccinimide (NHS)-modified poly(CBMA) brushes. Immobilization of anti-hCG results in specific binding of hCG protein. Poly(CBMA) brushes were modified with NHS in the presence of 1-[3-(dimethylamino)propyl]-3-ethylcarbodiimide hydrochloride (EDC). Redrawn from Zhang, Z.; Chen, S. F.; Jiang, S. Y. *Biomacromolecules* **2006**, *7*, 3311-3315.

Scheme 1.7. Fabrication of protein-functionalized poly(oligo(ethylene glycol)methacrylate) brushes: **(a)** grafting of ATRP initiator and surface-initiated ATRP of oligo(ethylene glycol)methacrylate; **(b)** activation of hydroxyl groups with p-nitrophenyl chloroformate; **(c)** functionalization with O^6-(4-(13-amino-2,5,8,11-tetraoxatridecyl)oxymethylbenzyl)guanine and quenching of residual *p*-nitrophenyl chloroformate groups; **(d)** immobilization of O^6-alkylguanine-DNA-alkyltransferase (AGT) fusion protein on benzylguanine surfaces. Redrawn from Tugulu, S.; Arnold, A.; Sielaff, I.; Johnsson, K.; Klok, H. A. *Biomacromolecules* **2005**, *6*, 1602-1607.

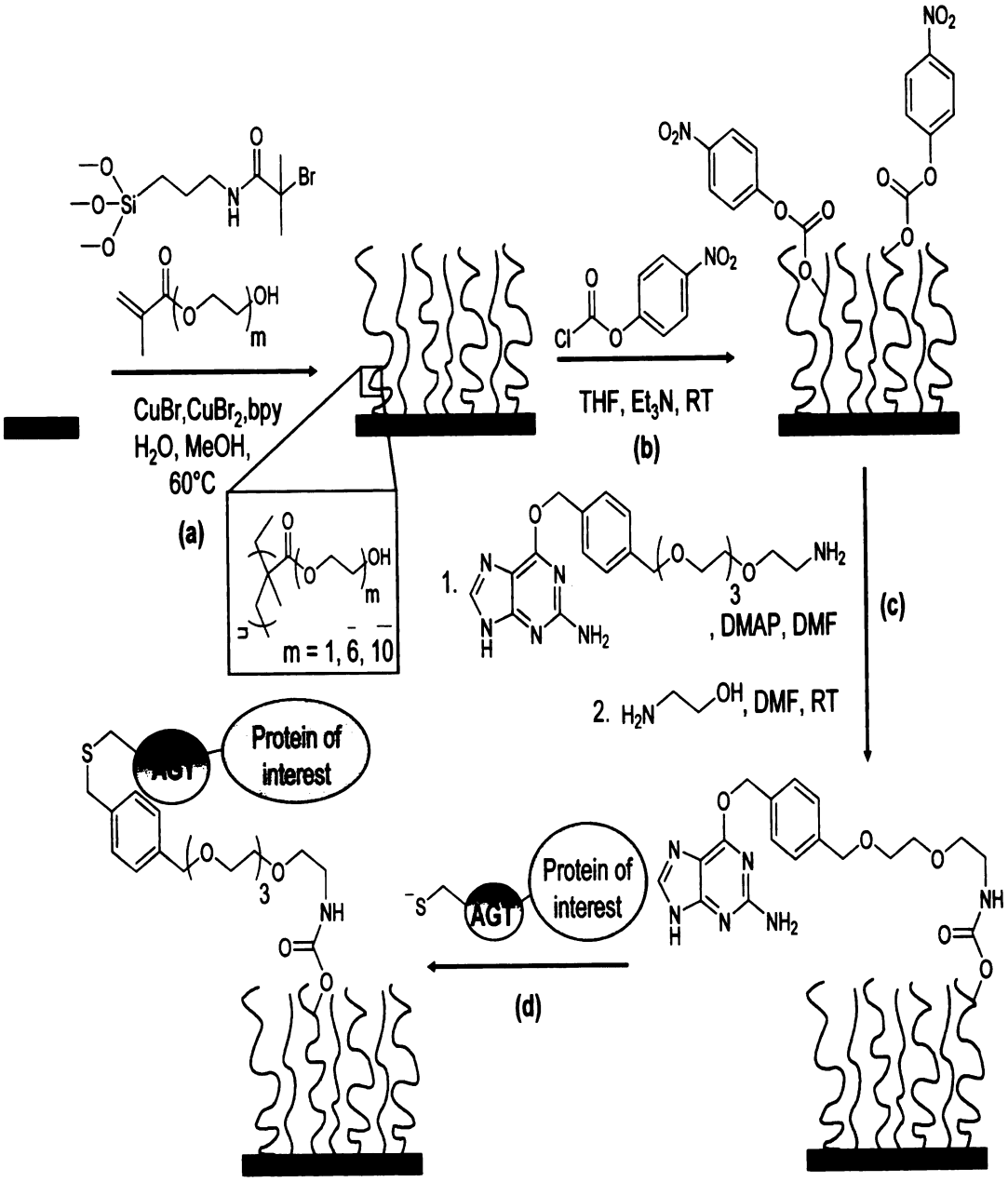
CuBr,CuBr2,bpy
H2O, MeOH,
60°C
(a)
m = 1, 6, 10
THF, Et3N, RT
(b)
1.
3
, DMAP, DMF
2. H2N
OH, DMF, RT
(c)
Protein of interest
AGT
(d)

In addition to minimizing non-specific interactions, substrates for protein microarrays should also prevent denaturation of protein molecules. Ober and coworkers developed a lithographic method (**Scheme 1.8.**) to produce protein patterns with minimal denaturation and a low level of non-specific interactions.[71] A patterned PEG surface was back-filled with ATRP initiators, and poly(AA) brushes were grown from the initiator-containing regions. FITC-labeled BSA was covalently immobilized on poly(AA) brushes that were activated with NHS/1-[3-(dimethylamino)propyl]-3-ethylcarbodiimide

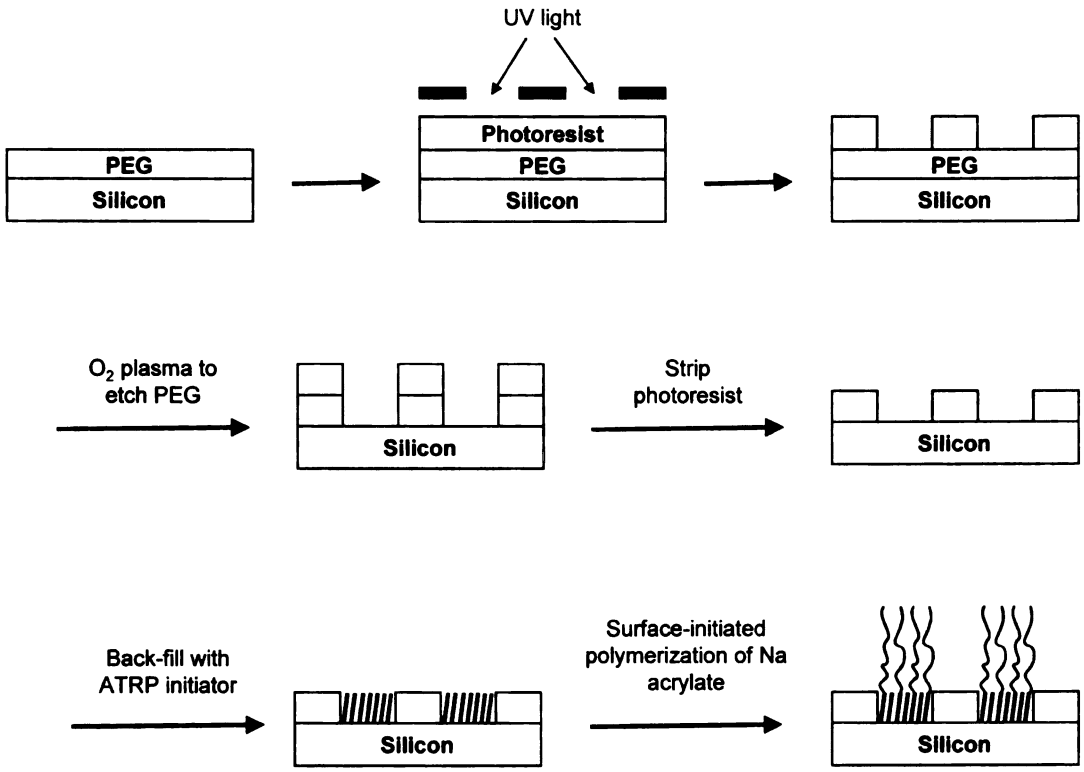

Scheme 1.8. Patterning of PEG and poly(AA) brushes on a silicon surface. Redrawn from Dong, R.; Krishnan, S.; Baird, B. A.; Lindau, M.; Ober, C. K. *Biomacromolecules* **2007**, *8*, 3082-3092.

hydrochloride (EDC). The fluorescence image of these films showed well-defined, bright BSA patterns. In contrast, the PEG modified regions were dark due to minimal attachment of BSA. Thus this method can yield protein microarrays with low non-specific binding.[71]

Proper orientation of an enzyme or antibody is required to maintain biological activity and should be taken into account when developing a substrate for immobilizing biomolecules. Randomly oriented proteins frequently show decreases in activity due to the inaccessibility of the active site. Control over protein orientation is generally achieved by (a) changing the surface charge,[72] or (b) using site-specific immobilization through biotin-streptavidin interactions or thiol-disulfide interchange reactions between polymer brushes and protein molecules.[67,69,73,74] Iwata and coworkers utilized well-defined block copolymer brushes consisting of poly(MPC) and poly(GMA) on silicon wafers to immobilize antibody F_{ab}' fragments in a defined orientation.[67,74] The orientation of the antibody fragments was defined by derivatizing the GMA units with pyridyl disulfide and immobilizing the antibodies via thiol-disulfide interchange reactions **(Scheme 1.9.)**. Increases in the length of poly(GMA) units resulted in increased loading of the antibody fragments due to the availability of more binding sites. The fluorescence intensity after reaction of immobilized antibody fragments with FITC-labeled antigen also increased with an increasing length of poly(GMA) units because of the increased loading of the antibody fragments. Polymer brushes without pyridyl disulfide moieties were also used to immobilize antibody F_{ab}' fragments via reaction with the epoxy groups on GMA units. The fluorescence intensity arising from binding of labeled antigen to antibodies linked to unmodified poly(GMA) blocks was 20 times lower than that

Scheme 1.9. Immobilization of Fab′ fragments in defined orientation on poly(MPC)-b-poly(GMA) brushes. The proper orientation was achieved by **(a)** introduction of pyridyl disulfide units onto the polymer brushes followed by **(b)** a thiol-disulfide interchange reaction between thiol groups in Fab′ fragments and pyridyl disulfide units in the polymer chain. The activity of the immobilized antibody fragments was investigated by **(c)** reaction with FITC-labeled mouse immuglobulin G. Redrawn from Iwata, R.; Satoh, R.; Iwasaki, Y.; Akiyoshi, K. *Colloid Surface B* **2008**, *62*, 288-298.

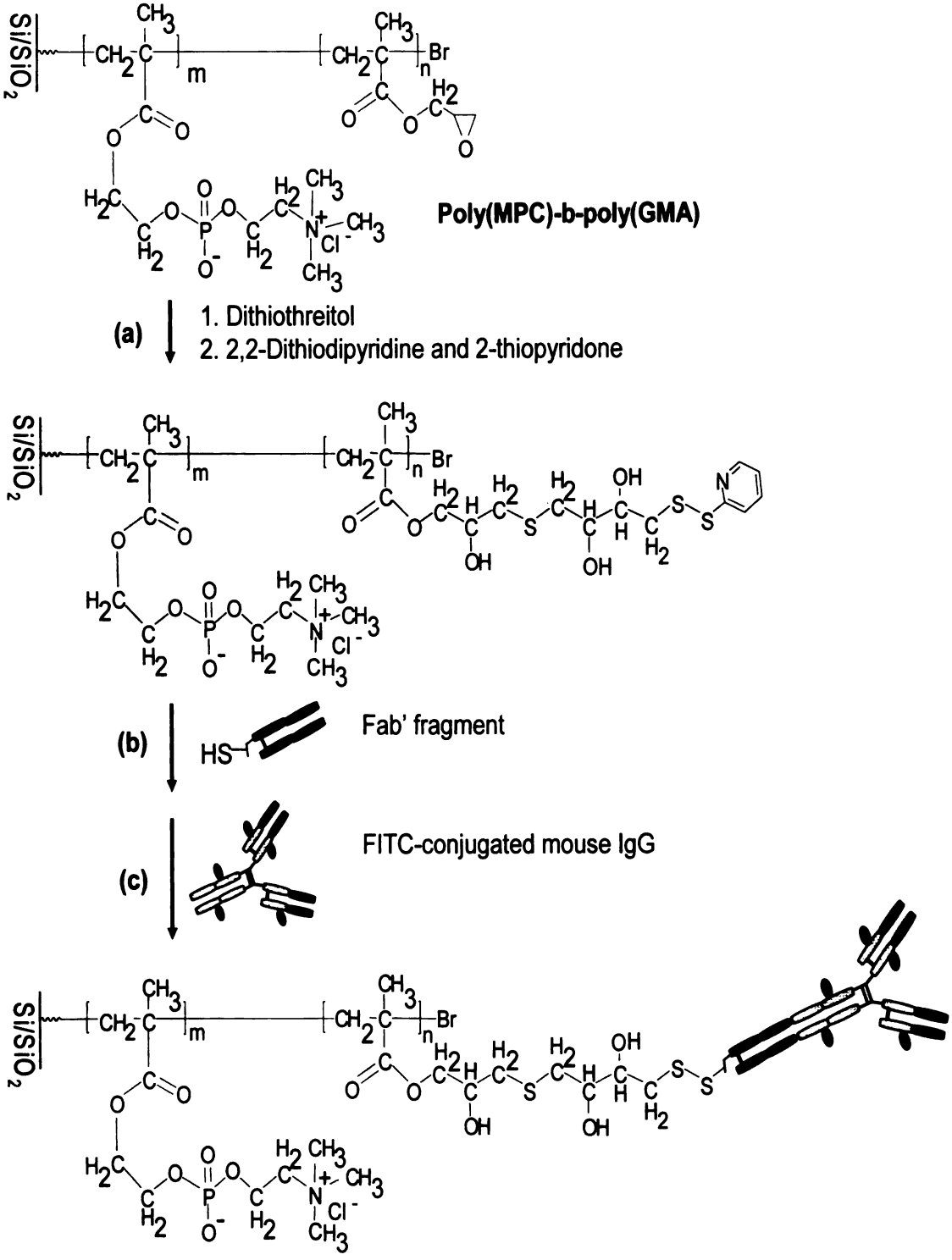
Poly(MPC)-b-poly(GMA)
(a)
1. Dithiothreitol
2. 2,2-Dithiodipyridine and 2-thiopyridone
(b)
Fab' fragment
(c)
FITC-conjugated mouse IgG

obtained using antibodies attached to pyridyl-disulfide-modified brushes. Presumably, the random orientation of antibodies attached to unmodified poly(GMA) results in a lower activity.

1.2.1-f. Polymer brushes for enzyme immobilization

Enzymatic reactions in non-aqueous media are also important in industrial applications,[75,76] but enzymes frequently do not show sufficient activity in non-aqueous solvents. To overcome this problem enzymes have been coated with surfactants[77] and immobilized on microspheres[78] and in polymer brush-modified membranes.[79-81] Enzymes immobilized in polymer brush-modified membranes show higher activity than enzymes coated with surfactants or immobilized on microspheres.[79-81] This is because convective flow brings the substrates to the immobilized enzymes and minimizes mass-transport limitations. Goto and coworkers immobilized lipases via ion-exchange inside a porous polyethylene hollow fiber (**Figure 1.3.**). The anion-exchange sites were created by radiation-induced grafting of poly(GMA) brushes followed by reaction of the GMA units with diethylamine.[80] The immobilized lipase showed 23-fold higher activity than the native lipase (suspended in substrate solution) in the esterification reaction between lauric acid and benzyl alcohol. The grafted poly(GMA) acts as a hydrophobic surfactant to stabilize the enzyme and enhance activity. Moreover, reuse of the immobilized lipase three times in a batch reactor over a period of 24 h resulted in no loss in activity, whereas there was a 75% decrease in the activity of native lipase under similar conditions.[81]

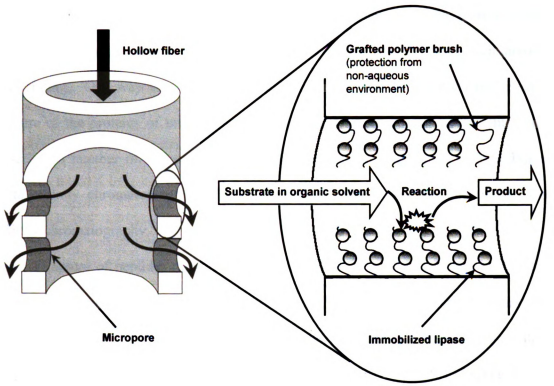

Figure 1.3. Schematic representation of lipase immobilized in a porous hollow-fiber polyethylene membrane. The pores of the membrane were modified with poly(GMA) brushes followed by reaction with diethylamine. Lipase immobilization occurred via ion-exchange interactions, and the lipase-containing membranes were used to study the esterification reaction between lauric acid and benzyl alcohol. Redrawn from Goto, M.; Kawakita, H.; Uezu, K.; Tsuneda, S.; Saito, K.; Goto, M.; Tamada, M.; Sugo, T. *Journal of the American Oil Chemists Society* **2006**, *83*, 209-213.

1.2.2. Polymer brush-based capture of proteins for analysis by mass spectrometry

The identification and analysis of the proteins associated with specific diseases is a major opportunity in analytical chemistry. Identification of phosphorylated proteins, in particular, is important because changes in phosphorylation states can cause various diseases including cancer.[82] Mass spectrometry is often employed for the identification

and analysis of phosphorylated proteins, but the low abundance of the phosphorylated proteins and suppression of signals by non-phosphorylated proteins make such analyses challenging. One way to overcome this problem is to develop methods for selective capture of the proteins of interest from a pool of unwanted proteins. A recent review describes a number of techniques for phosphopeptide enrichment such as immobilized metal-affinity chromatography (IMAC), reversible covalent binding, and metal oxide affinity chromatography.[82]

Capture of peptides directly in polymer brushes on a MALDI plate is attractive for high-throughput analysis of moderately complex samples. Dunn and coworkers used poly(HEMA) brushes in on-plate enrichment of phosphopeptides for analysis by matrix-assisted laser desorption/ ionization mass spectrometry (MALDI-MS) (**Figure 1.4.**).[83] Au-coated Si wafers were modified with poly(HEMA)-nitrilotriacetate (NTA)-Fe(III) brushes, and small volumes (~1μL) of digest containing phosphopeptide, non-phosphopeptides and salts were spotted on these films. After incubation, the films were washed and dried, and matrix was added for MALDI-MS analysis. In a specific example, mass spectra of a β-casein digest were obtained with and without enrichment on poly(HEMA)-NTA-Fe(III) brushes. Enrichment on the brushes yielded a 30-fold increase in the signal intensities of several phosphorylated peptides relative to the conventional MALDI-MS analysis. Additionally, the enrichment procedure resulted in signals from several phosphopeptides that were undetectable in conventional MALDI-MS, as well as decreased signals for nonphosphopeptides. Finally, enrichment decreased the detection limit to 15 fmol for the peptide with m/z 2062 in a β-casein digest. The effectiveness of polymer brushes in the enrichment of phosphopeptides is likely due to

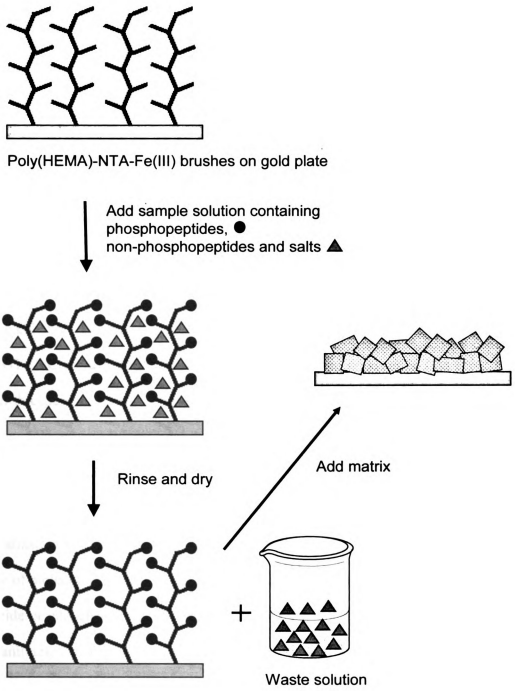

Figure 1.4. Protocol for phosphopeptide enrichment using poly(HEMA)- NTA-Fe(III) films on Au MALDI plates.

the high density of peptide-binding sites, as 60 nm-thick poly(HEMA)-NTA-Fe(III) brushes have a binding capacity of ~0.6 $\mu g/cm^2$ for phosphoangiotensin. Remarkably, these brushes showed ~70% recovery of a synthetic monophosphopeptide and 100% recovery of a diphosphopeptide. In contrast, MALDI plates modified with a monolayer of NTA-Fe(III) gave a monophosphopeptide recovery of only ~9%.

1.2.3. Polymer brushes for capillary chromatography and electrochromatography

Polymer brushes may also find use in capillary chromatography[84,85] and open-tubular capillary electrochromatography (OT-CEC),[86,87] where the polymers are grafted on the inner walls of the capillary and separation is achieved without the need for packing of the column. The advantages of using polymer brushes in capillary chromatography and OT-CEC include optimization of separation efficiency by controlling the polymer brush thickness as well as the ease of derivatization of the polymer chains for specific binding. Huang and Wirth found that polyacrylamide coated capillaries enhance protein separations by decreasing surface adsorption.[64] Miller and coworkers used substituted poly(HEMA) brushes as stationary phases in OT-CEC and demonstrated that derivatization of the brushes by appropriate reagents allows for separation of a wide range of molecules.[86] Specifically, derivatization of poly(HEMA) brushes with octanoyl chloride or ethylenediamine **(Scheme 1.10.)** facilitated separation of a series of phenols and anilines, which could not be separated using bare silica capillaries or underivatized brushes. They studied separation of three amines, aniline, 4-nitroaniline and 3, 5-dichloroaniline, using a bare silica column as well as a capillary coated with ethylenediamine-derivatized poly(HEMA). These amines could not be resolved using bare silica columns whereas the use of polymer-coated capillaries resulted in full

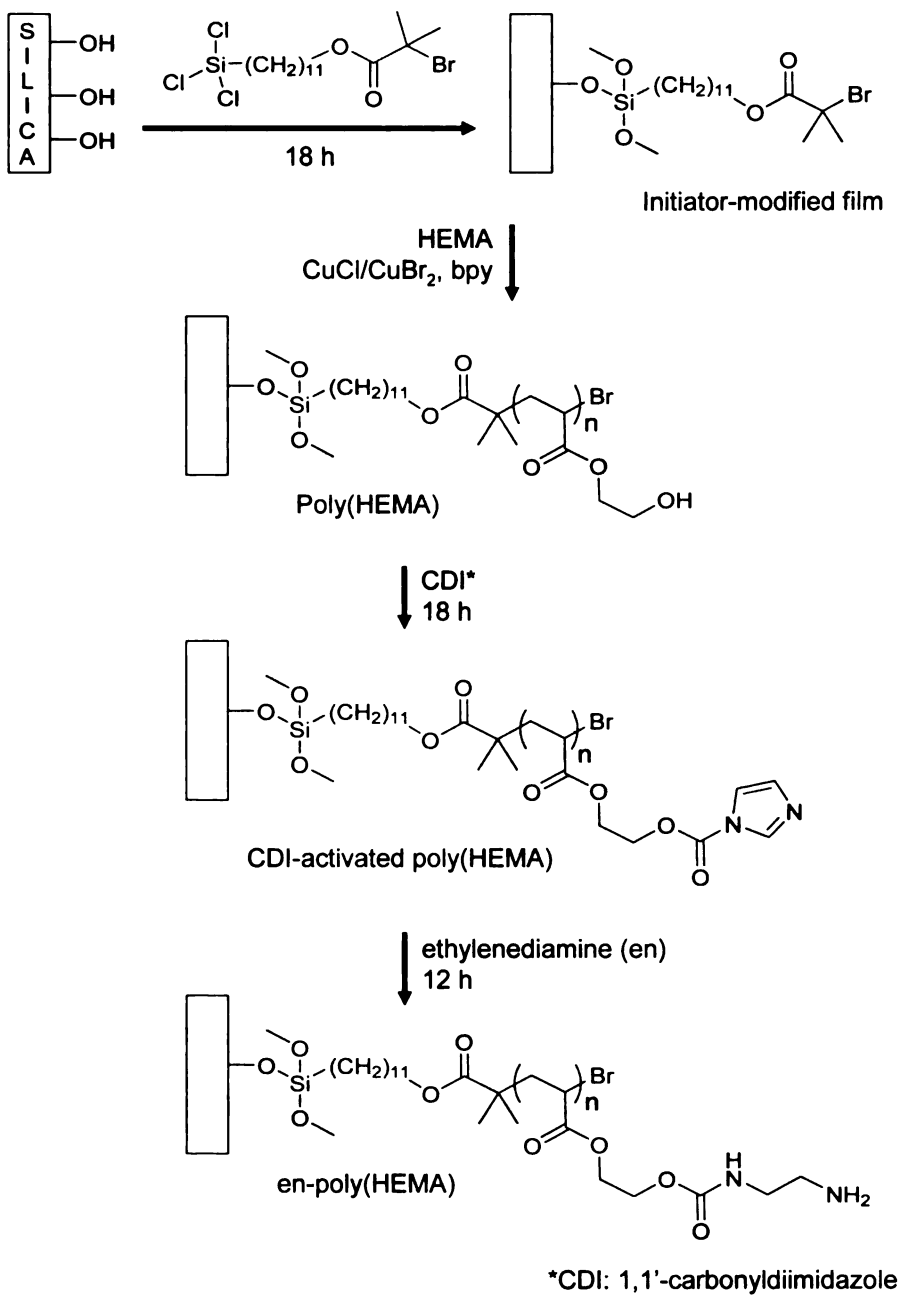

Scheme 1.10. Attachment of trichlorosilane initiator to a silica capillary surface, ATRP of HEMA from the immobilized initiator, activation of poly(HEMA) by 1,1′-carbonyldiimidazole (CDI), and derivatization with ethylenediamine (en). Redrawn from Miller, M. D.; Baker, G. L.; Bruening, M. L. *Journal of Chromatography A* **2004**, *1044*, 323-330.

resolution. Although the peaks were broad, they were fully separated. Moreover, increasing the thickness of the coatings enhanced the resolution for several aniline pairs presumably due to increase in effective stationary phase to mobile phase volume ratio.

1.2.4. Selective protein purification in polymer brush-modified membranes

1.2.4-a. Membrane absorbers for protein purification via affinity interactions

Purification is often the bottleneck step in producing proteins for therapeutic or research purposes. Perhaps the most powerful method for protein purification is affinity adsorption in which immobilized ligands interact specifically with an affinity tag that is genetically engineered into the protein of interest. Modified surfaces selectively bind the proteins containing the affinity tags, whereas other cellular proteins can be washed away. The most common affinity tags are polyhistidine,[88,89] streptavidin,[90] glutathione-S-transferrase,[91] and maltose binding protein.[92] The use of polyhistidine tags allows purification by IMAC where selectivity is usually based on the interaction of the polyhistidine with a Ni^{2+} complex immobilized on silica beads or in a gel **(Figure 1.5.)**. However, drawbacks to IMAC include slow diffusion of macromolecules into porous beads, difficulties in packing large columns, relatively high pressure drops, and long separation times.[93,94] These drawbacks become particularly important in large scale separations.

Membrane absorbers[95] have the potential to provide more rapid affinity purification than column-based methods because convective flow, rather than diffusion, brings proteins to binding sites in membrane pores. Convective rinsing of pores may also help to remove non-specifically adsorbed proteins.[89] Additionally, the development of

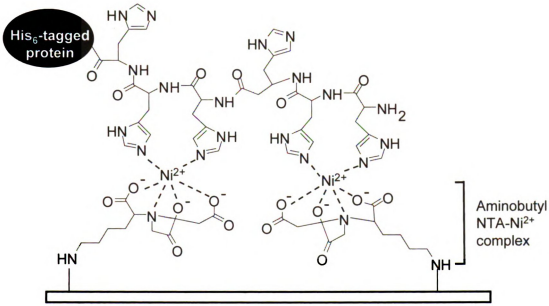

Figure 1.5. His-tagged protein binding to a NTA-Ni^{2+} modified surface.

disposable membranes for one time use would avoid challenges with crossover between samples.[44]

Unfortunately, typical protein-absorbing membranes suffer from low binding capacities relative to porous beads. In order to increase the capacity of membrane absorbers, the membrane pores can be modified with polymer brushes (**Figure 1.6.**).[20,89,96-98] The brushes are attractive because they have multiple protein binding sites and can be easily modified with ligands for specific biological recognition. A wide range of polymeric and inorganic membranes such as alumina,[20,89] silica,[99] PVDF,[98] nylon,[100] polyethersulfone,[22] regenerated cellulose,[101] and polyethylene[102] have been modified with polymer brushes to develop protein-absorbing membranes with high protein-binding capacity as well as selectivity towards the protein of interest. The ability of polymer brushes to enhance protein binding to membranes depends greatly on both membrane

geometry and the polymer brush. Sun *et al.* showed that modification of microporous alumina membranes with poly(HEMA) and subsequent derivatization of the poly(HEMA) brushes with NTA-Cu^{2+} gives membranes with a BSA-binding capacity as high as 130 mg/cm^3 of membrane (~95 mg of BSA per g of membrane), which is several fold higher than the capacities of other protein absorbing membranes.[18,20,99] This high capacity stems in part from both the relatively small pore diameter (0.2 μm) in the membrane and the thickness of the polymer brushes. Binding capacity should increase as pore size decreases, but unfortunately so does resistance to flow.

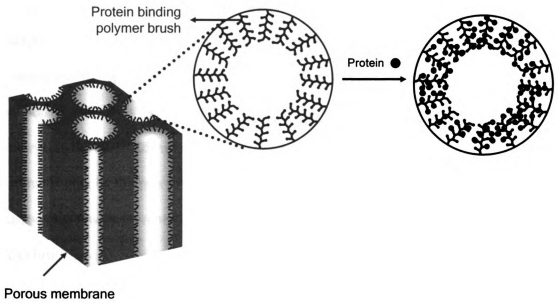

Figure 1.6. Protein binding to a polymer brush inside a membrane pore.

1.2.4-b. Membrane absorbers for protein purification via ion-exchange interactions

Membrane absorbers are also being used for protein immobilization via ion-exchange interactions. The separation is achieved by differential absorption of charged proteins at oppositely charged membrane surfaces. For instance, Kawakita and coworkers formed anion-exchange membranes through modification of porous glass with poly(GMA)-diethyl amine brushes. The resulting membranes showed a BSA binding capacity of 12 mg protein per g of membrane.[99] Kumar, *et al.* grafted poly(vinylbenzyltrimethylammonium chloride) **(Figure 1.1.(xi))** brushes onto cotton cellulose and achieved an equilibrium binding capacity of 40 mg BSA per g of membrane.[103] Ulbricht and coworkers formed cation-exchange microfiltration membranes by photo-grafting copolymers of acrylic acid and a cross-linking monomer, methylene bisacrylamide, inside the pores of polypropylene membranes.[31,45] The incorporation of cross-links within the grafted polymer layers led to higher dynamic protein-binding capacities than grafting of a linear polymer, even when the amount of functional groups was same in both cases.[45] Overall, the poly(acrylic acid-*co*-methylene bisacrylamide)-modified membranes exhibited a lysozyme binding capacity of 60 mg/cm^3, which is 30 times higher than the binding capacity of an unmodified membrane. Husson and coworkers reported that regenerated cellulose membranes modified with poly (AA) brushes via 1 h of ATRP show static lysozyme binding capacities of 99 mg/mL.[101] This capacity is 2-3 times higher than the capacity of commercial Sartobind C membranes. However, the Sartobind C membranes are 40 times more permeable because of a larger pore size.

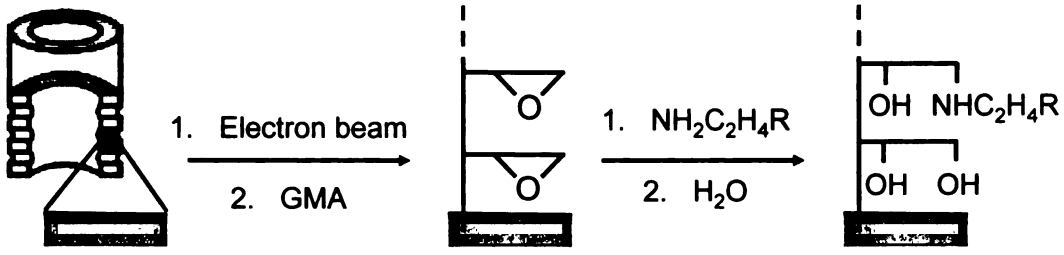

Inner diameter 2.0 mm
Outer diameter 2.0 mm
Porosity 70%
Pore diameter 0.36 μm

R	Fiber name
COOH	AC(x)-diol
PO_3H_2	AP(x)-diol
SO_3H	AS(x)-diol

Scheme 1.11. Modification of a porous high-density polyethylene hollow fiber membrane with poly(GMA) brushes and subsequent reaction of the brushes with 3-aminopropionic acid (AC), (2-aminoethyl)phosphonic acid (AP), or 2-aminoethane-1-sulfonic acid (AS). Redrawn from Iwanade, A.; Umeno, D.; Saito, K.; Sugo, T. *Biotechnology Progress* **2007**, *23*, 1425-1430.

Iwanade and coworkers modified porous hollow fiber membranes with poly(GMA) brushes and reacted the epoxide groups of the polymer with ampholite molecules containing amino and anionic groups such as carboxylic acids (**Scheme 1.11.**).[104] The resulting membranes showed multilayer protein binding for lactoferrin, cytochrome C, and lysozyme. In a specific example, membranes containing (2-aminoethyl)phosphonic acid as an ampholite had equilibrium adsorption capacities of 130 mg/g, 150 mg/g and 190 mg/g for lysozyme (feed concentration of 0.2 g/L), cytochrome C (feed concentration of 0.5 g/L) and lactoferrin (feed concentration of 1.0 g/L), respectively. Moreover the elution efficiency was >99%. However, mutual repulsion

between the anionic groups caused extension of the polymer brush and a 3-fold decrease in the flux relative to unmodified membranes. In fact, decreased membrane permeability due to extended polymer brushes is the major disadvantage of grafting charged polymer brushes into porous membranes. To overcome this drawback, Iwanade and coworkers suggested ionic cross-linking of the negatively charged polymer brushes with divalent cations.[105]

Growth of polymer brushes in membranes can also help to decrease the dispersity of pore sizes. A relatively narrow pore-size distribution is important for obtaining narrow breakthrough curves. Singh and coworkers tuned the ion-exchange capacity and the pore size of commercially available microporous PVDF membranes using controlled polymerization of poly(2-vinylpyridine) **(Figure 1.1.(xii))** inside membrane pores.[98] Growth of the brushes decreased the width of the pore-size distribution and prevented premature breakthrough of proteins in the largest pores. Controlling the polymerization time also provided control over the average pore size of the membranes and the ion-exchange capacity.

1.3. Outline of the dissertation

This dissertation aims at developing affinity membranes for high-capacity protein binding as well as rapid and selective purification of His-tagged proteins. Chapter 2 shows that ATRP affords controlled growth of polymer brushes inside porous alumina membranes without clogging the pores. Growth of poly(HEMA) brushes inside porous alumina membranes and subsequent functionalization of poly(HEMA) with NTA-Ni^{2+} complexes allows rapid, highly selective purification of His-tagged proteins. Gel electrophoresis reveals that the purity of His-tagged ubiquitin eluted from these materials

is >99%, even when the initial solution contains 10% bovine serum or a 20-fold excess of BSA. Moreover, the binding capacity of the membrane is at least 5-fold greater than that for membranes reported in the literature.[20,31,99] Separations can be completely performed in 30 min or less and membranes are fully reusable.

Unfortunately, purification of His-tagged proteins using porous alumina membranes is limited to relatively simple solutions and low flow rates because of a limited pore size. Polymeric membranes, on the other hand, can have larger pore sizes than porous alumina, which should allow rapid purification with more complex solutions. In Chapter 3, I discuss the use of porous nylon membranes modified with poly(HEMA)-NTA-Ni^{2+} brushes for purification of His-tagged cellular retinaldehyde binding protein directly from a cell lysate with purities that are at least as good as those obtained with Ni^{2+} columns.

Nevertheless, nylon membranes modified with poly(HEMA)-NTA-Ni^{2+} brushes have a relatively low protein binding capacity (25 mg protein/cm^3 of the membrane), perhaps because the organic solvents employed in the brush synthesis and derivatization partially damage the membrane structure. Chapter 4 of this dissertation focuses on a completely aqueous procedure for growth of polymer brushes inside polymeric membranes. The aqueous process avoids the use of organic solvents that may dissolve or corrupt porous substrates. This chapter describes the use of aqueous layer-by-layer adsorption of polyelectrolyte macroinitiators and subsequent aqueous ATRP from these immobilized initiators for successful, aqueous growth of poly(HEMA) brushes on polymeric substrates.

Despite the successful growth of poly(HEMA) brushes with aqueous initiation, the creation of protein-binding brushes requires conversion of hydroxyl groups in poly(HEMA) to carboxylic acid moieties. The formation of acid groups involves reaction of poly(HEMA) with succinic anhydride in an organic solvent for several hours. Chapter 5 describes surface-initiated aqueous ATRP of an acidic monomer, 2-(methacryloyloxy)ethyl succinate (MES), that allows rapid, one-step synthesis of acidic polymer brushes. This procedure avoids the need to react the brush with succinic anhydride in an organic solvent. Also, poly(MES) brushes and their derivatives exhibit high protein-binding capacities. Through FTIR and ellipsometry studies, I show that poly(MES) brushes are capable of binding many monolayers of BSA as well as lysozyme.

Modification of polymeric membranes with poly(MES) should allow for high-capacity purification of His-tagged proteins directly from a cell lysate. In Chapter 6, I describe the growth, derivatization, and characterization of poly(MES) brushes inside the pores of nylon membranes to form protein absorbers. Analysis of the protein breakthrough curves give a high binding capacity of 80 ± 2 and 118 ± 8 mg protein per cm^3 of the membrane for BSA and lysozyme respectively. Finally these membranes are utilized to purify His-tagged proteins from cell lysate.

In the last chapter, I will present the conclusions drawn from my research and some proposed future work.

1.4. References

(1) Milner, S. T. *Science* **1991**, *251*, 905-914.

(2) Bhat, R. R.; Tomlinson, M. R.; Wu, T.; Genzer, J. *Advances in Polymer Science* **2006**, *198*, 51-124.

(3) Huang, W.; Kim, J.-B.; Bruening, M. L.; Baker, G. L. *Macromolecules* **2002**, *35*, 1175-1179.

(4) Ulbricht, M.; Yang, H. *Chem. Mater.* **2005**, *17*, 2622-2631.

(5) Brown, H. R.; Char, K.; Deline, V. R. *Macromolecules* **1990**, *23*, 3383-3385.

(6) Andruzzi, L.; Senaratne, W.; Hexemer, A.; Sheets, E. D.; Ilic, B.; Kramer, E. J.; Baird, B.; Ober, C. K. *Langmuir* **2005**, *21*, 2495-2504.

(7) Ma, H. W.; Hyun, J. H.; Stiller, P.; Chilkoti, A. *Advanced Materials* **2004**, *16*, 338-341.

(8) Zhang, Z.; Chen, S. F.; Jiang, S. Y. *Biomacromolecules* **2006**, *7*, 3311-3315.

(9) Parsonage, E.; Tirrell, M.; Watanabe, H.; Nuzzo, R. G. *Macromolecules* **1991**, *24*, 1987-1995.

(10) Kent, M. S. *Macromolecular Rapid Communications* **2000**, *21*, 243-270.

(11) Jordan, R.; Graf, K.; Riegler, H.; Unger, K. K. *Chemical Communications* **1996**, 1025-1026.

(12) Huang, W. X.; Skanth, G.; Baker, G. L.; Bruening, M. L. *Langmuir* **2001**, *17*, 1731-1736.

(13) Prucker, O.; Rühe, J. *Macromolecules* **1998**, *31*, 592-601.

(14) Prucker, O.; Rühe, J. *Macromolecules* **1998**, *31*, 602-613.

(15) Jones, D. M.; Brown, A. A.; Huck, W. T. S. *Langmuir* **2002**, *18*, 1265-1269.

(16) Yamamoto, S.; Ejaz, M.; Tsujii, Y.; Fukuda, T. *Macromolecules* **2000**, *33*, 5608-5612.

(17) Bao, Z. Y.; Bruening, M. L.; Baker, G. L. *Journal of the American Chemical Society* **2006**, *128*, 9056-9060.

(18) Bruening, M. L.; Dotzauer, D. M.; Jain, P.; Ouyang, L.; Baker, G. L. *Langmuir* **2008**, *24*, 7663-7673.

(19) Huang, W. X.; Baker, G. L.; Bruening, M. L. *Angewandte Chemie-International Edition* **2001**, *40*, 1510-1512.

(20) Sun, L.; Dai, J. H.; Baker, G. L.; Bruening, M. L. *Chemistry of Materials* **2006**, *18*, 4033-4039.

(21) Chen, X. Y.; Armes, S. P.; Greaves, S. J.; Watts, J. F. *Langmuir* **2004**, *20*, 587-595.

(22) Jain, P.; Dai, J.; Grajales, S.; Saha, S.; Baker, G. L.; Bruening, M. L. *Langmuir* **2007**, *23*, 11360-11365.

(23) Advincula, R. C.; Brittain, W. J.; Caster, K. C.; Rühe, J. *Polymer Brushes: Synthesis, Characterization, Applications*, 2004.

(24) Edmondson, S.; Osborne, V. L.; Huck, W. T. S. *Chemical Society Reviews* **2004**, *33*, 14-22.

(25) Minko, S. *Polymer Reviews* **2006**, *46*, 397-420.

(26) Zhao, B.; Brittain, W. J. *Macromolecules* **2000**, *33*, 342-348.

(27) Choi, I. S.; Langer, R. *Macromolecules* **2001**, *34*, 5361-5363.

(28) Huang, X. Y.; Wirth, M. J. *Analytical Chemistry* **1997**, *69*, 4577-4580.

(29) Juang, A.; Scherman, O. A.; Grubbs, R. H.; Lewis, N. S. *Langmuir* **2001**, *17*, 1321-1323.

(30) Moon, J. H.; Swager, T. M. *Macromolecules* **2002**, *35*, 6086-6089.

(31) Ulbricht, M.; Yang, H. *Chemistry of Materials* **2005**, *17*, 2622-2631.

(32) Yang, H.; Ulbricht, M. *Macromolecular Materials and Engineering* **2008**, *293*, 419-427.

(33) Dauginet-Da Pra, L.; Demoustier-Champagne, S. *Polymer* **2005**, *46*, 1583-1594.

(34) Wang, J. S.; Matyjaszewski, K. *Macromolecules* **1995**, *28*, 7901-7910.

(35) Matyjaszewski, K.; Xia, J. H. *Chemical Reviews* **2001**, *101*, 2921-2990.

(36) Kato, M.; Kamigaito, M.; Sawamoto, M.; Higashimura, T. *Macromolecules* **1995**, *28*, 1721-1723.

(37) Mitsukami, Y.; Donovan, M. S.; Lowe, A. B.; McCormick, C. L. *Macromolecules* **2001**, *34*, 2248-2256.

(38) Boyer, C.; Bulmus, V.; Liu, J. Q.; Davis, T. P.; Stenzel, M. H.; Barner-Kowollik, C. *Journal of the American Chemical Society* **2007**, *129*, 7145-7154.

(39) Husemann, M.; Morrison, M.; Benoit, D.; Frommer, K. J.; Mate, C. M.; Hinsberg, W. D.; Hedrick, J. L.; Hawker, C. J. *Journal of the American Chemical Society* **2000**, *122*, 1844-1845.

(40) Chung, I.-D.; Britt, P.; Xie, D.; Harth, E.; Mays, J. *Chemical Communications* **2005**, 1046-1048.

(41) Tsarevsky, N. V.; Pintauer, T.; Matyjaszewski, K. *Macromolecules* **2004**, *37*, 9768-9778.

(42) Kim, J.-B.; Huang, W.; Miller, M. D.; Baker, G. L.; Bruening, M. L. *Journal of Polymer Science Part A: Polymer Chemistry* **2003**, *41*, 386-394.

(43) Odian, G. *Principles of Polymerization*; Fourth ed.; Wiley-Interscience, 2004, pp 316-317.

(44) Singh, N.; Chen, Z.; Tomer, N.; Wickramasinghe, S. R.; Soice, N.; Husson, S. M. *Journal of Membrane Science* **2008**, *311*, 225-234.

(45) Yusof, A. H. M.; Ulbricht, M. *Journal of Membrane Science* **2008**, *311*, 294-305.

(46) Dai, J. H.; Baker, G. L.; Bruening, M. L. *Analytical Chemistry* **2006**, *78*, 135-140.

(47) Sage, L. *Analytical Chemistry* **2004**, *76*, 137A-142A.

(48) Xu, F. J.; Cai, Q. J.; Li, Y. L.; Kang, E. T.; Neoh, K. G. *Biomacromolecules* **2005**, *6*, 1012-1020.

(49) Cullen, S. P.; Liu, X.; Mandel, I. C.; Himpsel, F. J.; Gopalan, P. *Langmuir* **2008**, *24*, 913-920.

(50) Dai, J. H.; Bao, Z. Y.; Sun, L.; Hong, S. U.; Baker, G. L.; Bruening, M. L. *Langmuir* **2006**, *22*, 4274-4281.

(51) Arica, M. Y.; Yilmaz, M.; Yalcin, E.; Bayramoğlu, G. *Journal of Chromatography B-Analytical Technologies in the Biomedical and Life Sciences* **2004**, *805*, 315-323.

(52) Bayramoğlu, G.; Ekici, G.; Beşirli, N.; Arica, M. Y. *Colloids and Surfaces a-Physicochemical and Engineering Aspects* **2007**, *310*, 68-77.

(53) Su, C. K.; Chiang, B. H. *Process Biochemistry* **2006**, *41*, 257-263.

(54) Huang, J. S.; Han, B. Z.; Yue, W.; Yan, H. *Journal of Materials Chemistry* **2007**, *17*, 3812-3818.

(55) Xu, C. J.; Xu, K. M.; Gu, H. W.; Zhong, X. F.; Guo, Z. H.; Zheng, R. K.; Zhang, X. X.; Xu, B. *Journal of the American Chemical Society* **2004**, *126*, 3392-3393.

(56) Huang, J. S.; Li, X. T.; Zheng, Y. H.; Zhang, Y.; Zhao, R. Y.; Gao, X. C.; Yan, H. S. *Macromolecular Bioscience* **2008**, *8*, 508-515.

(57) Cai, C. F.; Bakowsky, U.; Rytting, E.; Schaper, A. K.; Kissel, T. *European Journal of Pharmaceutics and Biopharmaceutics* **2008**, *69*, 31-42.

(58) Savina, I. N.; Galaev, I. Y.; Mattiasson, B. *Journal of Molecular Recognition* **2006**, *19*, 313-321.

(59) Tsujii, Y.; Ohno, K.; Yamamoto, S.; Goto, A.; Fukuda, T. *Advances in Polymer Science* **2006**, *197*, 1-45.

(60) Yoshikawa, C.; Goto, A.; Tsujii, Y.; Ishizuka, N.; Nakanishi, K.; Fukuda, T. *Journal of Polymer Science Part a-Polymer Chemistry* **2007**, *45*, 4795-4803.

(61) Kanazawa, H.; Matsushima, Y.; Okano, T. *Temperature-responsive chromatography*; Marcel Dekker: New York, 2001; Vol. 41, pp 311-336.

(62) Kikuchi, A.; Okano, T. *Progress in Polymer Science* **2002**, *27*, 1165-1193.

(63) Kobayashi, J.; Kikuchi, A.; Sakai, K.; Okano, T. *Analytical Chemistry* **2003**, *75*, 3244-3249.

(64) Huang, X. Y.; Doneski, L. J.; Wirth, M. J. *Analytical Chemistry* **1998**, *70*, 4023-4029.

(65) Phizicky, E.; Bastiaens, P. I. H.; Zhu, H.; Snyder, M.; Fields, S. *Nature* **2003**, *422*, 208-215.

(66) Kusnezow, W.; Jacob, A.; Walijew, A.; Diehl, F.; Hoheisel, J. D. *Proteomics* **2003**, *3*, 254-264.

(67) Iwata, R.; Satoh, R.; Iwasaki, Y.; Akiyoshi, K. *Colloids and Surfaces B-Biointerfaces* **2008**, *62*, 288-298.

(68) Pirri, G.; Chiari, M.; Damin, F.; Meo, A. *Analytical Chemistry* **2006**, *78*, 3118-3124.

(69) Tugulu, S.; Arnold, A.; Sielaff, I.; Johnsson, K.; Klok, H. A. *Biomacromolecules* **2005**, *6*, 1602-1607.

(70) Wang, A. J.; Xu, J. J.; Chen, H. Y. *Journal of Chromatography A* **2007**, *1147*, 120-126.

(71) Dong, R.; Krishnan, S.; Baird, B. A.; Lindau, M.; Ober, C. K. *Biomacromolecules* **2007**, *8*, 3082-3092.

(72) Chen, S. F.; Liu, L. Y.; Zhou, J.; Jiang, S. Y. *Langmuir* **2003**, *19*, 2859-2864.

(73) Peluso, P.; Wilson, D. S.; Do, D.; Tran, H.; Venkatasubbaiah, M.; Quincy, D.; Heidecker, B.; Poindexter, K.; Tolani, N.; Phelan, M.; Witte, K.; Jung, L. S.; Wagner, P.; Nock, S. *Analytical Biochemistry* **2003**, *312*, 113-124.

(74) Iwasaki, Y.; Omichi, Y.; Iwata, R. *Langmuir* **2008**, *24*.

(75) Bastida, A.; Sabuquillo, P.; Armisen, P.; Fernandez-Lafuente, R.; Huguet, J.; Guisan, J. M. *Biotechnology and Bioengineering* **1998**, *58*, 486-493.

(76) Saxena, R. K.; Ghosh, P. K.; Gupta, R.; Davidson, W. S.; Bradoo, S.; Gulati, R. *Current Science* **1999**, *77*, 101-115.

(77) Fadnavis, N. W.; Deshpande, A. *Current Organic Chemistry* **2002**, *6*, 393-410.

(78) Schilke, K. F.; Kelly, C. *Biotechnology and Bioengineering* **2008**, *101*, 9-18.

(79) Kobayashi, S.; Yonezu, S. J.; Kawakita, H.; Saito, K.; Sugita, K.; Tamada, M.; Sugo, T.; Lee, W. *Biotechnology Progress* **2003**, *19*, 396-399.

(80) Goto, M.; Kawakita, H.; Uezu, K.; Tsuneda, S.; Saito, K.; Goto, M.; Tamada, M.; Sugo, T. *Journal of the American Oil Chemists' Society* **2006**, *83*, 209-213.

(81) Goto, M.; Okubo, T.; Kawakita, H.; Uezu, K.; Tsuneda, S.; Saito, K.; Goto, M.; Tamada, M.; Sugo, T. *Biochemical Engineering Journal* **2007**, *37*, 159-165.

(82) Dunn, J. D.; Reid, G. E.; Bruening, M. L. *Mass Spectrometry Reviews* **(in press)**.

(83) Dunn, J. D.; Igrisan, E. A.; Palumbo, A. M.; Reid, G. E.; Bruening, M. L. *Analytical Chemistry* **2008**, *80*, 5727-5735.

(84) Schleimer, M.; Pirkle, W. H.; Schurig, V. *Journal of Chromatography A* **1994**, *679*, 23-34.

(85) Idota, N.; Kikuchi, A.; Kobayashi, J.; Akiyama, Y.; Okano, T. *Langmuir* **2006**, *22*, 425-430.

(86) Miller, M. D.; Baker, G. L.; Bruening, M. L. *Journal of Chromatography A* **2004**, *1044*, 323-330.

(87) Zou, H. F.; Ye, M. L. *Electrophoresis* **2000**, *21*, 4073-4095.

(88) Groll, J.; Haubensak, W.; Ameringer, T.; Moeller, M. *Langmuir* **2005**, *21*, 3076-3083.

(89) Jain, P.; Sun, L.; Dai, J. H.; Baker, G. L.; Bruening, M. L. *Biomacromolecules* **2007**, *8*, 3102-3107.

(90) Groll, J.; Amirgoulova, E. V.; Ameringer, T.; Heyes, C. D.; Röcker, C.; Nienhaus, G. U.; Möller, M. *Journal of the American Chemical Society* **2004**, *126*, 4234-4239.

(91) Draveling, C.; Ren, L.; Haney, P.; Zeisse, D.; Qoronfleh, M. W. *Protein Expression and Purification* **2001**, *22*, 359-366.

(92) Boi, C.; Cattoli, F.; Facchini, R.; Sorci, M.; Sarti, G. C. *Journal of Membrane Science* **2006**, *273*, 12-19.

(93) Zou, H. F.; Luo, Q. Z.; Zhou, D. M. *Journal of Biochemical and Biophysical Methods* **2001**, *49*, 199-240.

(94) Che, S.; Liu, Z.; Ohsuna, T.; Sakamoto, K.; Terasaki, O.; Tatsumi, T. *Nature* **2004**, *429*, 281-284.

(95) Brandt, S.; Goffe, R. A.; Kessler, S. B.; Oconnor, J. L.; Zale, S. E. *Bio-Technology* **1988**, *6*, 779-782.

(96) Kawai, T.; Saito, K.; Lee, W. *Journal of Chromatography B-Analytical Technologies in the Biomedical and Life Sciences* **2003**, *790*, 131-142.

(97) Endres, H. N.; Johnson, J. A. C.; Ross, C. A.; Welp, J. K.; Etzel, M. R. *Biotechnology and Applied Biochemistry* **2003**, *37*, 259-266.

(98) Singh, N.; Husson, S. M.; Zdyrko, B.; Luzinov, I. *Journal of Membrane Science* **2005**, *262*, 81-90.

(99) Kawakita, H.; Masunaga, H.; Nomura, K.; Uezu, K.; Akiba, I.; Tsuneda, S. *Journal of Porous Materials* **2007**, *14*, 387-391.

(100) Castilho, L. R.; Deckwer, W. D.; Anspach, F. B. *Journal of Membrane Science* **2000**, *172*, 269-277.

(101) Singh, N.; Wang, J.; Ulbricht, M.; Wickramasinghe, S. R.; Husson, S. M. *Journal of Membrane Science* **2008**, *309*, 64-72.

(102) Kubota, N.; Kounosu, M.; Saito, K.; Sugita, K.; Watanabe, K.; Sugo, T. *Biotechnology Progress* **1997**, *13*, 89-95.

(103) Kumar, V.; Bhardwaj, Y. K.; Jamdar, S. N.; Goel, N. K.; Sabharwal, S. *Journal of Applied Polymer Science* **2006**, *102*, 5512-5521.

(104) Iwanade, A.; Umeno, D.; Saito, K.; Sugo, T. *Biotechnology Progress* **2007**, *23*, 1425-1430.

(105) Sasagawa, N.; Saito, K.; Sugita, K.; Kunori, S.; Sugo, T. *Journal of Chromatography A* **1999**, *848*, 161-168.

This chapter is adapted from our published work in Biomacromolecules (Jain, P.; Sun, L.; Dai, J.; Baker, G. L.; Bruening, M. L., *Biomacromolecules* **2007,** *8*, 3102-3107).

Some of the research was done with Dr. Lei Sun.

Chapter 2

High-capacity purification of His-tagged proteins by alumina membranes containing functionalized poly(HEMA) brushes

2.1. Introduction

The expansion of recombinant protein expression has generated a great need for rapid and convenient methods of protein purification.[1,2] Typical purifications involve a series of steps, the most important of which frequently rely on affinity binding. Affinity methods are based on specific interactions between immobilized ligands and an affinity tag (e.g., polyhistidine,[3] glutathione-S-transferrase,[4] streptavidin,[5] or maltose binding protein[6]) that is appended to the protein of interest. Proteins containing an affinity tag are selectively bound to the chromatographic matrix, while other cellular proteins are washed away.[7]

Affinity purification has several assests such as ligand stability, high protein loading, mild elution conditions, simple regeneration and low cost.[8] However, this technique often presents a bottleneck in the purification process because of slow diffusion of proteins into the pores of chromatographic gels, which leads to long separation times. Difficulties in packing large columns and relatively high pressure drops, are also drawbacks to column-based affinity separations.[9-11] These limitations will be particularly important for large-scale separations. (The use of commercially available Gravity-flow and Spin-trap columns allows some reduction in purification times for small-scale separations[12]).

Protein-absorbing membranes[13] can overcome diffusional limitations in protein separations because convective flow through membrane pores provides rapid mass transport to binding sites.[14-18] Moreover, scale-up of membrane separations simply involves increasing membrane area, which should avoid the challenges of packing large columns and provide low pressure drops. Unfortunately, however, the low internal surface area of membrane absorbers (when compared to porous beads) yields a relatively low binding capacity. To overcome this problem, membranes are modified with polymer brushes that have multiple protein-binding sites.[19-25]

We aim to develop affinity membranes for high-capacity protein binding as well as rapid and selective purification of His-tagged proteins **(Figure 2.1.)**. Previously, Sun *et al.* demonstrated that growth of poly(HEMA) from initiators bound to a porous alumina membrane and subsequent functionalization of the poly(HEMA) with NTA-Cu^{2+} complexes yields a remarkable binding capacity of more than 100 mg BSA/cm^3 of membrane.[23] The high binding capacity is due to the strong interaction of NTA-Cu^{2+} complex with histidine residue on proteins. However, since many proteins have exposed histidine residues, NTA-Cu^{2+} complexes are non-selective and thus not suitable for protein purification. The NTA-Ni^{2+} complex, on the other hand, is highly selective for His-tagged proteins due to the relatively weak interaction of NTA-Ni^{2+} with histidine groups, thereby requiring a polyhistidine tag for efficient binding.[3,26]

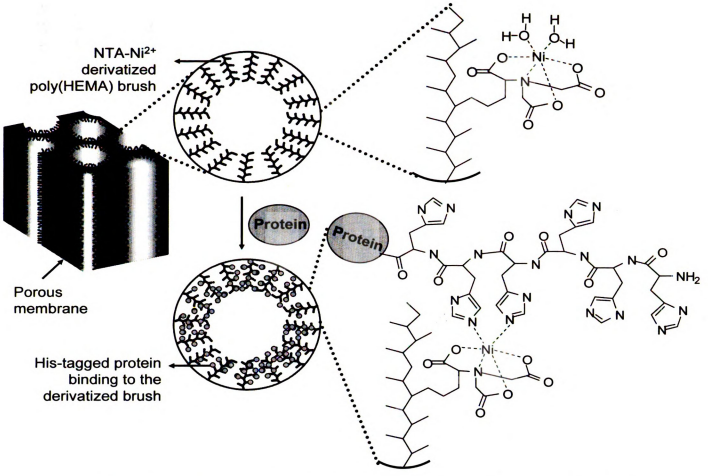

Figure 2.1. Binding of His-tagged protein to a NTA-Ni^{2+} derivatized poly(HEMA) brush inside a membrane pore.

This chapter shows that the use of alumina membranes modified with poly(HEMA)-NTA-Ni^{2+} brushes allows rapid and highly selective purification of His-tagged proteins. Gel electrophoresis reveals that the purity of His-tagged ubiquitin (HisU) eluted from these membranes is greater than 99%, even when the initial solution contains 10% bovine serum or a 20-fold excess of BSA. The binding capacity of the membrane is as high as 120 mg HisU/cm^3 of membrane, which is at least 5-fold greater than that for membranes reported in the literature.[23,24,27] Moreover, separations can be completely performed in 30 min or less and membranes are fully reusable.

2.2. Experimental section

2.2.1. Materials

Anodisc™ porous alumina membranes with 0.2 μm-diameter surface pores were obtained from Fisher Scientific. Dimethylformamide (DMF, anhydrous, 99.8%), 11-mercaptoundecanol (97%), 2-bromoisobutyryl bromide (98%), CuCl (99.999%), $CuBr_2$ (99%), 2,2'-bipyridyl (bpy, 99%), EDC, NHS, 4-dimethylaminopyridine (DMAP), ethylenediamine tetraacetic acid (EDTA), imidazole (99%), TWEEN-20 surfactant, BSA, lysozyme, ubiquitin, N-terminal histidine$_6$ tagged ubiquitin (HisU), and myoglobin were used as received from Sigma Aldrich. Fetal bovine serum was obtained from HyClone. $NiSO_4 \cdot 5H_2O$ (Columbus Chemical), NaH_2PO_4 (CCI), Na_2HPO_4 (Aldrich), N_α, N_α–*bis*(carboxymethyl)-L-lysine hydrate (Fluka, aminobutyl NTA), succinic anhydride (Matheson Coleman & Bell), and Coomassie protein assay reagent (Pierce) were also used without purification. HEMA (Aldrich, 97%, inhibited with 300 ppm hydroquinone monomethyl ether) was purified by passing it through a column of activated basic alumina (Aldrich), and trichlorosilane initiator (11-(2-bromo-2-

methyl)propionyloxy)undecyltrichlorosilane) was synthesized according to a literature procedure.[28] Buffers were prepared using analytical grade chemicals and deionized (Milli-Q, 18.2 MΩ cm) water.

2.2.2. Polymerization of HEMA in porous alumina membranes

The procedure for polymerizing HEMA inside alumina membranes was reported previously.[23] Briefly, the alumina membrane was sandwiched inside a membrane cell (Millipore, Swinnex 25), and a solution of the trichlorosilane initiator, (11-(2-bromo-2-methyl)propionyloxy)undecyltrichlorosilane, was passed through the membrane followed by subsequent rinsing. Polymerization of HEMA from the immobilized initiator occurred by circulating a degassed solution containing 15 mL of purified HEMA, 15 mL methanol, 82.5 mg (0.825 mmol) of CuCl, 54 mg (0.24 mmol) of $CuBr_2$, and 320 mg (2.04 mmol) of bpy through the initiator-modified membrane for 1 hour. (The use of a mixed halide system sometimes provides better control over polymerization[29,30]). After polymerization, the membrane was cleaned with flowing ethanol (20 mL), deionized water (Milli-Q, 18.2 MΩ cm, 20 mL), and acetone (20 mL).

2.2.3. Polymerization of HEMA on Au substrates

Au-coated silicon wafers were coated with a mercaptoundecanol monolayer that was subsequently allowed to react with 2-bromoisobutyryl bromide as described previously.[30,31] Polymerization of HEMA from these substrates occurred as described in section 2.2.2. except that the substrate was simply immersed in a polymerization solution that was kept in a glove bag, and water was used instead of methanol to give thicker films.[31]

2.2.4. Poly(HEMA) derivatization and protein immobilization

The derivatization procedure was also described previously and is shown in **Scheme 2.1.**[23] However, in the present case the aminobutyl NTA derivatized membrane was exposed to a 0.1 M $NiSO_4$, rather than 0.1 M $CuSO_4$ solution and rinsed with buffer (20 mM phosphate buffer, pH 7.2). After loading of membranes with Ni^{2+}, a solution containing pure protein or a mixture of proteins (in 20 mM phosphate buffer, pH 7.2) was then pumped through the membrane using a peristaltic pump, and the permeate was collected for analysis at specific time intervals. Subsequently, the membrane was rinsed with 20 mL pH 7.2 washing buffer (20 mM phosphate buffer containing 0.1% Tween-20 surfactant and 0.15 M NaCl) and 20 mL phosphate buffer, and protein was then eluted using 5-10 mL of a solution containing 20 mM sodium phosphate, 0.5 M NaCl, and 0.5 M imidazole at pH 7.4. Ni^{2+} was later eluted using a 50 mM EDTA solution (pH 7.2), and the poly(HEMA)-NTA film was recharged with Ni^{2+} prior to reuse.

To prepare derivatized films for reflectance Fourier transform infrared (FTIR) characterization, a poly(HEMA) film on a gold substrate was treated in a similar procedure by immersing the substrate in appropriate solutions and rinsing with solutions (20 mL each) from a pipette.

2.2.5. Film characterization methods

FTIR spectra of films on gold-coated wafers were obtained with a Nicolet Magna-IR 560 spectrometer containing a PIKE grazing angle (80°) accessory, and film thicknesses were measured using a rotating analyzer ellipsometer (model M-44; J.A. Woollam) at an incident angle of 75°, assuming a film refractive index of 1.5. Ellipsometric measurements were performed on at least three spots on a film. A UV/ozone-cleaned gold-coated wafer was used as a background for reflectance FTIR

spectra. Film growth inside alumina membranes was verified using transmission FTIR spectroscopy (Mattson Galaxy Series 3000) with an air background.

2.2.6. Determination of the amount of coordinated Ni^{2+} in the membrane

A calibration curve was determined by measuring the absorbance of $NiSO_4$ standard solutions in 50 mM EDTA (pH 7.2) using a Varian Spectra AA-200 atomic absorption spectrophotometer, and a sample solution was obtained by eluting Ni^{2+} from a poly(HEMA)-NTA-Ni^{2+}-coated membrane with 5.0 mL of 50 mM EDTA (pH 7.2). The amount of Ni^{2+} in the stripping solution was calculated from its absorbance using the calibration curve.

2.2.7. Protein quantification

To determine the concentration of protein bound to poly(HEMA)brushes in a membrane, 50 μL of eluent was added to 2.95 mL of a solution of Coomassie reagent, and the mixture was shaken a few times and allowed to react for 5 min at room temperature. The UV/vis absorbance spectra of these solutions were then obtained with a Perkin-Elmer UV/Vis (model Lambda 40) spectrophotometer. Calibration curves for the absorbance of BSA, HisU and myoglobin solutions at 595 nm were prepared using a series of protein solutions (concentration range of 100 μg to 1 mg of protein per mL) that were mixed with Coomassie reagent. All spectra were measured against a Coomassie reagent background.

To quantify the amount of protein bound to poly(HEMA) brushes on gold-coated Si, the method reported previously by Dai and coworkers was employed.[19] Briefly, a calibration curve was obtained by plotting the ellipsometric thickness of spin-coated

BSA, myoglobin, lysozyme, or ubiquitin films against the reflectance FTIR absorbance of their amide I band.

2.2.8. Determination of protein purity by sodium dodecyl sulfate-polyacrylamide gel electrophoresis (SDS-PAGE)

The protein solutions were analyzed by SDS-PAGE with a 16% cross-linked separating gel and a 4% cross-linked stacking gel (acrylamide). Protein bands were visualized using a standard silver staining procedure.[10]

2.3. Results and discussion

2.3.1. Characterization of poly(HEMA)-derivatized membranes

To form brush-modified membranes, poly(HEMA) was first grown from ATRP initiators that were immobilized within porous alumina via silanization.[23] The brushes were derivatized as shown in **Scheme 2.1.**, with reactant solutions being flowed through the membrane using a peristaltic pump.

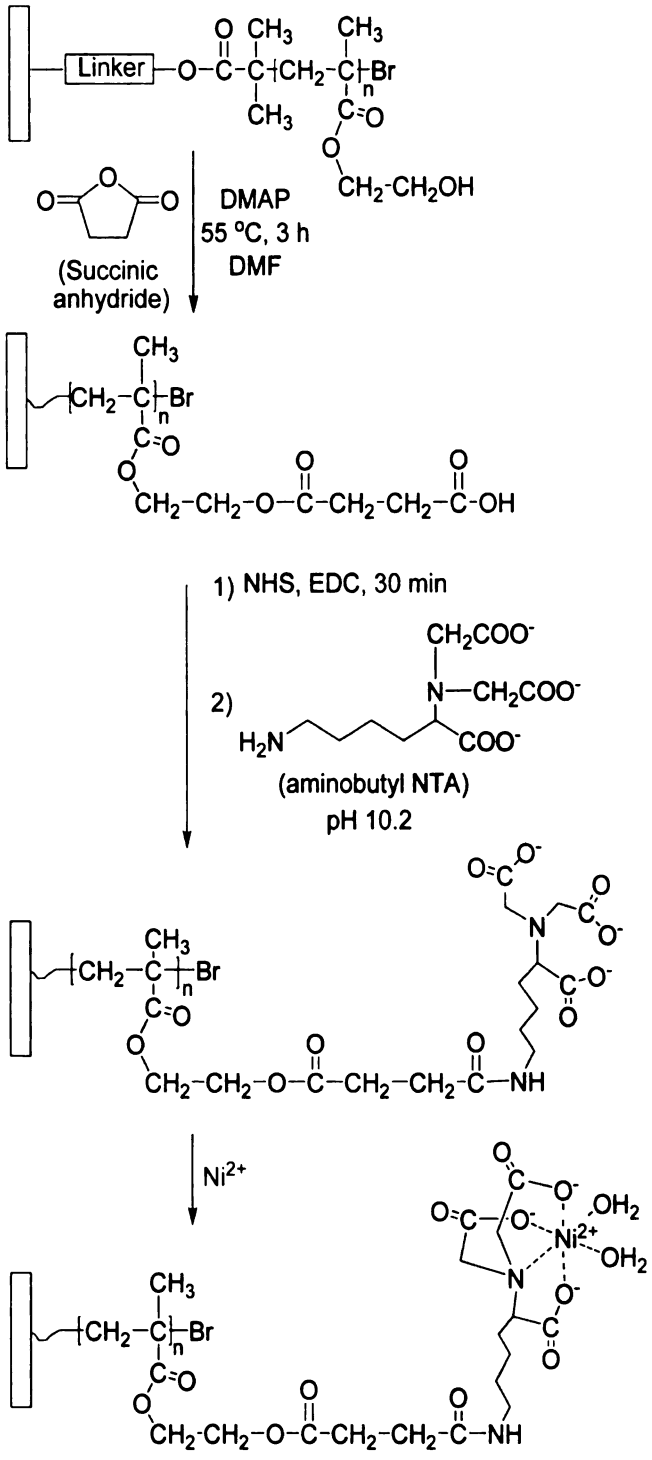

Scheme 2.1. Derivatization of poly(HEMA) with NTA-Ni^{2+} prior to protein adsorption.

Transmission IR spectra of membranes **(Figure 2.2.)** after polymerization and each derivatization step provide evidence for formation of poly(HEMA), subsequent reaction with succinic anhydride (SA) and finally, successful linking of aminobutyl NTA to these

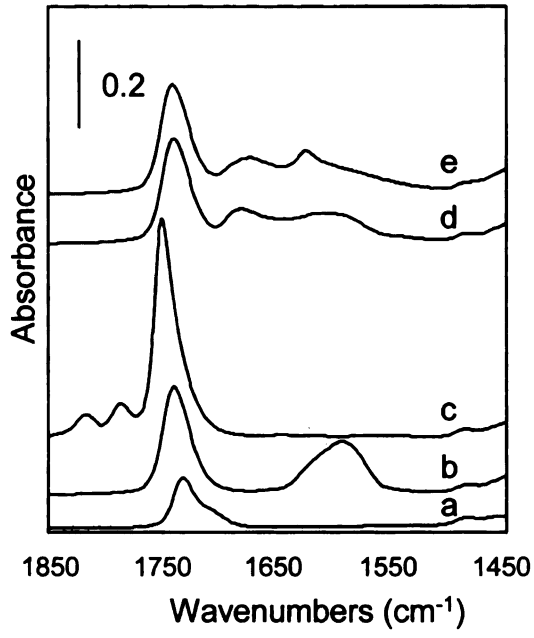

Figure 2.2. Transmission FTIR spectra of an alumina membrane modified with poly(HEMA) brushes before **(a)** and after the following sequential steps: **(b)** reaction with succinic anhydride, **(c)** activation with EDC/NHS, **(d)** reaction with aminobutyl NTA, and **(e)** exposure to 0.1 M $NiSO_4$.

polymer brushes. These transmission IR spectra are consistent with previous spectra of poly(HEMA) films grown on Au-coated Si.[23] To prepare poly(HEMA)-NTA-Ni^{2+} films in porous alumina, we first passed a solution of succinic anhydride in DMF through a poly(HEMA)-derivatized membrane to create free –COOH groups in the film. We then immersed the membrane in pH 9.9 buffer for 15 min and rinsed with ethanol and acetone before taking a transmission IR spectrum. The peak at ~1740 cm^{-1} doubled in intensity

after reaction with succinic anhydride due to ester formation **[Figure 2.2., spectrum b]**, suggesting that a large fraction of the –OH groups of poly(HEMA) reacted with succinic anhydride. The smaller peak at ~1594 cm^{-1} in **spectrum (b)** most likely results from newly formed carboxylic acid groups that are deprotonated.

Passing a 0.1 M mixture of EDC and NHS in water (pH~4.9) through the membrane converted –COOH groups to succinimidyl esters. Peaks due to the succinimide ester appeared at 1817 and 1786 cm^{-1} **[Figure 2.2., spectrum c].**[32] The asymmetric succinimide stretch at ~1753 cm^{-1} overlaps with the carbonyl band (1740 cm^{-1}) of the previously formed esters, resulting in a broad peak with a height that is about double that for the ester carbonyls present after reaction with succinic anhydride only.

Subsequently, the EDC/NHS-activated poly(HEMA) was allowed to react with aminobutyl-NTA. After this reaction, the membrane was immersed in pH 9.9 buffer for 15 min and rinsed with ethanol and acetone. This reaction resulted in a loss of the absorbance due to the active ester, and a shifting of the peak at 1753 cm^{-1} back to 1740 cm^{-1} **[Figure 2.2., spectrum d]**. The new absorbance at 1680 cm^{-1} suggests NTA immobilization, as it likely results from a combination of absorbance due to the carboxylate groups of NTA and amide bonds formed between succinic anhydride and NTA. The broad peak around 1600 cm^{-1} could be due to carboxylate groups from either NTA or hydrolyzed active esters.

Immersion of membranes modified with NTA-derivatized poly(HEMA) in 0.1 M $NiSO_4$ and subsequent rinsing with water gave immobilized NTA-Ni^{2+} that should selectively bind His-tagged proteins. However, there was no dramatic change in the IR spectrum **[Figure 2.2., spectrum e]** of membranes after Ni^{2+} complexation, but the peak

at 1600 cm^{-1} seems to move to around 1630 cm^{-1} and sharpen. This spectral change could occur because **spectrum (d)** was obtained after immersion in pH 9.9 buffer, while the membrane represented in **spectrum (e)** was not immersed in this buffer to avoid precipitation of $Ni(OH)_2$, which may occur at high pH. XPS data for a poly(HEMA)-NTA-Ni^{2+} film on a gold substrate confirmed the presence of Ni^{2+} in these films and showed a Ni:N ratio of 0.5 : 1, which is consistent with our previous results and indicative of one Ni^{2+} per NTA moiety.[19,23] We also determined the amount of Ni^{2+} in the membrane by passing 5 mL of 50 mM EDTA through a modified membrane and subsequently analyzing the EDTA solution for Ni^{2+} using atomic absorption spectroscopy. This procedure revealed that 14±1 μmol Ni^{2+} was present in a 2 cm-diameter, 60 μm-thick modified membrane. Assuming that every NTA moiety bound a Ni^{2+} ion, and that each hydroxyl group of poly(HEMA) was derivatized with one NTA moiety, these results suggest that prior to derivatization the poly(HEMA) consisted of 12 nm-thick annuli inside the 230 nm-diameter pores in the alumina. (This calculation also assumes a poly(HEMA) density of 1 g/cm^3 and a membrane porosity of 50%).

2.3.2. HisU binding to poly(HEMA)-NTA-Ni^{2+} brushes on gold-coated silicon substrates

We first examined absorption of His-tagged proteins in films formed on Au-coated Si to allow characterization of binding using ellipsometry and reflectance FTIR spectroscopy. These films were grown from monolayers of initiator as reported previously.[33] In initial studies, absorption of HisU occurred during a 2 h immersion of the poly(HEMA)-NTA-Ni^{2+}-modified gold substrate in a stirred solution containing 0.01 mg/mL HisU in pH 7.2 phosphate buffer. The film was then rinsed with 20 mL washing

buffer (20 mM phosphate buffer containing 0.1% Tween-20 surfactant and 0.15 M NaCl), immersed in phosphate buffer (pH 7.2) for 15 min, and finally rinsed with ethanol. To examine whether protein binds to poly(HEMA)-NTA-Ni^{2+}, the reflectance FTIR spectrum of the film prior to protein exposure was subtracted from the corresponding spectrum measured after protein exposure and rinsing. The subtracted spectra of films immersed in 0.01 mg/mL HisU show strong amide I (1680 cm^{-1}) and amide II (1545 cm^{-1}) bands **(Figure 2.3., spectrum a)**, indicative of extensive protein binding. (The small

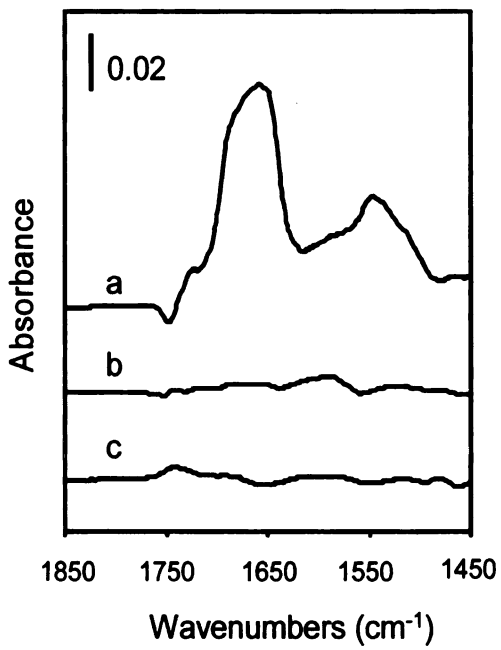

Figure 2.3. Subtracted reflectance FTIR spectra of protein immobilized on poly(HEMA)-NTA-Ni^{2+} brushes after exposure of the films to **(a)** 0.01 mg/mL HisU or **(b)** 0.1 mg/mL BSA or **(c)** 0.1 mg/mL ubiquitin. The spectra were obtained by subtracting the spectrum of poly(HEMA)-NTA-Ni^{2+} from that of poly(HEMA)-NTA-Ni^{2+}-protein (both films were rinsed with buffer and ethanol prior to the measurement).

negative peak at 1740 cm^{-1} likely result from deprotonation of some —COOH groups.) In contrast to HisU, the subtracted spectrum of a poly(HEMA)-NTA-Ni^{2+} coating exposed to 0.1 mg/mL BSA for 6 h **(Figure 2.3., spectrum b)** shows no amide absorbances, even though the concentration of BSA in the exposure solution was 10-fold more than the concentration used for HisU. To further demonstrate that histidine tags are crucial for binding to poly(HEMA)-NTA-Ni^{2+} brushes, we immersed a film in a 0.1 mg/mL ubiquitin solution in phosphate buffer (pH 7.2) and stirred the solution for 6 h. No ubiquitin binding was detected **(Figure 2.3., spectrum c)**. Thus, these films exhibit no detectable non-specific adsorption and should maintain the high selectivities that are available through adsorption of His-tagged proteins to NTA-Ni^{2+} complexes.

Previously, Dai *et al.* correlated the subtracted-spectrum amide absorbance of BSA with the amount of BSA bound to poly(HEMA)-NTA-Cu^{2+} films using calibration curves of ellipsometric thickness versus amide absorbance for films of pure, spin-coated BSA.[19] However, obtaining a calibration curve by spin-coating of HisU is not practical due to the high cost of this protein. To overcome this challenge, we showed that calibration curves of thickness versus amide I absorbance are essentially independent of the protein employed to obtain the curve **(Figure 2.4.)**. The slopes of calibration curves for BSA, myoglobin, lysozyme, and ubiquitin absorption were all 0.0017 absorbance units/nm protein. The uniformity of slopes is reasonable, as the extinction coefficient for the amide absorbance should be similar for all proteins. Given the value of 0.0017 absorbance units/nm, **spectrum (a)** in **Figure 2.3.** suggests that the poly(HEMA)-NTA-Ni^{2+} film absorbed 31 nm of HisU. This corresponds to binding of 3.1 μg HisU/cm^2 or

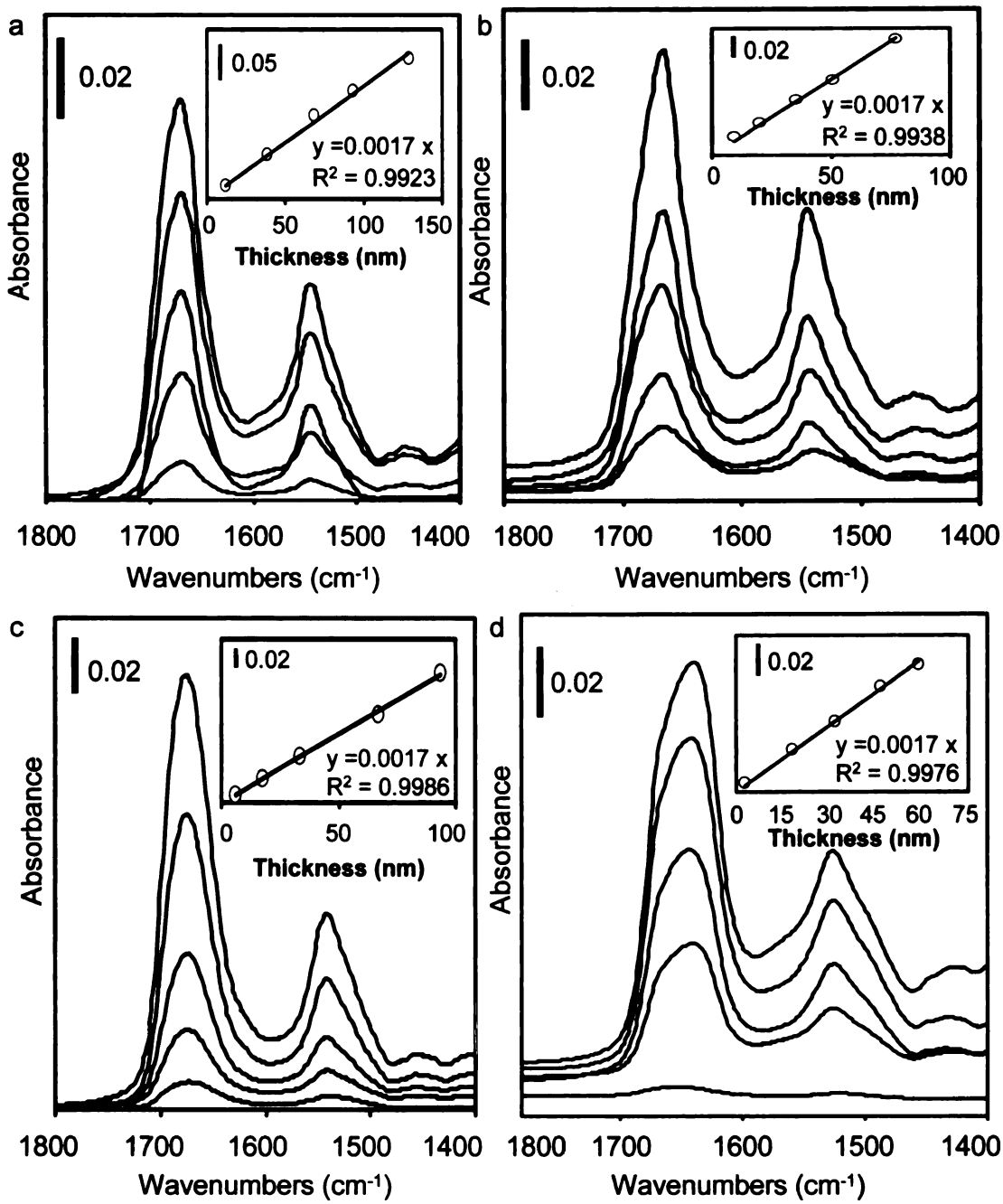

Figure 2.4. Reflectance FTIR spectra of spin-coated **(a)** BSA, **(b)** myoglobin, **(c)** lysozyme, and **(d)** ubiquitin films on Au. Films of different thicknesses were prepared using aqueous solutions containing from 0.1 to 10 mg/mL protein solution. The insets in the figures show the correlation between film ellipsometric thickness and amide I absorbance (1680 cm^{-1}).

about 10 monolayers of HisU (assuming a HisU density of 1 g/cm^3 and a monolayer thickness of 2.9 nm[34]).

Figure 2.5. shows how the amount of HisU bound to poly(HEMA)-NTA-Ni^{2+} films on Au varies as a function of **(a)** concentration and **(b)** time. (Data were obtained using a combination of reflectance FTIR spectroscopy and calibration curves of thickness versus amide absorbance as described above.) **Figure 2.5.(a)** reveals that significant HisU binding occurs at concentrations as low as 0.001 mg/mL, and that saturation of the film is approached when HisU concentrations reach 0.04 mg/mL. The data in **Figure 2.5.(b)** demonstrate ~90% film saturation in 20 min when using a 0.05 mg/mL HisU solution. The maximum binding capacity of these 51 nm-thick (before derivatization) films was 40 nm of HisU or about 13 monolayers. Capacity increases with film thickness **(Figure 2.6.)** but eventually plateaus when poly(HEMA) thickness reaches 115 nm. The highest binding capacity obtained was 70 nm of HisU or the equivalent of about 23 monolayers.

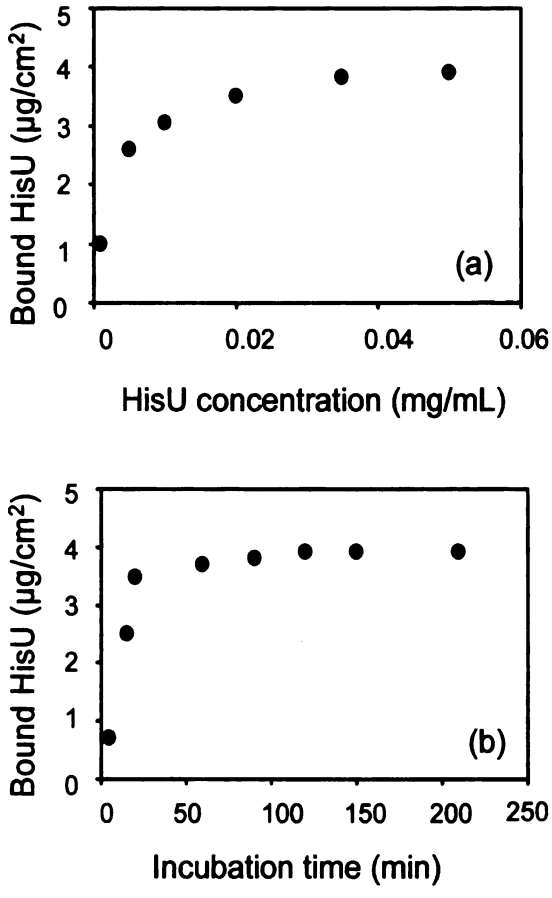

Figure 2.5. Amount of HisU bound to poly(HEMA)-NTA-Ni^{2+} films as a function of (**a**) concentration and (**b**) time. To obtain the data in (**a**), a 51 nm-thick (prior to derivatization) poly(HEMA) film was used, and the binding capacity was determined after 2 h. The same poly(HEMA)-NTA film was used throughout the experiment, with protein elution and reloading of Ni^{2+} after measurements at each concentration. For (**b**), 0.05 mg/mL HisU and a single 51 nm poly(HEMA) film were used. To test the reproducibility of the experiments, binding on a 51 nm film with a protein concentration of 0.01 mg/mL was repeated three times and found to be 3.01± 0.05 $\mu g/cm^2$.

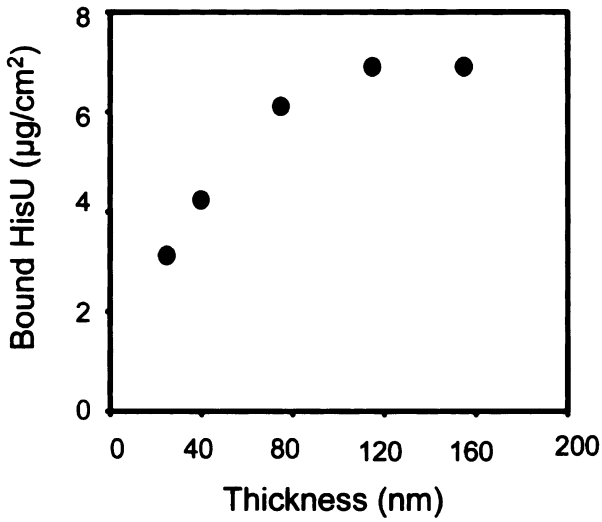

Figure 2.6. HisU binding capacity versus thickness of poly(HEMA) films that were subsequently derivatized with NTA-Ni^{2+}. The concentration of HisU in solution was 0.05 mg/mL. The binding on a 40 nm film was repeated using 3 different films and different protein samples. The binding capacity obtained was 4.3±0.1 μg/cm^2.

2.3.3. HisU binding to poly(HEMA)-NTA-Ni^{2+} brushes in membranes

To test the HisU binding capacity of poly(HEMA)-NTA-Ni^{2+} brushes in membranes, we pumped a solution of 0.3 mg/mL HisU in pH 7.2 phosphate buffer through the membrane, collected the permeate over specific time intervals, and analyzed these samples using a Bradford assay. **Figure 2.7.** shows the breakthrough curve for HisU binding to poly(HEMA)-NTA-Ni^{2+} brushes along with similar curves for BSA and myoglobin binding to poly(HEMA)–NTA-Cu^{2+}-modified membranes. (Poly(HEMA)-NTA-Ni^{2+} brushes do not bind a significant amount of BSA and myoglobin as shown below.) Integration of the differences between the feed concentrations and the permeate concentrations shown in the breakthrough curves gives binding capacities of 110 and 83 mg/cm^3, respectively, for binding of BSA and myoglobin to poly(HEMA)-NTA-Cu^{2+}-

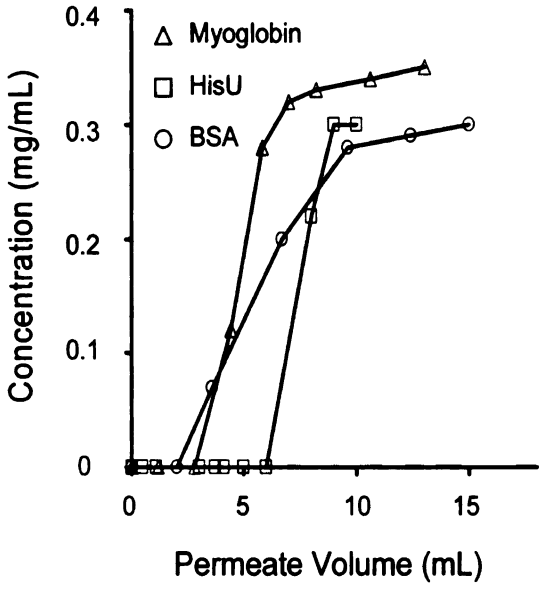

Figure 2.7. Breakthrough curves for absorption of 0.3 mg/mL HisU, 0.3 mg/mL BSA, and 0.35 mg/mL myoglobin in membranes modified with poly(HEMA)-NTA-Ni^{2+} (HisU) or poly(HEMA)-NTA-Cu^{2+} (BSA and myoglobin). The permeate flow rate was initially 2.4 mL/min and 0.9 mL/min at the end of the experiment. Solid lines are added to guide the eyes.

modified membranes, and 120 mg/cm^3 for HisU binding to a poly(HEMA)-NTA-Ni^{2+}-modified membrane. However, the breakthrough curves of HisU and myoglobin are slightly sharper than that for BSA. (Flow rate measurements at a constant pressure showed that flow rates are similar for all three proteins for a given permeate volume). The very sharp breakthrough curve for HisU may stem from its high affinity for the NTA-Ni^{2+} or its low molecular mass (10.7 kDa) relative to myoglobin (17 kDa) and BSA (67.5 kDa). A low molecular mass could allow rapid diffusion of smaller proteins into the polymer brushes, but future studies with several different His-tagged proteins are needed to determine if this is the case.

The linear flow velocity through the membrane is on average about 21 cm/h. This is about an order magnitude less than the flow rate through typical gel columns,[35-38] but the capacity of the membranes per cm^3 is also an order of magnitude greater than that of gels.[35-38] Still, linear velocities need to increase to make the membranes a more competitive technology, and this can be accomplished by increasing pore size (at a constant porosity, flow rate is proportional to the square of pore radius for assemblies of parallel pores).

After measuring the breakthrough curve of HisU, the poly(HEMA)-NTA-Ni^{2+}-HisU membrane was washed with 20 mL washing buffer followed by 20 mL phosphate buffer, and HisU was eluted with 5-10 mL elution buffer containing 0.5 M imidazole. Analysis of the eluent using a Bradford assay and comparison of this analysis with the capacity determined from the breakthrough curve showed that 99±1% of the bound HisU was recovered.

To prove that poly(HEMA)-NTA-Ni^{2+}-modified membranes selectively bind HisU, we also investigated the binding of BSA and myoglobin to poly(HEMA)-NTA-Ni^{2+} films in alumina. A poly(HEMA)-NTA-Ni^{2+}-derivatized membrane was loaded with 10 mL of 0.3 mg/mL BSA or 10 mL of 0.3 mg/mL myoglobin in buffer, rinsed with washing buffer, and treated with eluent. BSA was not detected in the imidazole eluent (<0.001 mg/cm^3), while a small amount (0.05 mg/cm^3) of myoglobin binding was observed. However, the amount of myoglobin bound was only 3% of the amount of HisU bound when using 0.3 mg/mL HisU. (Eleven of the 153 residues of myoglobin are histidine, which could enhance the undesired adsorption of this protein to NTA-Ni^{2+}).

2.3.4. Separation of protein mixtures using poly(HEMA)-NTA-Ni^{2+} brushes on Au substrates

We first tested the ability of Au-poly(HEMA)-NTA-Ni^{2+} films to purify His tagged proteins due to ease in handling and characterization. In an initial experiment, a gold substrate modified with poly(HEMA)-NTA-Ni^{2+} was immersed in 10 mL of phosphate buffer containing BSA, myoglobin and HisU (0.05 mg/mL each), and the solution was stirred for 2 h. The film was then rinsed with 20 mL washing buffer followed by 20 mL phosphate buffer, followed by ethanol and dried under a stream of nitrogen. Finally, we immersed the film in 1 mL elution buffer (20 mM phosphate buffer, 0.5 M NaCl, and 0.5 M imidazole, pH 7.2) for 30 min to recover the bound protein and then analyzed this eluent by electrophoresis. The gel electropherogram of the eluent (**Figure 2.8.(a),** lane 6) shows no bands due to BSA or myoglobin and an intense band for HisU, demonstrating that highly pure HisU can be obtained using this procedure. (Lanes 1-5 are given to show positions of proteins)

In a second test of selectivity, another film was immersed in 10 mL of phosphate buffer containing 1 mg/mL BSA and 0.05 mg/mL HisU for 2 h, and the solution was stirred for 2 h. The film was rinsed, treated with elution buffer, and analyzed as described above. Even though this sample contained a 20-fold excess of BSA, the eluent showed only a band for HisU (**Figure 2.8.(a),** lane 8).

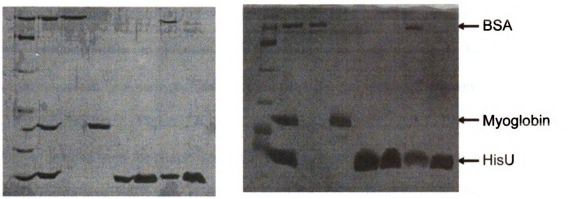

Figure 2.8. SDS-PAGE analysis (silver staining) of protein solutions and eluents from **(a)** Au-poly(HEMA)-NTA-Ni^{2+} films and **(b)** poly(HEMA)-NTA-Ni^{2+} modified alumina membranes. Samples for both electropherograms are: **lane 1**, standard broad range ladder; **lane 2**, mixture of BSA, myoglobin and HisU (0.05 mg/mL each); **lane 3**, BSA; **lane 4**, myoglobin; **lane5**, HisU; **lane 6**, eluent from a film (a) or membrane (b) loaded with a mixture of BSA, myoglobin and HisU (0.05 mg/mL each); **lane 7**, mixture of BSA and HisU; **lane 8**, eluent from a film (a) or membrane (b) loaded with 10 mL of a solution containing 1 mg/mL BSA and 0.05 mg/mL HisU.

2.3.5. Separation of protein mixtures using poly(HEMA)-NTA-Ni^{2+} brushes in membranes

After obtaining promising results with Au-poly(HEMA)-NTA-Ni^{2+} films, we utilized poly(HEMA)-NTA-Ni^{2+}-modified alumina membranes to purify HisU. Three sets of experiments were performed. In the first experiment, 6 mL of phosphate buffer containing BSA, myoglobin and HisU (0.05 mg/mL of each protein) was passed through the poly(HEMA)-NTA-Ni^{2+}-derivatized membrane, and the membrane was then rinsed

with 20 mL washing buffer followed by 20 mL phosphate buffer. Finally, we used 5-10 mL elution buffer to recover the bound protein and analyzed this eluent by electrophoresis. As with purification on a film, the gel electropherogram of the eluent from the membrane (**Figure 2.8. (b),** Lane 6) shows no bands due to BSA or myoglobin and an intense band for HisU. This demonstrates that one pass through the membrane is sufficient to give >99% pure HisU. The purity was calculated assuming that the amount of BSA in the 15 μL protein solution that was loaded on the gel is <20 ng. Approximately 0.75 μg of HisU was loaded on the gel based on a Bradford assay of the protein sample, which was possible because of the high purity of the eluent. Moreover, the membranes can be used multiple times. Gel electrophoresis confirmed that the purity of eluted HisU was not affected by reusing the membrane four times.

After this initial experiment, we washed the membrane with 10 mL of 50 mM EDTA, rinsed it with water, recharged it with 0.1 M Ni^{2+}, and rinsed with 20 mL water and 20 mL phosphate buffer. To further test the membranes, 10 mL of phosphate buffer containing 1 mg/mL BSA and 0.05 mg/mL HisU was passed through the membrane, and the membrane was rinsed, treated with elution buffer, and analyzed as described above. Here also, the eluent showed only a band for HisU (**Figure 2.8.(b)**, Lane 8) even in the presence of 20-fold excess of BSA.

In a final experiment, 10% Bovine serum in 10 mL phosphate buffer containing 45 mM imidazole (pH 7.2) was spiked with 0.3 mg/mL HisU. (Imidazole was added to help prevent adsorption of non His-tagged proteins.) This solution was passed through the membrane, which was then rinsed, treated with elution buffer, and analyzed using the procedure described above.

Figure 2.9. shows the SDS-PAGE analysis of the spiked bovine serum (left) and the eluent from the membrane (right). Although the diluted serum contains about 4 mg/mL of protein and only 0.3 mg/mL of HisU, the electropherogram of the eluent shows a strong band for HisU and only a very faint band of BSA. The HisU in this case is more than 99% pure, assuming that the faint band of BSA represents <40 ng of BSA. (Approximately 4.5 μg of HisU was loaded on the gel, as determined using a Bradford assay of the eluent, and separate gels showed that 40 ng of BSA gave a readily visible band.) **Figure 2.9.** clearly shows the selectivity of the membrane for HisU over other proteins present in serum. Moreover, similar results were obtained upon reusing the membrane.

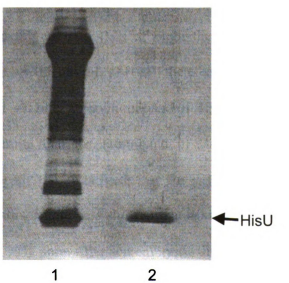

Figure 2.9. SDS-PAGE analysis (silver staining) of 10% bovine serum spiked with 0.3 mg/mL HisU **(lane 1)** and the imidazole eluent from an alumina-poly(HEMA)-NTA-Ni^{2+} membrane loaded with this solution **(lane 2)**.

2.4. Conclusions

This work demonstrates that growth of poly(HEMA)-NTA-Ni^{2+} brushes inside porous alumina supports yields high-capacity membranes that selectively bind His-tagged proteins. The membranes show a binding capacity of 120 mg HisU/cm^3 of membrane along with minimal non-specific adsorption. Moreover, 99% of the bound HisU could be recovered, and membranes can be reused.

Studies of poly(HEMA)-NTA-Ni^{2+} brushes on flat, gold-coated silicon substrates show that significant HisU binding occurs at concentrations as low as 0.001 mg/mL, and saturation of the film is approached in 20 min or less at HisU concentrations of 0.05 mg/mL. Thus, even at His-tagged protein concentrations of 0.04 mg/mL, it should be possible to make full use of binding sites in a few minutes. The time required to approach saturation should be even less at higher concentrations and in membranes, where convection through the membrane will help to overcome diffusion limitations. However, comparison of breakthrough curves of BSA and myoglobin suggest that binding times may increase for large proteins.

Gel electrophoresis results indicate that the membrane is selective towards HisU even in the presence of a 20-fold excess of BSA or in 10% Bovine serum. The recovered HisU in such cases is 99% pure. These membranes should also be effective for whole-cell extracts provided the solution does not clog the membrane. Increases in membrane pore sizes should help to avoid clogging and increase linear velocities, but large pores may also require some optimization of brush thickness and density to achieve rapid binding and high capacities.

Importantly, the time required for membrane-based purification included only 10 min for loading, 10 min for washing, and 5 min for elution. Thus purification of His-tagged proteins can be achieved in less than 30 min, and further time reductions could likely be achieved by using more permeable membrane supports and higher pressures. Hence, these membranes are attractive for rapid, selective purification of His-tagged proteins.

2.5. References:

(1) Arnau, J.; Lauritzen, C.; Petersen, G. E.; Pedersen, J. *Protein Expression and Purification* **2006**, *48*, 1-13.

(2) Zhen, G. L.; Falconnet, D.; Kuennemann, E.; Voros, J.; Spencer, N. D.; Textor, M.; Zurcher, S. *Advanced Functional Materials* **2006**, *16*, 243-251.

(3) Stiborova, H.; Kostal, J.; Mulchandani, A.; Chen, W. *Biotechnology and Bioengineering* **2003**, *82*, 605-611.

(4) Draveling, C.; Ren, L.; Haney, P.; Zeisse, D.; Qoronfleh, M. W. *Protein Expression and Purification* **2001**, *22*, 359-366.

(5) Skerra, A.; Schmidt, T. G. M. *Biomolecular Engineering* **1999**, *16*, 79-86.

(6) Cattoli, F.; Boi, C.; Sorci, M.; Sarti, G. C. *Journal of Membrane Science* **2006**, *273*, 2-11.

(7) Suen, S. Y.; Liu, Y.-C.; Chang, C. S. *Journal of Chromatography B-Analytical Technologies in the Biomedical and Life Sciences* **2003**, *797*, 305-319.

(8) Özkara, S.; Yavuz, H.; Denizli, A. *Journal of Applied Polymer Science* **2003**, *89*, 1567-1572.

(9) Che, S.; Liu, Z.; Ohsuna, T.; Sakamoto, K.; Terasaki, O.; Tatsumi, T. *Nature* **2004**, *429*, 281-284.

(10) Clairbois, A.-S.; Letourneur, D.; Muller, D.; Jozefonvicz, J. *Journal of Chromatography B* **1998**, *706*, 55-62.

(11) Zou, H. F.; Luo, Q. Z.; Zhou, D. M. *Journal of Biochemical and Biophysical Methods* **2001**, *49*, 199-240.

(12) Luzinov, I.; Minko, S.; Tsukruk, V. V. *Soft Matter* **2008**, *4*, 714-725.

(13) Brandt, S.; Goffe, R. A.; Kessler, S. B.; O'Connor, J. L.; Zale, S. E. *Bio-Technology* **1988**, *6*, 779-782.

(14) Boi, C.; Cattoli, F.; Facchini, R.; Sorci, M.; Sarti, G. C. *Journal of Membrane Science* **2006**, *273*, 12-19.

(15) Boi, C.; Facchini, R.; Sorci, M.; Sarti, G. C. *Desalination* **2006**, *199*, 544-546.

(16) Endres, H. N.; Johnson, J. A. C.; Ross, C. A.; Welp, J. K.; Etzel, M. R. *Biotechnology and Applied Biochemistry* **2003**, *37*, 259-266.

(17) Sorci, M.; Boi, C.; Facchini, R.; Sarti, G. C. *Desalination* **2006**, *199*, 550-552.

(18) Yang, H. W.; Viera, C.; Fischer, J.; Etzel, M. R. *Industrial & Engineering Chemistry Research* **2002**, *41*, 1597-1602.

(19) Dai, J. H.; Bao, Z. Y.; Sun, L.; Hong, S. U.; Baker, G. L.; Bruening, M. L. *Langmuir* **2006**, *22*, 4274-4281.

(20) Hicke, H.-G.; Becker, M.; Paulke, B.-R.; Ulbricht, M. *Journal of Membrane Science* **2006**, *282*, 413-422.

(21) Kawai, T.; Saito, K.; Lee, W. *Journal of Chromatography B-Analytical Technologies in the Biomedical and Life Sciences* **2003**, *790*, 131-142.

(22) Singh, N.; Husson, S. M.; Zdyrko, B.; Luzinov, I. *Journal of Membrane Science* **2005**, *262*, 81-90.

(23) Sun, L.; Dai, J. H.; Baker, G. L.; Bruening, M. L. *Chemistry of Materials* **2006**, *18*, 4033-4039.

(24) Ulbricht, M.; Yang, H. *Chemistry of Materials* **2005**, *17*, 2622-2631.

(25) Yusof, A. H. M.; Ulbricht, M. *Desalination* **2006**, *200*, 462-463.

(26) Johnson, R. D.; Arnold, F. H. *Biotechnology and Bioengineering* **1995**, *48*, 437-443.

(27) Kawakita, H.; Masunaga, H.; Nomura, K.; Uezu, K.; Akiba, I.; Tsuneda, S. *Journal of Porous Materials* **2007**, *14*, 387-391.

(28) Matyjaszewski, K.; Miller, P. J.; Shukla, N.; Immaraporn, B.; Gelman, A.; Luokala, B. B.; Siclovan, T. M.; Kickelbick, G.; Vallant, T.; Hoffmann, H.; Pakula, T. *Macromolecules* **1999**, *32*, 8716-8724.

(29) Matyjaszewski, K.; Shipp, D. A.; Wang, J.-L.; Grimaud, T.; Patten, T. E. *Macromolecules* **1998**, *31*, 6836-6840.

(30) Huang, W. X.; Kim, J. B.; Bruening, M. L.; Baker, G. L. *Macromolecules* **2002**, *35*, 1175-1179.

(31) Kim, J.-B.; Huang, W. X.; Bruening, M. L.; Baker, G. L. *Macromolecules* **2002**, *35*, 5410-5416.

(32) Xiao, S.-J.; Brunner, S.; Wieland, M. *Journal of Physical Chemistry B* **2004**, *108*, 16508-16517.

(33) Kim, J.-B.; Bruening, M. L.; Baker, G. L. *Journal of the American Chemical Society* **2000**, *122*, 7616-7617.

(34) Cook, W. J.; Suddath, F. L.; Bugg, C. E.; Goldstein, G. *Journal of Molecular Biology* **1979**, *130*, 353-355.

(35) Yusof, A. H. M.; Ulbricht, M. *Journal of Membrane Science* **2008**, *311*, 294-305.

(36) Motornov, M.; Sheparovych, R.; Katz, E.; Minko, S. *Acs Nano* **2008**, *2*, 41-52.

(37) Goto, M.; Okubo, T.; Kawakita, H.; Uezu, K.; Tsuneda, S.; Saito, K.; Goto, M.; Tamada, M.; Sugo, T. *Biochemical Engineering Journal* **2007**, *37*, 159-165.

(38) Bayramoğlu, G.; Ekici, G.; Beşirli, N.; Arica, M. Y. *Colloids and Surfaces a-Physicochemical and Engineering Aspects* **2007**, *310*, 68-77.

Chapter 3

Purification of His-tagged proteins by polymer membranes containing functionalized poly(HEMA) brushes

3.1. Introduction

Chapter 2 shows that the use of alumina membranes modified with poly(HEMA)-NTA-Ni^{2+} brushes allows rapid and highly selective purification of His-tagged proteins. Unfortunately, the largest pore diameter available in commercial alumina membranes is 0.25 μm,[1,2] which limits the use of these membranes to relatively simple solutions and low flow rates because complex solutions such as cell extracts often plug the relatively small pores. Moreover porous alumina is expensive and frequently breaks both because of its fragility and the pressure needed to achieve required flow rates. Polymeric membranes, on the other hand, can have larger pore diameters than porous alumina (1-10 μm),[3,4] which should facilitate rapid purification with more complex solutions. Higher permeabilities through membranes with larger pores will also allow for lower pressures during separations and the use of thicker membranes that can bind more protein.

This chapter describes the growth of poly(HEMA) brushes inside porous polymer (nylon and PVDF) membranes, and the use of nylon membranes modified with poly(HEMA)-NTA-Ni^{2+} brushes to purify His-tagged cellular retinaldehyde binding protein (CRALBP) from a cell extract. The purities of CRALBP eluted from these membranes are at least as good as those obtained with commercial Ni^{2+} columns.

3.2. Experimental section

3.2.1. Materials

Hydroxylated (LoProdyne® LP) nylon membranes with 1.2 and 5.0 μm-diameter surface pores were obtained from Pall Corporation, and hydrophilic PVDF membranes with a nominal 0.45 μm pore size were purchased from Millipore Corporation. 2-Bromoisobutyryl bromide (98%), CuCl (99.999%), $CuBr_2$ (99%), bpy (99%), EDC, NHS, DMAP, EDTA, imidazole (99%), TWEEN-20 surfactant, and BSA were used as received from Sigma Aldrich. $NiSO_4 \cdot 5H_2O$ (Columbus Chemical), NaH_2PO_4 (CCI), Na_2HPO_4 (Aldrich), aminobutyl NTA (Fluka), succinic anhydride (Matheson Coleman & Bell), and Coomassie protein assay reagent (Pierce) were also used without purification. Tetrahydrofuran (THF, Jade Scientific Inc., anhydrous, 99%) was distilled and stored over molecular sieves. HEMA (Aldrich, 97%, inhibited with 300 ppm hydroquinone monomethyl ether) was purified by passing it through a column of activated basic alumina (Aldrich), and trichlorosilane initiator (11-(2-bromo-2-methyl)propionyloxy)undecyltrichlorosilane) was synthesized according to a literature procedure.[5] Buffers were prepared using analytical grade chemicals and deionized (Milli-Q, 18.2 MΩ cm) water.

3.2.2. Polymerization of HEMA in porous polymer membranes

A polymer membrane was cleaned with UV/ozone (Boekel model 135500) for 10 min, and placed inside a home-built Teflon cell. Subsequently a 1 mM solution of the trichlorosilane initiator in 20 mL of anhydrous THF was circulated through the membrane for 2 h at a flow rate of 3 mL/min, followed by rinsing with 20 mL of ethanol. Polymerization of HEMA from the immobilized initiator occurred by circulating a

degassed solution containing 15 mL of purified HEMA, 15 mL water, 82.5 mg (0.825 mmol) of CuCl, 54 mg (0.24 mmol) of $CuBr_2$, and 320 mg (2.04 mmol) of bpy through the initiator-modified membrane for 1 hour inside a glove bag (flow rate of 1 mL/min). (The use of a mixed halide system sometimes provides better control over polymerization[6,7]). After polymerization, the membrane was cleaned with flowing ethanol (20 mL) followed by 20 mL of deionized water (Milli-Q, 18.2 MΩ cm, 20 mL). (Acetone should not be used with nylon membrane as it partially damages the membrane structure).

3.2.3. Poly(HEMA) derivatization and protein immobilization

Chapter 2 described the derivatization procedure, however, in the present case succinic anhydride was dissolved in THF instead of DMF because DMF partially damages nylon membranes. Additionally, triethylamine was used instead of DMAP as the latter does not dissolve in THF. Moreover, the reaction took place at room temperature unlike with alumina membranes where heating to 55 °C was required **(Scheme 3.1)**.

To study BSA binding, a solution of BSA in 20 mM phosphate buffer (pH 7.2) was pumped through the poly(HEMA)-NTA-Cu^{2+} modified membrane using a peristaltic pump, and the permeate was collected for analysis at specific time intervals. Subsequently, the membrane was rinsed with 20 mL of pH 7.2 washing buffer (20 mM phosphate buffer containing 0.1% Tween-20 surfactant and 0.15 M NaCl) followed by 20 mL of phosphate buffer. The protein was then eluted using 5-10 mL of a solution containing 20 mM sodium phosphate, 0.5 M NaCl, and 0.5 M imidazole at pH 7.4. Cu^{2+}

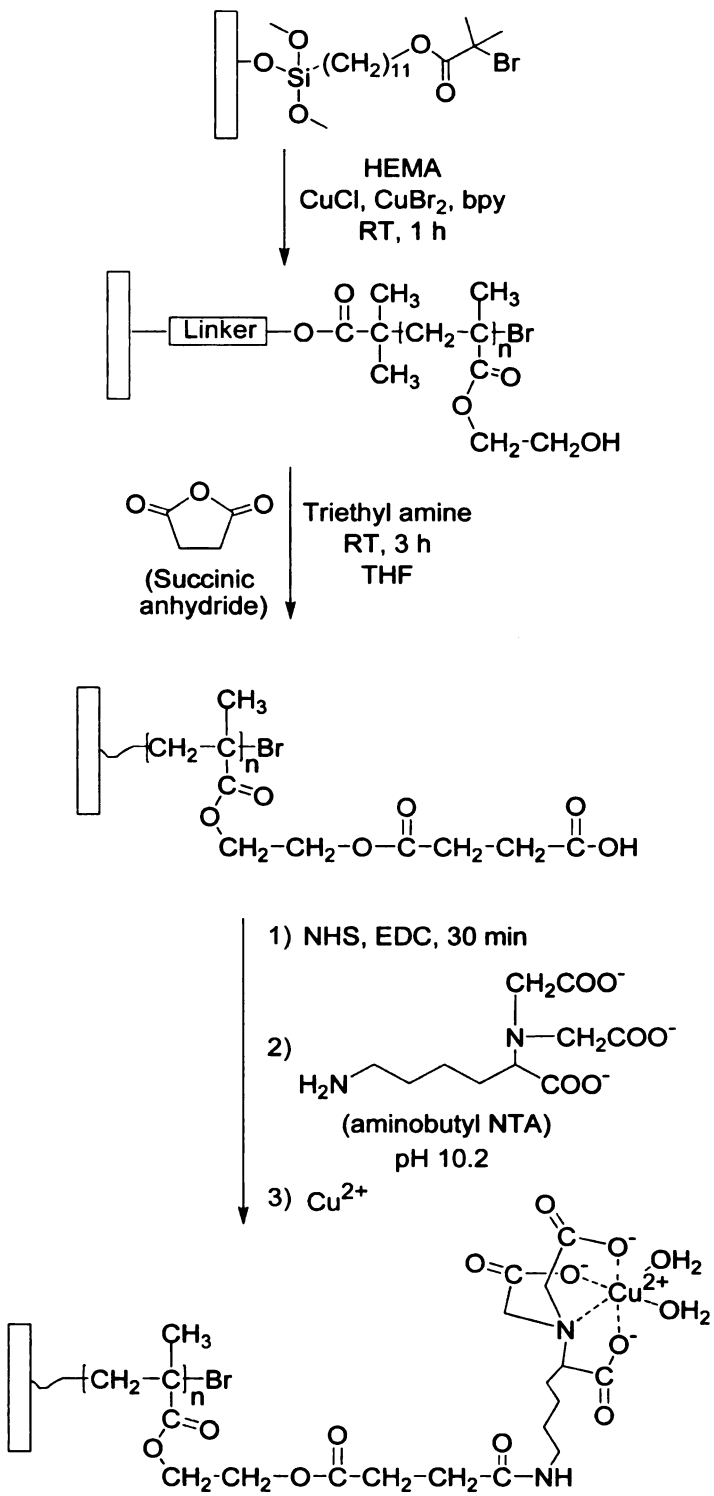

Scheme 3.1. Schematic illustration of the growth and derivatization of poly(HEMA) brushes inside polymer (nylon or PVDF) membranes.

was later eluted using a 50 mM EDTA solution (pH 7.2), and the poly(HEMA)-NTA film was recharged with Cu^{2+} prior to reuse.

3.2.4. Characterization methods

Film growth inside polymer membranes was verified using attenuated total reflectance (ATR) FTIR spectroscopy (Perkin Elmer Spectrum One Instrument, air background) as well as field-emission scanning electron microscopy (FESEM, Hitachi S-4700II equipped with an EDAX Phoenix energy dispersive X-ray spectrometer system, acceleration voltage of 15V).

3.2.5. Protein quantification

To determine the amount of protein eluted from poly(HEMA) brushes in a membrane, 50 μL of eluent was added to 2.95 mL of a solution of Coomassie reagent, and the mixture was shaken a few times and allowed to react for 5 min at room temperature. The UV/vis absorbance spectra of these solutions were then obtained with a Perkin-Elmer UV/Vis (model Lambda 40) spectrophotometer. A calibration curve for the absorbance of BSA solutions at 595 nm was prepared using a series of protein solutions (concentration range of 100 μg to 1 mg of protein per mL) that were mixed with Coomassie reagent. All spectra were measured against a Coomassie reagent background.

To quantify the amount of protein bound to poly(HEMA) brushes on gold-coated Si, the method reported by Dai and coworkers was employed.[8] Briefly, a calibration curve was obtained by plotting the ellipsometric thickness of spin-coated BSA, myoglobin, lysozyme, or ubiquitin films against the reflectance FTIR absorbance of their amide I band (for more details refer to page 60).

3.2.6. Determination of protein purity by sodium dodecyl sulfate-polyacrylamide gel electrophoresis (SDS-PAGE)

The protein solutions were analyzed by SDS-PAGE with a 16% cross-linked separating gel and a 4% cross-linked stacking gel (acrylamide). Protein bands were visualized using standard silver staining[9] or coomassie blue staining[10] procedures.

3.3. Results and discussion

3.3.1. Characterization of poly(HEMA)-derivatized membranes

To form brush-modified membranes, poly(HEMA) was grown from ATRP initiators that were immobilized via silanization within the porous polymer membrane.[11] The brushes were derivatized as shown in **Scheme 3.1.**, with reactant solutions being circulated through the membrane using a peristaltic pump. **Figure 3.1.** shows the ATR-FTIR spectra of (a) a pristine membrane and a similar membrane after (b) polymerization of HEMA, and subsequent reaction with (c) succinic anhydride, (d) activation with NHS/EDC and finally, (e) derivatization with aminobutyl NTA. A bare nylon membrane shows amide I and amide II peaks at 1630 and 1530 cm^{-1} respectively **(Figure 3.1., spectrum (a))**. The small peak at 1720 cm^{-1} might be due to carbonyl groups introduced during hydroxylation of the membrane (however we are not sure as the procedure for hydroxylation is not disclosed by the vendors). The growth of poly(HEMA) is evident by the increase in the carbonyl peak intensity at 1720 cm^{-1} **(Figure 3.1., spectrum (b))**. The difference in intensity of amide peaks before and after derivatization is due to differences in the pressure applied to hold the membrane against the ATR crystal. We applied a lower pressure to the polymer-modified membrane to prevent any damage, and hence the

amide peaks of the modified membrane are less intense than those for the bare membrane.

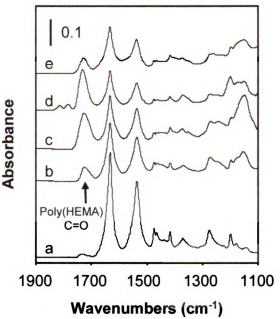

Figure 3.1. ATR-FTIR spectra of a hydroxyl functionalized nylon membrane before (**a**) and after the following sequential steps: (**b**) formation of poly(HEMA) brushes inside the membrane; (**c**) reaction with succinic anhydride; (**d**) activation with EDC/NHS; (**e**) reaction with aminobutyl NTA.

The peak at ~1720 cm^{-1} further increased in intensity after reaction with succinic anhydride due to ester formation **(Figure 3.1., spectrum (c),** the membrane swells after reaction with succinic anhydride, thus it is difficult to quantify the increase in ester peak intensity.) Passing a mixture of EDC and NHS in water through the membrane converted —COOH groups to succinimidyl esters. Peaks due to the succinimide ester appeared at 1810 and 1776 cm^{-1} **(Figure 3.1., spectrum (d)).** Subsequently, the EDC/NHS-activated poly(HEMA) was allowed to react with aminobutyl-NTA. This reaction resulted in a loss of the absorbance due to the succinimide ester, **(Figure 3.1., spectrum (e)).** NTA immobilization is difficult to characterize because of the nylon amide peaks, but there is an absorbance due to the carboxylate groups of NTA (~1680 cm^{-1}) that appears under the amide peaks.

SEM images corroborate the growth of poly(HEMA)-NTA-Cu^{2+} brushes in the polymer membranes. The image of a pristine membrane **(Figure 3.2.(a))** contains open pores, whereas modified pores **(Figure 3.2(b))** appear less open, presumably because they are covered with a polymer film. The energy dispersive X-ray (EDAX) spectrum of a membrane cross-section shows the presence of copper ions throughout the sample (the thickness of the nylon membrane is ~110 μm, **Figure 3.2(c)),** confirming that the growth and derivatization of poly(HEMA) was not limited to the membrane surface.

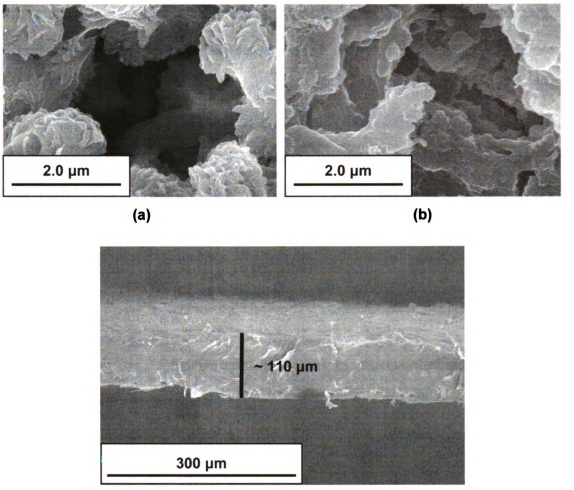

Figure 3.2. SEM images of **(a)** a bare nylon membrane with a 1.2 μm nominal filtration cutoff, **(b)** a similar membrane modified with poly(HEMA)-NTA-Cu^{2+} and **(c)** a cross-sectional image of the membrane.

3.3.2. BSA binding to poly(HEMA)-NTA-Cu^{2+} brushes in membranes

To test the protein binding capacity of poly(HEMA)-NTA-Cu^{2+} brushes in polymer membranes, we pumped a 1 mg/mL solution of BSA in pH 7.2 phosphate buffer through the membrane, collected the permeate over specific time intervals, and analyzed these samples using a Bradford assay. **Figure 3.3.** shows the breakthrough curve for

BSA binding to a poly(HEMA)-NTA-Cu^{2+}-modified nylon membrane (1.2 μm). Integration of the differences between the feed concentrations and the permeate concentrations in the breakthrough curves gives a binding capacity of 25 mg/cm^3. This binding capacity is only 20% of that in alumina membranes modified with poly(HEMA)-NTA-Cu^{2+} (see Chapter 2) and thus is difficult to determine. Similar experiments with PVDF-poly(HEMA)-NTA-Cu^{2+} membranes yield a BSA binding capacity of only 15 mg/cm^3.

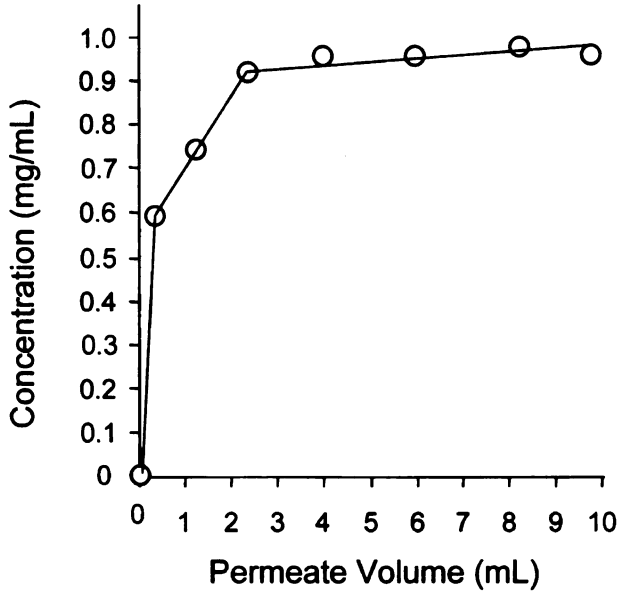

Figure 3.3. Breakthrough curve for absorption of 1 mg/mL BSA in a nylon membrane (1.2 μm pore diameter) modified with poly(HEMA)-NTA-Cu^{2+}. The permeate flow rate was 0.77 mL/min. The solid line is a guide to the eyes.

After measuring the breakthrough curve of BSA, the poly(HEMA)-NTA-Cu^{2+}-BSA membrane was washed with 20 mL washing buffer followed by 20 mL phosphate buffer, and the bound BSA was eluted with 5-10 mL EDTA. Analysis of the eluent using a Bradford assay and comparison of this analysis with the capacity determined from the breakthrough curve showed that >94% of the bound BSA was recovered. (Most likely,

essentially all of the protein eluted from the membrane, but the uncertainty in the amount of binding determined from the breakthrough curve only allows us to say that >94% of the protein was eluted.)

The low BSA binding capacity in polymer membranes relative to alumina membranes may be due to the larger pore size in the polymer membranes and the inability of protein to penetrate thick brushes, or less polymer grafting in the polymer substrates. To examine whether the amount of polymer grafted in the membrane affects protein binding capacity, we increased the polymerization time. However, increasing the polymerization time from 1 h to 2 h did not lead to an increase in BSA binding capacity. Presuming that the longer polymerization time results in more polymer growth, this result suggests that the interior of long brushes is not accessible for protein binding. Longer brushes may also block some pores to decrease binding capacity. We also tried increasing the nominal pore size of the membrane from 1.2 to 5 μm. However, the protein binding capacities for the two types of membranes were similar. Nevertheless, the 5 μm membranes are advantageous over 1.2 μm membranes because of an increase in permeability. After modification with poly(HEMA)-NTA-Cu^{2+}, flow rate at 6.9 X 10^4 Pascal (10 psig) was 1.5 mL/min and 3.0 mL/min for 1.2 μm and 5 μm membranes, respectively .

3.3.3. Purification of His-Tagged CRALBP using nylon membranes modified with poly(HEMA)-NTA-Ni^{2+} brushes

As discussed in chapter 2, alumina membranes modified with poly(HEMA)-NTA-Ni^{2+} brushes are promising for purification of His-tagged proteins. However it is difficult to purify complex mixtures with alumina membranes due to the small pore diameter (0.25

μm). Nylon membranes, on the other hand, have larger pore sizes (1.2-5.0 μm) than alumina so they can potentially purify His-tagged proteins directly from a cell extract. We tested the performance of poly(HEMA)-NTA-Ni^{2+}-modified nylon membranes towards purification of His-tagged CRALBP (36 kD) that was over-expressed in *E. coli*[12] (Dr. James Geiger and Dr. Xiaofei Jia kindly provide the cell extracts.) The cells were lysed by sonication, centrifuged at 4 °C, and 1.25 mL of the supernatant was added to 3.75 mL of 20 mM phosphate buffer (containing 10 mM imidazole and 300 mM NaCl, pH 7.2). This solution was pumped through the poly(HEMA)-NTA-Ni^{2+} modified nylon membrane in an amicon cell at 6.9 X 10^4 Pascal (10 psig) at room temperature. (The flow rate was 0.12 mL of extract/min.) Subsequently, the membrane was rinsed with 20 mL pH 7.2 washing buffer I (20 mM phosphate buffer containing 0.1% Tween-20 surfactant and 0.15 M NaCl) followed by 20 mL pH 7.2, washing buffer II (20 mM phosphate buffer containing 45 mM imidazole and 0.15 M NaCl), and protein was then eluted using a solution containing 20 mM sodium phosphate, 0.5 M NaCl, and 0.5 M imidazole at pH 7.2. The flow rate increased to >1 mL/min during elution at $6.9x10^4$ Pascal.

Figure 3.4.a shows the electropherograms of the cell extract (lane 1) and the eluate from the membrane (lane 2). The eluate contains remarkably pure protein (~99% pure based on the faintness of all other bands). Unfortunately, we cannot establish the protein binding capacity or elution efficiency in this case because the concentration of CRALBP in the cell extract is unknown. We reused the membrane twice without a change in protein purity or flow rate. Future studies should further establish how many times these membranes can be reused without affecting protein purity.

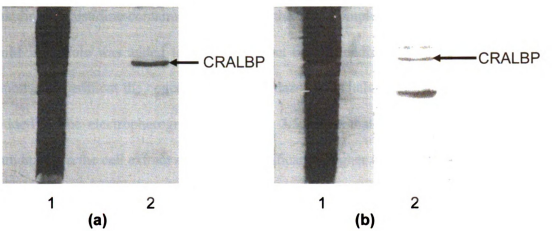

Figure 3.4. SDS-PAGE analysis (silver staining) of an extract from E. coli containing over-expressed His-tagged CRALBP **(Lanes 1 in gels (a) and (b))**; and CRALBP purified from these extracts using flow-through **(gel (a), lane 2)** and immersion methods **(gel (b), lane 2)**. In the flow-through method, the cell extract, washing and elution solutions were flowed through the nylon-poly(HEMA)-NTA-Ni^{2+} membrane whereas in the immersion method, the membrane was immersed in the solutions.

To determine whether flow through the membrane plays an important role in obtaining high protein purity, we attempted to isolate His-tagged CRALBP by simply immersing a membrane in the cell extract, washing, and elution solutions. **Figure 3.4.b.** shows that the protein isolated by the immersion method is much less pure than the protein purified by flowing the cell extract, washing and elution solutions through the membrane. This result suggests that that the flowing solution removes non-specifically adsorbed proteins from the membranes, which may be a major advantage of membranes over columns because the nanopores in resins will not be rinsed with flow.

We also studied the effect of the imidazole concentration in the loading buffer on the purity of CRALBP eluted from membranes. Imidazole may inhibit the unwanted

binding of histidine-containing proteins to the Ni^{2+} complexes. In one experiment, 10 mM imidazole was added to the cell extract before loading on the membrane, and in another experiment the concentration of imidazole was halved (i.e. 5 mM imidazole was added). The electropherograms in **Figure 3.5.** show that the higher concentration of imidazole in the cell extract results in a significantly higher CRALBP purity in the eluate. However, too much imidazole in the binding buffer is undesirable because it will compete with His-tagged protein for the binding sites and decrease the protein binding capacity.

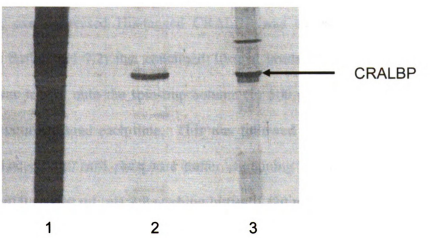

Figure 3.5. SDS-PAGE analysis (silver staining) of an extract from E. coli containing over-expressed His-tagged CRALBP **(Lane 1)** and CRALBP purified from cell extracts containing 10 mM **(Lane 2)** and 5 mM imidazole **(Lane 3).** CRALBP was purified with a poly(HEMA)-NTA-Ni^{2+}-modified nylon membrane (1.2 μm nominal pore size) using procedures described in the text. Solutions were flowed through the membrane.

The goal of this research is to develop affinity membranes for purification of His-tagged proteins in order to overcome the limitations in column-based protein separations. To establish how well our membranes perform, we first compared the performance of poly(HEMA)-NTA-Ni^{2+}-modified nylon membranes with commercial spin-trap columns, in the purification of His-tagged CRALBP. Spin-trap columns are small scale purification "columns" (100 μL resin in each tube) where solutions are passed through a small amount of resin using a centrifuge.[13] They have a protein binding capacity of 750 μg per column.

In CRALBP purification with the spin-trap columns, 1.25 mL of cell-free extract containing over-expressed His-tagged CRALBP was added to 3.75 mL of 20 mM phosphate buffer (pH 7.2) that contained 10 mM imidazole and 300 mM NaCl. The solution was loaded onto the spin-trap column (in 500 μL fractions, 10 times) and the column was centrifuged each time. This was followed by rinsing with 20 mL pH 7.2 washing buffer I (20 mM phosphate buffer containing 0.1% Tween-20 surfactant and 0.15 M NaCl) and 20 mL pH 7.2 washing buffer II (20 mM phosphate buffer containing 45 mM imidazole and 0.15 M NaCl). The protein was then eluted using a 600 μL solution containing 20 mM sodium phosphate, 0.5 M NaCl, and 0.5 M imidazole at pH 7.2. The electropherogram of the eluate **(Figure 3.6., lane 3 and 4)** shows a high protein purity similar to that obtained with membrane purification.

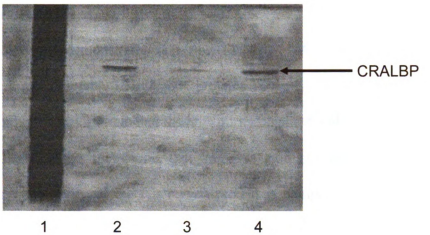

Figure 3.6. SDS-PAGE analysis (silver staining) of an extract from *E. coli* containing over-expressed His-tagged CRALBP **(Lane 1)** and CRALBP purified from the cell extracts using poly(HEMA)-NTA-Ni^{2+}-modified membranes **(Lane 2)** and spin-trap columns **(Lanes 3 and 4)**. 8 μL of eluate was loaded in lane 3 whereas 15 μL was loaded onto lanes 2 and 4.

We further compared membrane-based isolation of CRALBP with purification using a relatively large scale Ni-NTA column (Qiagen, Ni-NTA-Agarose, 6xHis-tagged protein purification kit[14]). These columns have a protein binding capacity of 50 mg per mL of resin. Gel electrophoresis of the eluate shows that the membranes were comparable to the columns interms of purity and time of purification. However these membranes have lower protein-binding capacities compared to the column. Thus, in order to compete with the column-based purification, we need to increase the protein-binding capacities of these membranes as well as decrease the time of purification, which can be accomplished with the use of larger pore sized membranes (e.g. 5 μm). Chapter 6 demonstrates that new methods of membrane formation offer significantly higher capacities and much shorter purification times.

3.4. Conclusions

This work demonstrates that poly(HEMA)-NTA-Ni^{2+}-modified porous nylon membranes can isolate His-tagged proteins directly from cell extracts. Gel electrophoresis results indicate that the high purity obtained with membranes is partly due to flow through the membrane that removes non-specifically adsorbed proteins. Importantly, the purity of the His-tagged protein is comparable to that obtained with commercial spin-trap columns and large columns. However, the membranes have potential advantage over commercial columns in terms of separation rates and higher capacities. Hence, these modified membranes are attractive for selective purification of His-tagged proteins.

3.5. References:

(1) http://www.whatman.com/PRODAnoporeInorganicMembranes.aspx (accessed July 9, 2009).

(2) Cai, C. F.; Bakowsky, U.; Rytting, E.; Schaper, A. K.; Kissel, T. *European Journal of Pharmaceutics and Biopharmaceutics* **2008**, *69*, 31-42.

(3) Kawakita, H.; Masunaga, H.; Nomura, K.; Uezu, K.; Akiba, I.; Tsuneda, S. *Journal of Porous Materials* **2007**, *14*, 387-391.

(4) Coad, B. R.; Kizhakkedathu, J. N.; Haynes, C. A.; Brooks, D. E. *Langmuir* **2007**, *23*, 11791-11803.

(5) Matyjaszewski, K.; Miller, P. J.; Shukla, N.; Immaraporn, B.; Gelman, A.; Luokala, B. B.; Siclovan, T. M.; Kickelbick, G.; Vallant, T.; Hoffmann, H.; Pakula, T. *Macromolecules* **1999**, *32*, 8716-8724.

(6) Matyjaszewski, K.; Shipp, D. A.; Wang, J. L.; Grimaud, T.; Patten, T. E. *Macromolecules* **1998**, *31*, 6836-6840.

(7) Huang, W. X.; Kim, J. B.; Bruening, M. L.; Baker, G. L. *Macromolecules* **2002**, *35*, 1175-1179.

(8) Dai, J. H.; Bao, Z. Y.; Sun, L.; Hong, S. U.; Baker, G. L.; Bruening, M. L. *Langmuir* **2006**, *22*, 4274-4281.

(9) Wray, W.; Boulikas, T.; Wray, V. P.; Hancock, R. *Analytical Biochemistry* **1981**, *118*, 197-203.

(10) Bertolini, M. J.; Tankersley, D. L.; Schroeder, D. D. *Analytical Biochemistry* **1976**, *71*, 6-13.

(11) Sun, L.; Dai, J. H.; Baker, G. L.; Bruening, M. L. *Chemistry of Materials* **2006**, *18*, 4033-4039.

(12) Jia, X.; Michigan State University, 2008; Vol. Ph.D. Dissertation.

(13) Hsu, C. Y.; Lin, H. Y.; Thomas, J. L.; Wu, B. T.; Chou, T. C. *Biosensors & Bioelectronics* **2006**, *22*, 355-363.

(14) Zhang, L.; Li, W.; Zhang, A. *Progress in Chemistry* **2006**, *18*, 939-949.

This chapter is adapted from our published work in Langmuir (Jain, P.; Dai, J.; Grajales, S.; Saha, S.; Baker, G. L.; Bruening, M. L., *Langmuir* 2007, *23*, 11360-11365). Some of the research was done with Dr. Jinhua Dai.

Chapter 4

Completely aqueous procedure for growth of polymer brushes on polymeric substrates

4.1. Introduction

Chapter 2 demonstrated the high protein-binding capacities that can be achieved by modifying porous alumina membranes with polymer brushes. However, as noted in chapter 3, pore sizes in alumina membranes are limited to 0.25 μm, and this greatly limits both membrane permeability and the viscosity of solutions that can be processed. Development of more practical brush-modified membranes requires growth of brushes in polymer substrates that contain micron-sized pores. However, when creating such membranes, synthetic methods must afford both fine control over the rate of chain growth and compatibility with the porous membrane supports.

As explained previously, the first step in the synthesis of polymer brushes by ATRP is attachment of initiators to a surface, which is often realized by immersion of a hydroxyl-functionalized substrate in an anhydrous organic solvent containing an initiator precursor such as 2-bromoisobutyryl bromide or trichlorosilane.[1-5] Unfortunately, many polymer membrane materials such as polysulfone and polyethersulfone (PES)[6] are incompatible with the organic solvents used for initiator attachment. For such substrates, organic solvents should be completely avoided in the brush synthesis to preserve the pore structure of the membrane. Moreover robust membranes such as nylon are also affected by the use of organic solvents. As shown in the chapter 3, nylon membranes modified with poly(HEMA)-NTA-Ni^{2+} brushes have a relatively low protein binding capacity (25

mg protein/cm^3 of the membrane), perhaps because the organic solvents employed in the brush synthesis and derivatization partially damage the membrane structure.

This chapter presents a general, method for immobilizing ATRP initiators on polymer films and membranes via layer-by-layer adsorption of macroinitiators from water. Subsequent aqueous ATRP from these immobilized initiators yields polymer brushes on polymeric substrates (**Scheme 4.1.**), and the entirely water-based process avoids the use of organic solvents that may dissolve or corrupt porous, polymeric substrates. Initiator immobilization relies on adsorption of a polycationic macroinitiator (PMI) recently described by Armes and coworkers.[7-9] To facilitate PMI adsorption, we first prime the surface through adsorption of multilayer polyelectrolyte films comprised of poly(styrene sulfonate) (PSS) and poly(diallyldimethylammonium chloride)

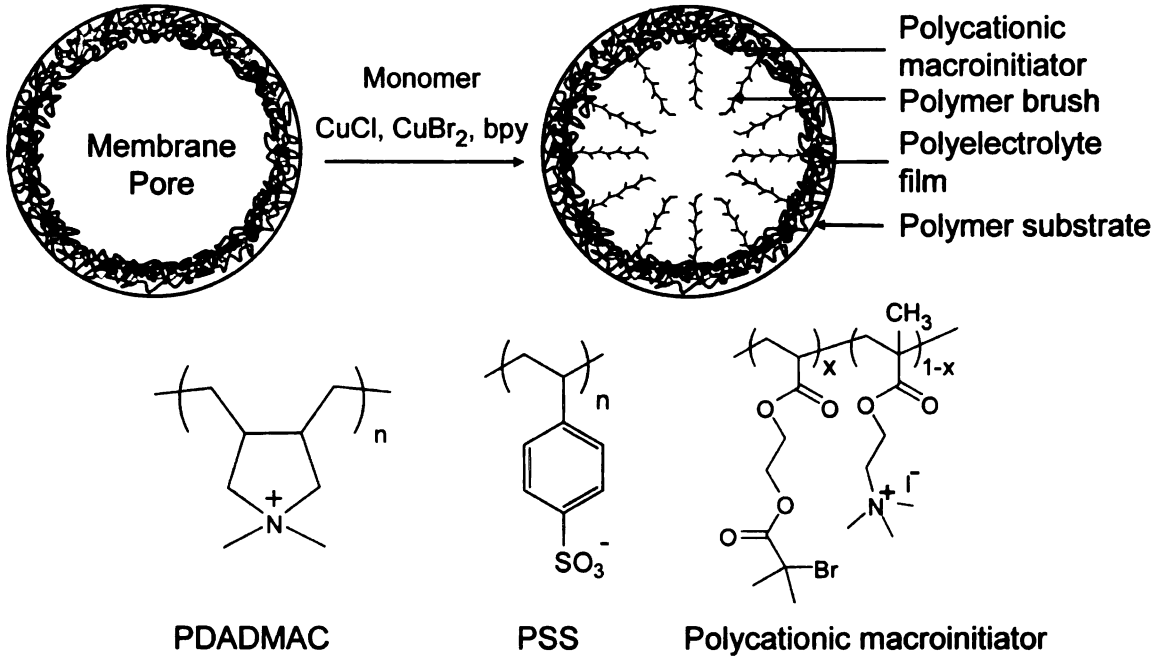

Scheme 4.1. Growth of polymer brushes by ATRP from macroinitiators adsorbed in a membrane pore.

(PDADMAC). Polycationic or polyanionic initiators readily adsorb onto oppositely charged surfaces through electrostatic interactions, as shown previously in adsorption on silica beads,[8] silicon,[9] and modified-colloidal particles.[10] This work builds on these previous studies to demonstrate macroinitiator adsorption and subsequent polymerization on PES films and membranes, which have a much different surface chemistry and morphology than previous substrates employed for macroinitiator adsorption and subsequent ATRP. Most importantly, the macroinitiator immobilization and polymerization occur from water so damage to PES substrates caused by the use of organic solvents is avoided. The adsorbed macroinitiators readily initiate polymerization on PES surfaces to allow growth of 100 nm-thick poly(HEMA) brushes in 30 min, and the procedure can be applied to porous PES membranes.

4.2. Experimental section

4.2.1. Materials

3-mercaptopropionic acid (MPA), 11-mercapto-1-undecanol (MUD), 2-bromoisobutyryl bromide, CuCl (99.999%), iodomethane (99%), PSS (M_w~70,000), PDADMAC (M_w~150,000), $CuBr_2$ (99.999%), 2,2′-bipyridyl (≥99%, bpy), and 2,2′-azobis(2-methylpropionitrile) (AIBN) were obtained from Sigma-Aldrich and used as received. HEMA (97%, Aldrich) and 2-(dimethylamino)ethyl methacrylate (98%, DMAEMA, Aldrich) were purified before use by passing the monomer through a column of activated basic alumina (Spectrum). PES membranes with a nominal 0.45 μm cutoff were obtained from GE Osmonics (Cat. #: S04WP02500). PES coatings on Au-coated Si wafers (200 nm of gold sputtered on 20 nm of Cr on Si(100)) were prepared by

dissolving a PES membrane (17 mg) in 10 mL CH_2Cl_2 and spin-coating the solution (1.0 mL) onto a substrate (1.1×2.4 cm) at a spin rate of 500 rpm.

4.2.2. Characterization methods

NMR Spectra were collected on a Varian Gemini-300 spectrometer. Polymer molecular weights were determined by GPC (Gel Permeation Chromatography) at 35°C using two PL-gel 10 mm mixed-B columns in series and an Optilab rEX differential refractometer (Wyatt Technology Co.) as a detector. THF was the eluting solvent at a flow rate of 1 mL/min. All samples were filtered through a 0.2 μm Whatman polytetrafluoroethylene (PTFE) syringe filter prior to GPC analysis. Films were examined by reflectance FTIR spectroscopy and ellipsometry after each step leading to brush growth. Reflectance FTIR spectra were acquired with a Nicolet Magna-IR 560 spectrophotometer containing a PIKE grazing angle (80°) attachment, and a UV/O_3-cleaned gold slide served as a background. Film thicknesses were determined using a rotating analyzer ellipsometer (model M-44; J. A. Woollam) at an incident angle of 75° and assuming a film refractive index of 1.5. The films were imaged in tapping-mode with a Dimension 3100 scanning probe microscope equipped with a Nanoscope IIIA control station. Film growth inside PES membranes was verified using transmission FTIR spectroscopy (Mattson Galaxy Series 3000) with an air background as well as field-emission scanning electron microscopy (FESEM, Hitachi S-4700II, acceleration voltage of 15 kV).

4.2.3. Determination of the internal surface area of a PES membrane

The internal surface area of these membranes was determined using N_2 adsorption measurements. N_2 adsorption/desorption isotherms were obtained on a Micromeritics

ASAP 2010 Sorptometer using static adsorption procedures at -196 °C. 15 Pieces of PES membranes (255 mg) were degassed for 48 hrs at 80 °C and 10^{-6} torr prior to analysis. The BET surface area was calculated to be 1800 cm^2/membrane from the linear part of the BET plot according to IUPAC recommendations.[11]

4.2.4. Synthesis of 2-(2-bromoisobutyryloxy)ethyl acrylate

2-(2-bromoisobutyryloxy)ethyl acrylate (BIEA) was synthesized according to a modified literature procedure.[12,13] 2-Hydroxyethyl acrylate (11.6 g, 0.1 mol) and triethylamine (11.2 g, 0.11 mol), dried over 4-Å molecular sieves, were dissolved in dry dichloromethane (150 mL). The mixture was cooled in an ice bath, and a 15 mL solution of 2-bromoisobutyryl bromide (24 g, 0.10 mol) in dry dichloromethane was added drop-wise. After the addition was complete, the ice bath was removed, and the reaction mixture was stirred at room temperature for 3h. The solution was filtered to remove triethylammonium bromide and the salt was washed with dichloromethane (100 mL). The organic solutions were combined and washed sequentially with 250 mL of 0.1 M HCl, 250 mL saturated $NaHCO_3$, and 250 mL water. After drying the organic phase over anhydrous Na_2SO_4, the solvent was removed in vacuum to provide 24.2 g of BIEA in 92% yield. ^1H NMR (**Figure 4.1.**, $CDCl_3$): δ 6.41 (dd, J = 18 Hz, J = 2.2 Hz, 1H), 6.11 (dd, J = 18 Hz, J = 18 Hz, 1H), 5.84 (dd, J = 11 Hz, J = 2.2 Hz, 1H), 4.40 (s, 4H), 1.90 (s, 6H).

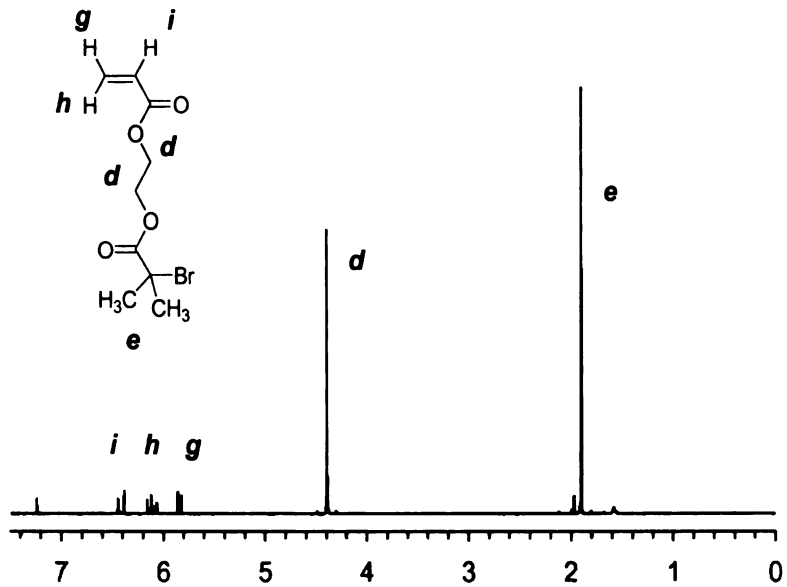

Figure 4.1. ^{1}H NMR (300 MHz, $CDCl_3$) of 2-(2-bromoisobutyryloxy)ethyl acrylate (BIEA).

4.2.5. Synthesis of poly(2-(dimethylamino)ethyl methacrylate-*co*-2-(2-bromoisobutyryloxy)ethyl acrylate) (poly(DMAEMA-*co*-BIEA), the precursor of the polycationic initiator

DMAEMA (2.97 g, 18.9 mmol), BIEA (1.45 g, 5.47 mmol), and AIBN (82 mg, 0.5 mmol) were added to 5 mL of dry THF. The mixture was degassed via three freeze-pump-thaw cycles, and then polymerization was carried out at 60 °C with stirring for 2 h. The highly viscous polymer mixture was diluted with 15 mL of THF, and the polymer was precipitated into pH 11 water. After filtration, the polymer was dried under vacuum, re-dissolved in 15 mL THF, and precipitated into hexane. Filtration and drying under vacuum at room temperature gave 2.1 g of the copolymer. The ^{1}H NMR spectrum of the polymer is shown in **Figure 4.2**, and indicates approximately 20% BIEA in the copolymer.

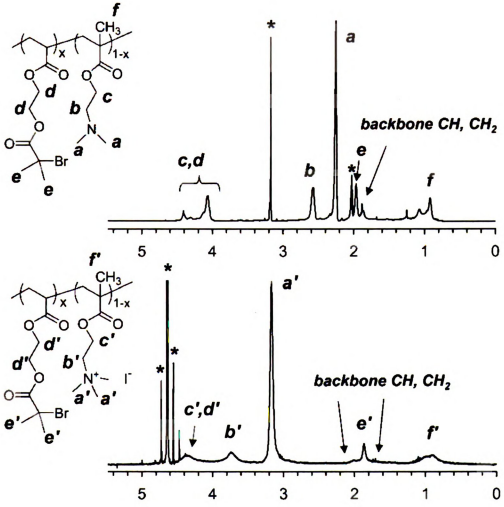

Figure 4.2. ^{1}H NMR spectra of poly(DMAEMA-*co*-BIEA) (top, acetone-d_6 + trace D_2O as solvent) and its quaternized product poly(TMAEMA-*co*-BIEA) (bottom, D_2O as solvent). The corresponding structures and proton assignments are given in the figure. * indicates resonances from solvents.

4.2.6. Synthesis of poly(2-(trimethylammonium iodide)ethyl methacrylate-*co*-BIEA) (poly(TMAEMA-*co*-BIEA)), the polycationic initiator

Poly (DMAEMA-*co*-BIEA) (1.71 g) was dissolved in 25 mL THF, and 1.0 mL of CH_3I was added to the stirred solution at room temperature. Within 2 min, the reaction

mixture became turbid with a butter-like color. After 1 h of stirring, the solution was added dropwise to vigorously stirred hexane to precipitate the polymer as a fine powder. Washing with hexane and drying under vacuum at room temperature for 12 h provided 2.52 g of polymer. The ^{1}H NMR spectrum of the polymer is shown in **Figure 4.2.**

4.2.7. Polymer brush synthesis

Poly(HEMA) and poly(DMAEMA) were grown from poly(TMAEMA-*co*-BIEA)-modified Au and PES surfaces. In the case of Au surfaces, an Au-coated silicon wafer was UV/ozone cleaned and immersed overnight in a 5 mM MPA solution in ethanol to form a MPA self-assembled monolayer. This substrate was then alternatively immersed in aqueous solutions of 0.02 M PDADMAC (containing 0.5 M NaCl) and 0.02 M PSS (containing 0.5 M NaCl) for 5 min, with a 1-min water rinse between each immersion. (Polymer concentrations are given with respect to the repeating unit, and the pH of these solutions was ~7.0). After deposition of a $(PDADMAC/PSS)_2$ film, the substrate was immersed in a solution of poly(TMAEMA-*co*-BIEA) (2.0 mg/mL in water) for 10 min, rinsed with water, and dried under a stream of N_2. PES substrates (both membranes and spin-coated films) were modified similarly but with slightly thicker polyelectrolyte films, $(PSS/PDADMAC)_4PSS$. (Deposition on polymers begins with PSS instead of PDADMAC because PSS adsorption on PES should be more favorable due to hydrophobic interactions.) For poly(TMAEMA-*co*-BIEA)/PSS multilayer films on gold, we used the same deposition solutions and times as above.

Brush growth from adsorbed initiators followed procedures reported previously.[3] Briefly, 15 mL of monomer (HEMA or DMAEMA) was mixed with 15 mL of water in a Schlenk flask, and this solution was degassed via three freeze-pump-thaw cycles.

Catalyst and ligand were added, and the solution was subjected to one additional freeze-pump-thaw cycle. The molar ratio of the reagents was monomer:CuCl:$CuBr_2$:bpy = 50:1:0.3:2.6. In a glovebag, initiator-modified substrates were immersed in the degassed solution, and polymerization was allowed to proceed at room temperature for the desired time. Polymer-coated substrates were then removed from the glovebag and rinsed sequentially with ethanol and water.

4.3. Results and discussion

4.3.1. Synthesis of polycationic macroinitiator

The macroinitiator, poly(TMAEMA-*co*-BIEA), is closely related to that reported by Armes et al.[8,17] The primary difference is the method used to incorporate the ATRP initiator into the macroinitiator. Armes used a post-polymerization strategy, acylating a HEMA-DMAEMA copolymer, while we copolymerized DMAEMA with 2-(2-bromoisobutyryloxy)ethyl acrylate (BIEA), a monomer capable of initiating ATRP. Quaternization of the resulting copolymer is the final step in both syntheses.

The copolymer intermediate, poly(DMAEMA-*co*-BIEA), is insoluble in water but easily dissolves in acetone and THF. The mole fraction of BIEA in the copolymer determined from the ^{1}H NMR integration ratios (**Figure 4.2.**, top) was ~20%, in reasonable agreement with the initial ratio of monomers in the polymerization solution (DMAEMA/BIEA = 3.46/1). The broad resonances in the ^{1}H NMR spectra imply a high molecular weight for the copolymer, but GPC data acquired in THF and calibrated with polystyrene standards reveal a bimodal molecular weight distribution with molecular weights <3000 g/mol **(Figure 4.3.).** Since GPC separates molecules on the basis of their size in solution, the data may indicate that poly(DMAEMA-*co*-BIEA) has a smaller

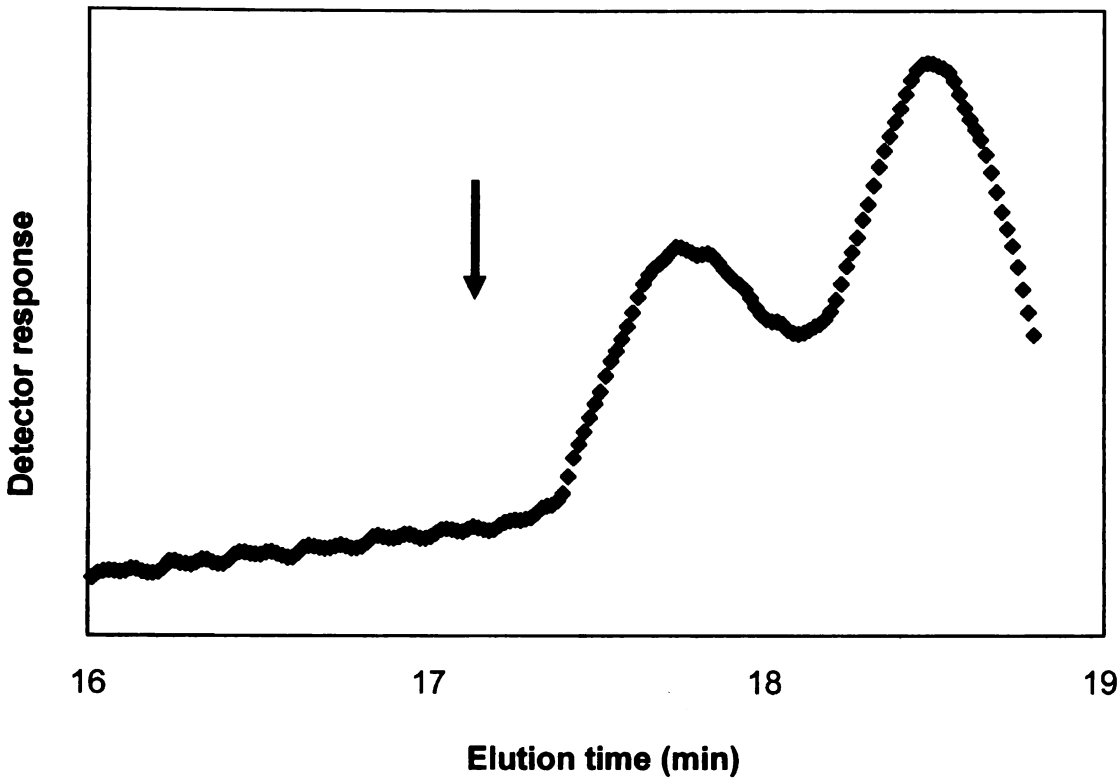

Figure 4.3. GPC trace of poly(TMAEMA-*co*-BIEA). The sample was run at 35 °C using two PL gel 10 mm mixed-B columns in series, and THF as the eluting solvent at a flow rate of 1 mL/min. The samples were filtered through a 0.2 μm Whatman PTFE syringe filter prior to GPC analysis. The arrow indicates the elution time for the lowest polystyrene standard (2727 g/mol) used for calibrating the columns. The elution time for pure solvent is ~20 minutes.

hydrodynamic radius than polystyrene of comparable molecular weight. Thus, using polystyrene standards may underestimate the true molecular weight of poly(DMAEMA-*co*-BIEA). In addition, the AIBN-initiated free radical copolymerization of DMAEMA with BIEA may provide branched rather than linear polymers since the bromine atom in BIEA is activated (α to a carbonyl) and can act as an internal chain transfer agent. Bromine atom abstraction by initiator or growing polymer chains is expected to cause

branching from the BIEA segments resulting in a more compact copolymer. However, the extent of chain transfer is difficult to characterize by ^{1}H and ^{13}C NMR. When growing polymer chains abstract bromine from BIEA segments, the polymer chains are terminated in α-bromocarbonyls, which will have reactivities comparable to that of BIEA. Solutions of poly(DMAEMA-*co*-BIEA) have limited stability and eventually become insoluble, precluding extensive characterization of the copolymer; we suspect cross-linking via intra and intermolecular quaternization of DMAEMA with BIEA. Poly(TMAEMA-*co*-BIEA), the quaternized polymer, is stable and water soluble, but insoluble in common organic solvents. The NMR spectrum of poly(TMAEMA-*co*-BIEA) shows downfield shifting of the methyl groups attached to nitrogen (**a′** in **Figure 4.2.**), indicating successful quaternization. The NMR spectrum of this polymer is essentially the same as that reported by Armes and coworkers for a similar macroinitiator prepared by acylation of the hydroxyl groups after polymerization. To verify that the α-bromo ester survived the quaternization step, we precipitated an aqueous solution of the polymer in acetone and analyzed the dried polymer using X-ray photoelectron spectroscopy (**Figure 4.4.**). The atom ratio of Br to N was 0.28, which is reasonably consistent with 20% BIEA in poly(TMAEMA-*co*-BIEA). Thus, the initiating moiety is at least temporarily stable to the quaternization process and to exposure to water.[14] However, over time it appears that the Br is slowly abstracted. In the NMR spectrum of a 10-month old sample of poly(TMAEMA-*co*-BIEA), the peak due to the methyl groups adjacent to the Br, **e** in **Figure 4.2.**, split into two peaks, suggesting that about half of the Br had been extracted (**Figure 4.5.**). Still, as shown below, 10-month old macroinitiator was capable of effectively initiating polymerization.

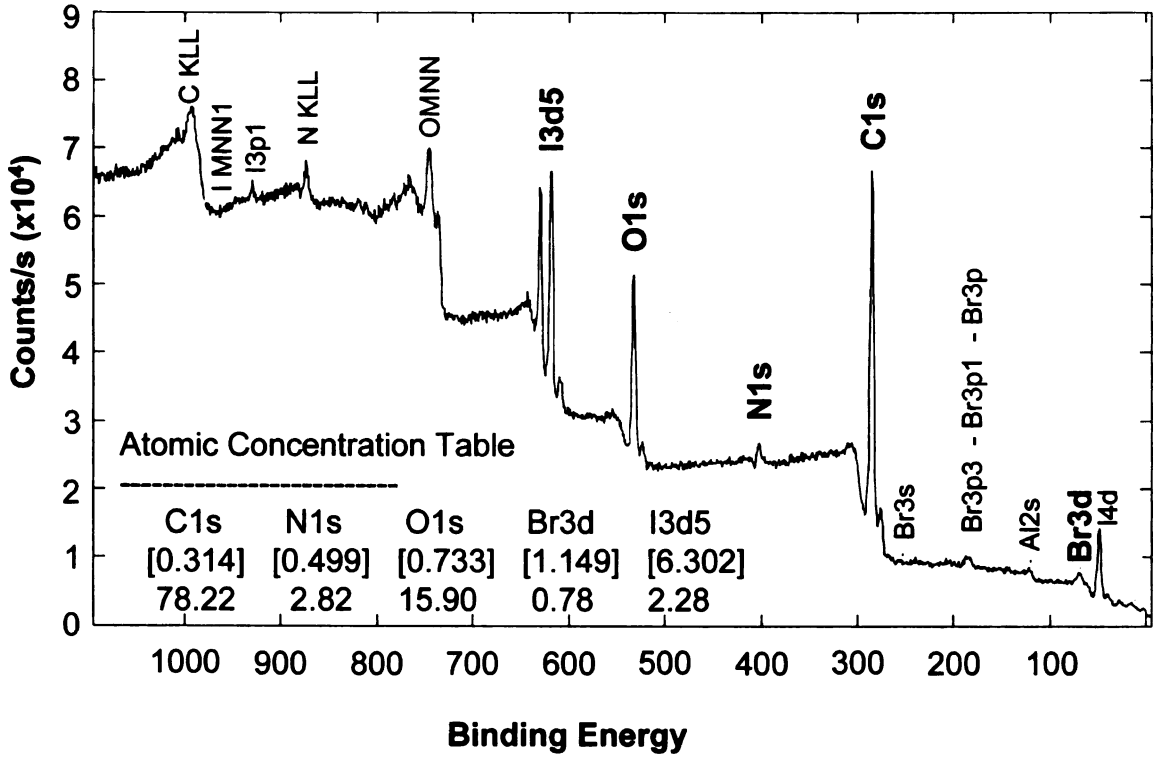

Figure 4.4. XPS elemental analysis of quaternized poly(DMAEMA-*co*-BIEA).

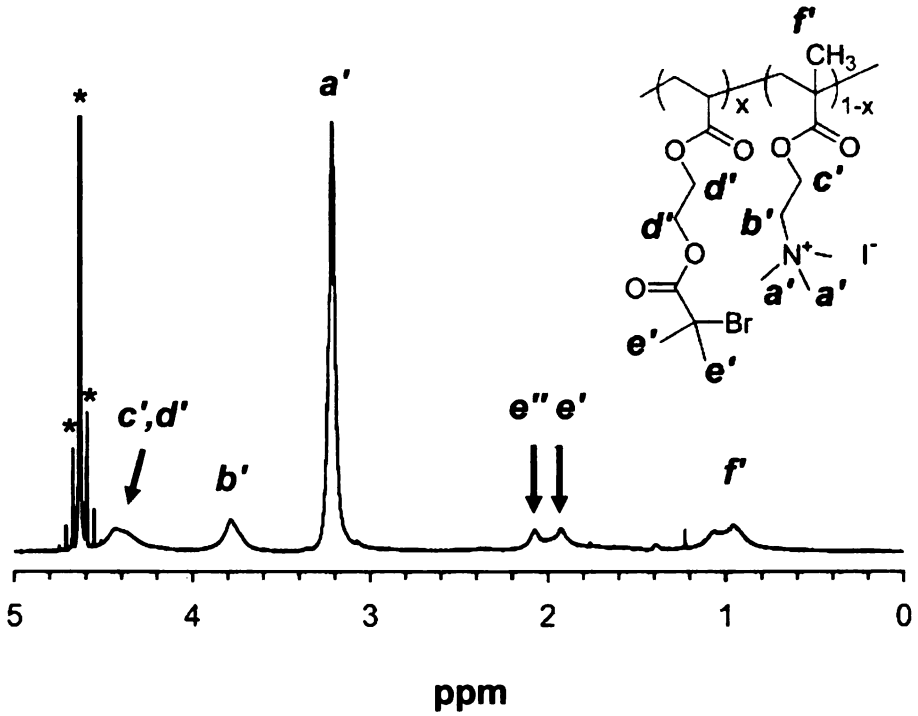

Figure 4.5. ^{1}H NMR spectrum of a 10-month old sample of poly(TMAEMA-*co*-BIEA) (D_2O as solvent), showing evolution of the α-methyl resonances (**e', e"**) . The corresponding structures and proton assignments are given in the figure. * indicates resonances from solvents.

4.3.2. Polymer brush growth from surfaces modified with poly(TMAEMA-*co*-BIEA)

The first step in growing polymer brushes from poly(TMAEMA-*co*-BIEA) is adsorption of the macroinitiator on a surface. To examine the adsorption properties of this polymer, we fabricated multilayer initiator-containing films by alternating deposition of poly(TMAEMA-*co*-BIEA) and PSS on a MPA-modified Au surface. Reflectance FTIR spectra of these films **(Figure 4.6.)** show a linear increase in the absorbance at 1730 cm^{-1} (attributed to the ester carbonyl groups of poly(TMAEMA-*co*-BIEA)) as a

function of the number of deposited bilayers, confirming controlled macroinitiator adsorption. Trends in absorbances due primarily to CH_3 and CH_2 bands (around 1490 cm^{-1}) in poly(TMAEMA-*co*-BIEA) as well as several PSS vibrations (1200-1225, 1040, and 1010 cm^{-1}) are also consistent with regular film growth. Plots of ellipsometric thickness versus the number of deposited bilayers showed a growth rate of 4.3 nm/bilayer.

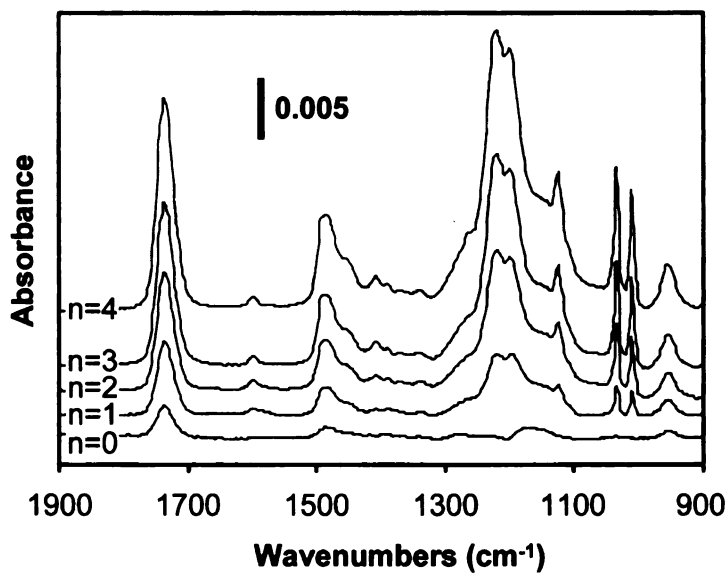

Figure 4.6. Reflectance FTIR spectra of poly(TMAEMA-*co*-BIEA)/ $[PSS/poly(TMAEMA\text{-}co\text{-}BIEA)]_n$ films deposited on Au-MPA substrates (n=0-4).

We investigated the ability of absorbed poly(TMAEMA-*co*-BIEA) multilayer films to initiate polymerization by growing poly(HEMA) brushes from such films via aqueous ATRP for 2 h. The appearance of broad hydroxyl peaks (3500-3300 cm^{-1}) and large ester carbonyl peaks at 1730 cm^{-1} in the reflectance FTIR spectra of these films **(Figure 4.7.)** confirmed the growth of poly(HEMA) from the macroinitiator-modified surfaces.

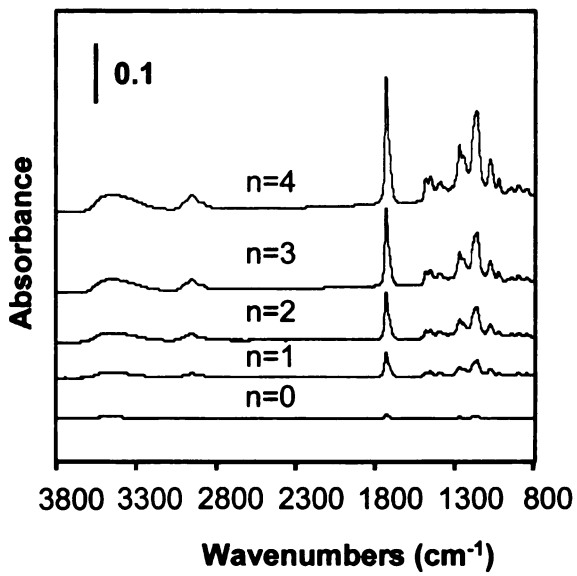

Figure 4.7. Reflectance FTIR spectra poly(HEMA) films grown from poly(TMAEMA-*co*-BIEA)/ $[PSS/poly(TMAEMA\text{-}co\text{-}BIEA)]_n$ films deposited on Au-MPA substrates (n = 0-4).

Moreover, both the absorbances due to poly(HEMA) and the ellipsometric thickness of the poly(HEMA) films **(Figure 4.8.)** increased monotonically with the number of PSS-macroinitiator bilayers. The enhanced polymer growth with more PSS/poly(TMAEMA -*co*-BIEA) bilayers suggests that initiators throughout the film can initiate brush growth. We should note that these brushes were polymerized from multilayer films that were prepared using macroinitiator that was about a year old, and about half of the Br groups may be removed from the initiator under such conditions **(Figure 4.5.)**. Still, films as thick as 160 nm can be obtained in just 2 h when polymerizing from poly(TMAEMA-*co*-BIEA)/$[PSS/poly(TMAEMA\text{-}co\text{-}BIEA)]_4$ films. (Unless specified, all other experiments reported here were performed within a few months of initiator synthesis.)

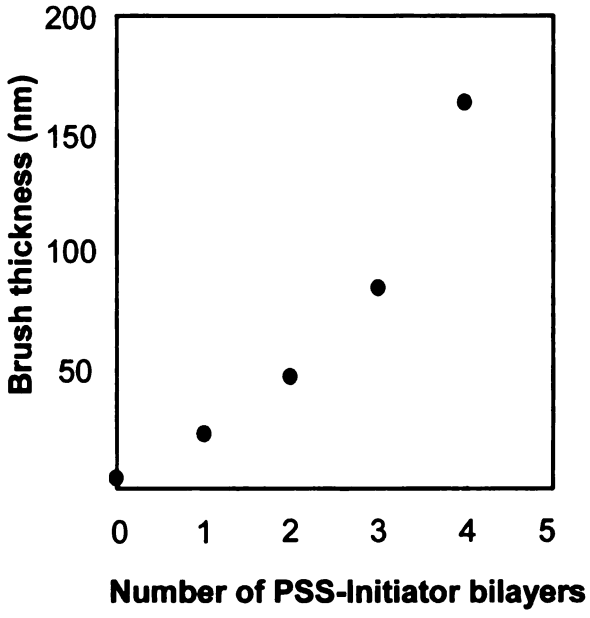

Figure 4.8. Poly(HEMA) brush ellipsometric thickness versus number of bilayers for growth from poly(TMAEMA-*co*-BIEA)/[PSS/poly(TMAEMA -*co*-BIEA)]$_n$ films deposited on Au-MPA substrates (n=0-4). The thickness of the initiator/polyelectrolyte layer was subtracted from the total thickness of the film.

We examined the kinetics of polymerization using a single macroinitiator layer adsorbed on a (PDADMAC/PSS)$_2$ film **(Figure 4.9.)**. Brush thickness increased with polymerization time to give films as thick as 200 nm in just 3 hours, but decreasing growth rates over time suggest some termination. As expected, control experiments with (PDADMAC/PSS)$_2$ films devoid of initiator layers showed no polymer growth, confirming that the polyelectrolyte layers are incapable of initiating polymerization in the absence of the macroinitiator.

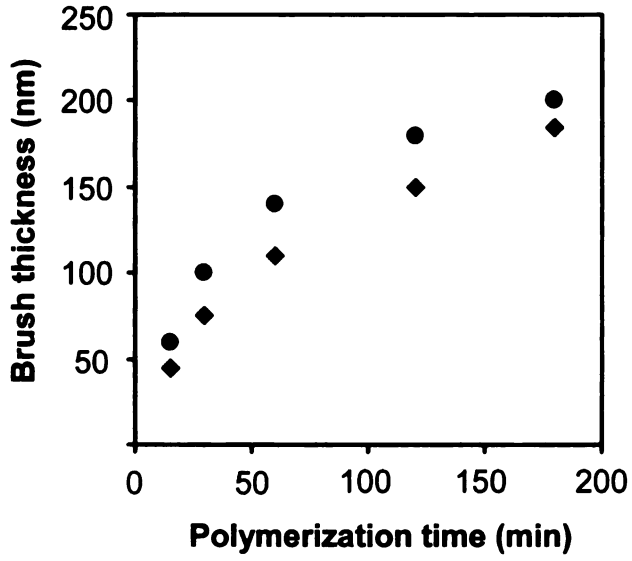

Figure 4.9. Poly(HEMA) brush thickness versus polymerization time for growth from Au-MPA-[PDADMAC/PSS]$_2$-poly(TMAEMA-*co*-BIEA) films (circles) and from Au-MUD-BribBr films (diamonds). The thickness of the initiator layer was subtracted from the total thickness of the film.

To compare the initiation performance of the adsorbed poly(TMAEMA-*co*-BIEA) to that of typical initiator monolayers, we also synthesized poly(HEMA) brushes from Au surfaces modified by a self-assembled monolayer of mercaptoundecanol that was subsequently reacted with 2-bromoisobutyryl bromide (BribBr). The initiating motifs of the BribBr-modified monolayer and the adsorbed poly(TMAEMA-*co*-BIEA) are the same (2-bromoisobutyryl ester). The poly(HEMA) growth rate from adsorbed poly(TMAEMA-*co*-BIEA) is comparable to or greater than that of the initiator monolayer, as shown in **Figure 4.9.** This might seem surprising considering the fact that only 20% of the repeat units in poly(TMAEMA-*co*-BIEA) contain the initiating motif. However, poly(TMAEMA-*co*-BIEA) likely adsorbed in a coiled form, which allows for deposition of a thick (~45 Å) layer with a reasonably high areal density of initiation

sites.[15,16] Given the thickness of the poly(TMAEMA-*co*-BIEA) layer and its composition, the total amount of transferable Br in the adsorbed macroinitiator is essentially the same as what we would expect for a fully derivatized self-assembled monolayer.[3] Moreover, most of the initiation sites in the monolayer film will not be active due to steric constraints.[17] Such constraints should be less demanding in the more three-dimensional poly(TMAEMA-*co*-BIEA) layer.

Film surface morphologies were examined using Atomic Force Microscopy (AFM) before and after polymerization. Figure **4.10.a.** and **4.10.b.** clearly show changes in surface roughness after polymerization. The root mean square roughness increased from 3.6 nm for a Au-MPA-$(PDADMAC/PSS)_2$-poly(TMAEMA-*co*-BIEA) film to 14.7 nm after poly(HEMA) growth for 2h. This topology may be indicative of patchy initiation because of the use of aged initiator in this case. However, the peak to trough distance of 51 nm is still considerably less than the film thickness of about 110 nm. Moreover, roughness may be a strong function of solvent treatment.

4.3.3. Polymer brush growth on PES

We selected PES as a representative material to demonstrate the use of the macroinitiator for synthesizing brushes on polymer substrates that can be formed into membranes. PES is widely used in membrane manufacturing because of its resistance to high temperature, acid, and base, but it has a very weak tolerance to organic solvents.[18] For convenience of characterization, we first dissolved a PES membrane in dichloromethane and spin-coated this solution on Au slides to obtain a PES film (~40 nm). A $PSS(PDADMAC/PSS)_4$ polyelectrolyte film was then deposited on the PES, followed by adsorption of poly(TMAEMA-*co*-BIEA).

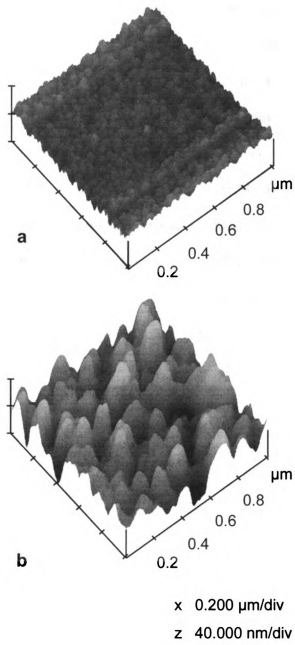

Figure 4.10. AFM Images of **(a)**: a Au-MPA-(PDADMAC/PSS)$_2$-poly(TMAEMA-co-BIEA) film; **(b)**: **(a)** + a poly(HEMA) brush. Note that these films were prepared using a 1-year old macroinitiator.

Reflectance FTIR spectroscopy **(Figure 4.11.)** confirmed each step in the initiator attachment and growth of polymer from these substrates. The peaks at 1040 and 1010 cm^{-1} **(Figure 4.11.b.**, under the thick arrow) stem from the adsorbed PSS, and indicate adsorption of $PSS(PDADMAC/PSS)_4$, while the ester carbonyl absorbance at 1730 cm^{-1} **(Figure 4.11.c.**, under the arrow) provides evidence for deposition of the poly(TMAEMA-*co*-BIEA). A 2 h polymerization of HEMA from these surfaces yielded a ~ 250 nm increase in the film's ellipsometric thickness, while the corresponding polymerization of 2-(dimethylamino)ethyl methacrylate resulted in growth of a 40 nm-thick brush. Large increases in carbonyl absorbances **(Figure 4.11.d.** and **Figure 4.11.e.)**

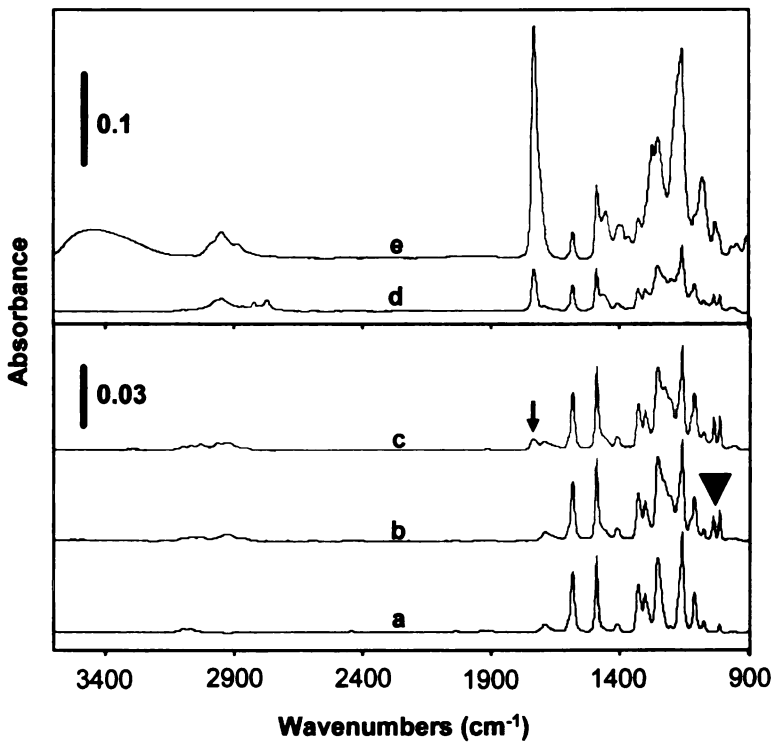

Figure 4.11. Reflectance FTIR of **(a):** spin-coated PES on Au; **(b): (a)** + $PSS(PDADMAC/PSS)_4$; **(c): (b)** + poly(TMAEMA-*co*-BIEA); **(d): (c)** + poly(DMAEMA) brush; and **(e): (c)** + poly(HEMA) brush.

also confirmed the growth of the brushes.

Lastly, we synthesized polymer brushes directly on porous PES membranes. In one case, the PES membrane was coated with a PSS(PDADMAC/PSS)$_4$/poly(TMAEMA-*co*-BIEA) film before poly(HEMA) brush growth, and the polymerization was performed for 1 h. Membranes were exposed to deposition and polymerization reagents by simple immersion in the solution. In a second case, to insure modification throughout the interior of the membranes, we used only a single PSS/poly(TMAEMA-*co*-BIEA) bilayer because PSS(PDADMAC/PSS)$_4$ bilayers blocked the pores at some point in the membrane as judged by our inability to flow water through these membranes using a peristaltic pump. The time of polymerization employed to grow polymer inside the pores was also reduced to 15 minutes to avoid blocking, and all solutions were flowed through the membrane during both initiator deposition and polymerization. Poly(HEMA) growth in both cases is evident from a new peak at 1724 cm^{-1} in transmission FTIR spectra (**Figure 4.12.b.** and **4.12.c.**, under the arrow).

We quantified the amount of poly(HEMA) brushes in PES membranes both gravimetrically and by calibrating the transmission IR absorbance of poly(HEMA)-modified membranes using spectra of pure poly(HEMA) in KBr pellets (**Figure 4.13.**). Results from these two methods match reasonably well. For example, the sample shown in **Figure 4.12.b.** has a poly(HEMA) ester carbonyl absorbance of 0.48, which corresponds to 1.7 mg poly(HEMA) per membrane according to an infrared calibration curve, while the direct mass measurement gave 2.3 mg poly(HEMA) in the membrane. The slightly larger value obtained gravimetrically could be attributed to incomplete removal of water and monomer/catalyst residues after polymerization. Assuming a

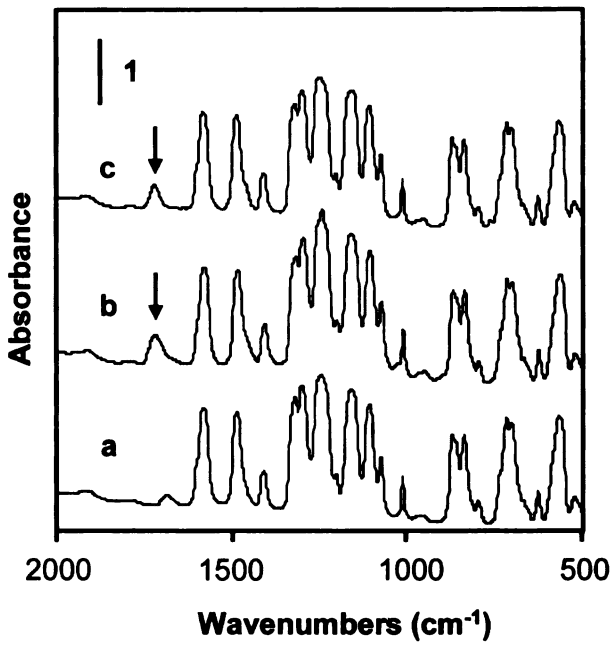

Figure 4.12. Transmission FTIR spectra of **(a)** a bare PES membrane, **(b)** a PES membrane modified with a PSS(PDADMAC/PSS)$_4$/poly(TMAEMA-*co*-BIEA) film and 1 h polymerization of poly(HEMA) (growth on the membrane surface), and **(c)** a PES membrane modified with a PSS/poly(TMAEMA-*co*-BIEA) bilayer and 15 min polymerization of poly(HEMA) (growth in the membrane pores).

porosity of about 80%, 1.7 mg of poly(HEMA) in a PES membrane is equivalent to about 5% of the initial open membrane volume. However, in this case much of the polymerization likely occurred on the membrane surface. Similarly for the sample shown in **Figure 4.12.c,** the poly(HEMA) ester carbonyl absorbance of 0.41 corresponds to 1.45 mg poly(HEMA) per membrane according to an infrared calibration curve, while the direct mass measurement gave 1.5 mg poly(HEMA) in the membrane. The unmodified membrane had an exposed diameter of 20 mm, a thickness of ~110 μm, and a N_2 adsorption-based internal surface area of 1800 cm^2. Assuming this pore surface area to

be flat, 1.5 mg of poly(HEMA) would correspond to brushes with a thickness of ~8.3 nm, which is reasonable given the short polymerization time (15 min for polymerization inside the pores).

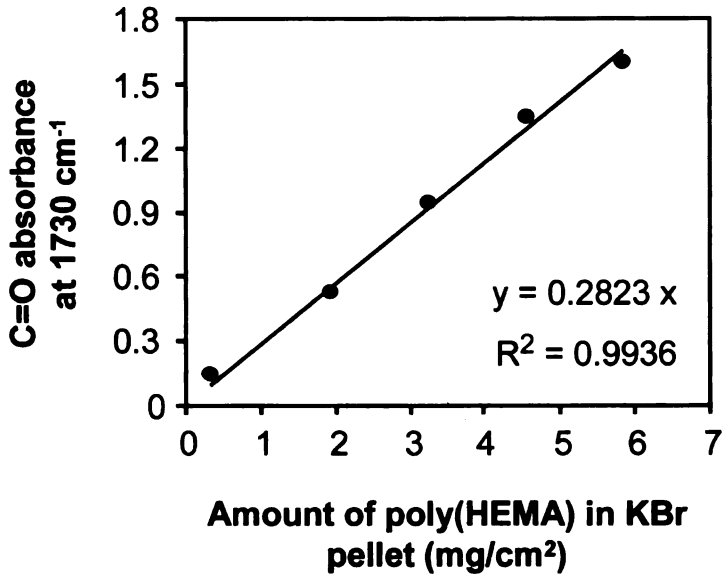

Figure 4.13. Calibration curve of the absorbance at 1730 cm^{-1} (attributed to the ester carbonyl of poly(HEMA) versus the areal concentration of poly(HEMA) in KBr pellets. Poly(HEMA) KBr pellets were prepared by thoroughly mixing different amounts of poly(HEMA) and KBr (the total amount of the mixture was 100 mg, and the face of the pellet had an area of 1.54 cm^2).

To investigate the morphology of poly(HEMA) grown within the pores of PES membranes, we dissolved away the PES framework using dichloromethane and examined the remaining material using SEM. Poly(HEMA) is partially cross-linked due to transesterification and thus insoluble in dichloromethane, and the FTIR spectrum of the material remaining after an overnight immersion in CH_2Cl_2 showed predominantly poly(HEMA). The SEM image of the dissolved PES-poly(HEMA) membrane shows

what appears to be to be a replica of the large pores of a bare PES membrane **(Figure 4.14.)**. The small pores are not present in the dissolved sample, however, which could be due to bridging of pores by poly(HEMA) or collapse of the structure during dissolution and swelling of poly(HEMA).

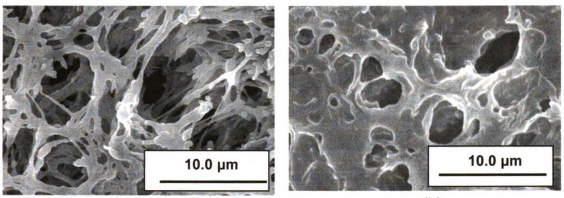

Figure 4.14. SEM image of **(a)** a bare PES membrane and **(b)** a PES membrane dissolved in dichloromethane after derivatization with poly(HEMA).

4.4 Conclusions

To conclude, layer-by-layer deposition of polyelectrolytes including at least one layer of a macroinitiator allows growth of polymer brushes from polymer supports in an entirely aqueous procedure, circumventing utilization of organic solvents that may dissolve or corrupt substrates.

4.5. References

(1) Tsujii, Y.; Ohno, K.; Yamamoto, S.; Goto, A.; Fukuda, T. *Advances in Polymer Science* **2006**, *197*, 1-45.

(2) Matyjaszewski, K.; Miller, P. J.; Shukla, N.; Immaraporn, B.; Gelman, A.; Luokala, B. B.; Siclovan, T. M.; Kickelbick, G.; Vallant, T.; Hoffmann, H.; Pakula, T. *Macromolecules* **1999**, *32*, 8716-8724.

(3) Huang, W.; Kim, J.-B.; Bruening, M. L.; Baker, G. L. *Macromolecules* **2002**, *35*, 1175-1179.

(4) Edmondson, S.; Osborne, V. L.; Huck, W. T. S. *Chemical Society Reviews* **2004**, *33*, 14-22.

(5) Matyjaszewski, K.; Xia, J. *Chemical Reviews* **2001**, *101*, 2921-2990.

(6) Baker, R. W. *Membrane Technology and Applications*; Second ed.; John Wiley & Sons Ltd., 2004.

(7) Chen, X.; Armes, S. P. *Advanced Materials* **2003**, *15*, 1558-1562.

(8) Chen, X. Y.; Armes, S. P.; Greaves, S. J.; Watts, J. F. *Langmuir* **2004**, *20*, 587-595.

(9) Edmondson, S.; Vo, C.-D.; Armes, S. P.; Unali, G.-F. *Macromolecules* **2007**, *40*, 5271-5278.

(10) Fulghum, T. M.; Patton, D. L.; Advincula, R. C. *Langmuir* **2006**, *22*, 8397-8402.

(11) Sing, K. S. W.; Everett, D. H.; Haul, R. A. W.; Moscou, L.; Pierotti, R. A.; Rouquerol, J.; Siemieniewska, T. *Pure and Applied Chemistry* **1985**, *57*, 603-619.

(12) Matyjaszewski, K.; Gaynor, S. G.; Kulfan, A.; Podwika, M. *Macromolecules* **1997**, *30*, 5192-5194.

(13) Zhai, G.; Kang, E. T.; Neoh, K. G. *Macromolecules* **2004**, *37*, 7240-7249.

(14) Boyer, C.; Bulmus, V.; Liu, J. Q.; Davis, T. P.; Stenzel, M. H.; Barner-Kowollik, C. *Journal of the American Chemical Society* **2007**, *129*, 7145-7154.

(15) Bertrand, P.; Jonas, A.; Laschewsky, A.; Legras, R. *Macromolecular Rapid Communications* **2000**, *21*, 319-348.

(16) Dubas, S. T.; Schlenoff, J. B. *Macromolecules* **1999**, *32*, 8153-8160.

(17) Bao, Z.; Bruening, M. L.; Baker, G. L. *Macromolecules* **2006**, *39*, 5251-5258.

(18) Nicolas, J.; Mantovani, G.; Haddleton, D. M. *Macromolecular Rapid Communications* **2007**, *28*, 1083-1111.

This chapter is adapted from our published work in Macromolecules (Jain, P.; Dai, J.; Baker, G. L.; Bruening, M. L., *Macromolecules* **2008**, *41*, 8413-8417).

Chapter 5

Rapid synthesis of functional polymer brushes by surface-initiated atom transfer radical polymerization of an acidic monomer

5.1. Introduction

The previous chapter describes aqueous methods for growth of poly(HEMA) brushes inside polymer membranes. However, our procedure for creation of protein-binding membranes requires conversion of hydroxyl groups in poly(HEMA) to carboxylic acid moieties. As explained in chapters 2 and 3, the formation of acid groups involves reaction of poly(HEMA) with succinic anhydride in an organic solvent for several hours **(Scheme 5.1.a)**, which partially damages the membrane structure and leads to low protein binding capacities. This chapter describes surface-initiated aqueous ATRP of an acidic monomer, 2-(methacryloyloxy)ethyl succinate (MES), that allows direct synthesis of poly(carboxylic acid) brushes, hence avoiding the need to react the brush with succinic anhydride in an organic solvent. Interestingly, this method yields the same polymer formula as obtained after reaction of poly(HEMA) with succinic anhydride **(Scheme 5.1.b)**.

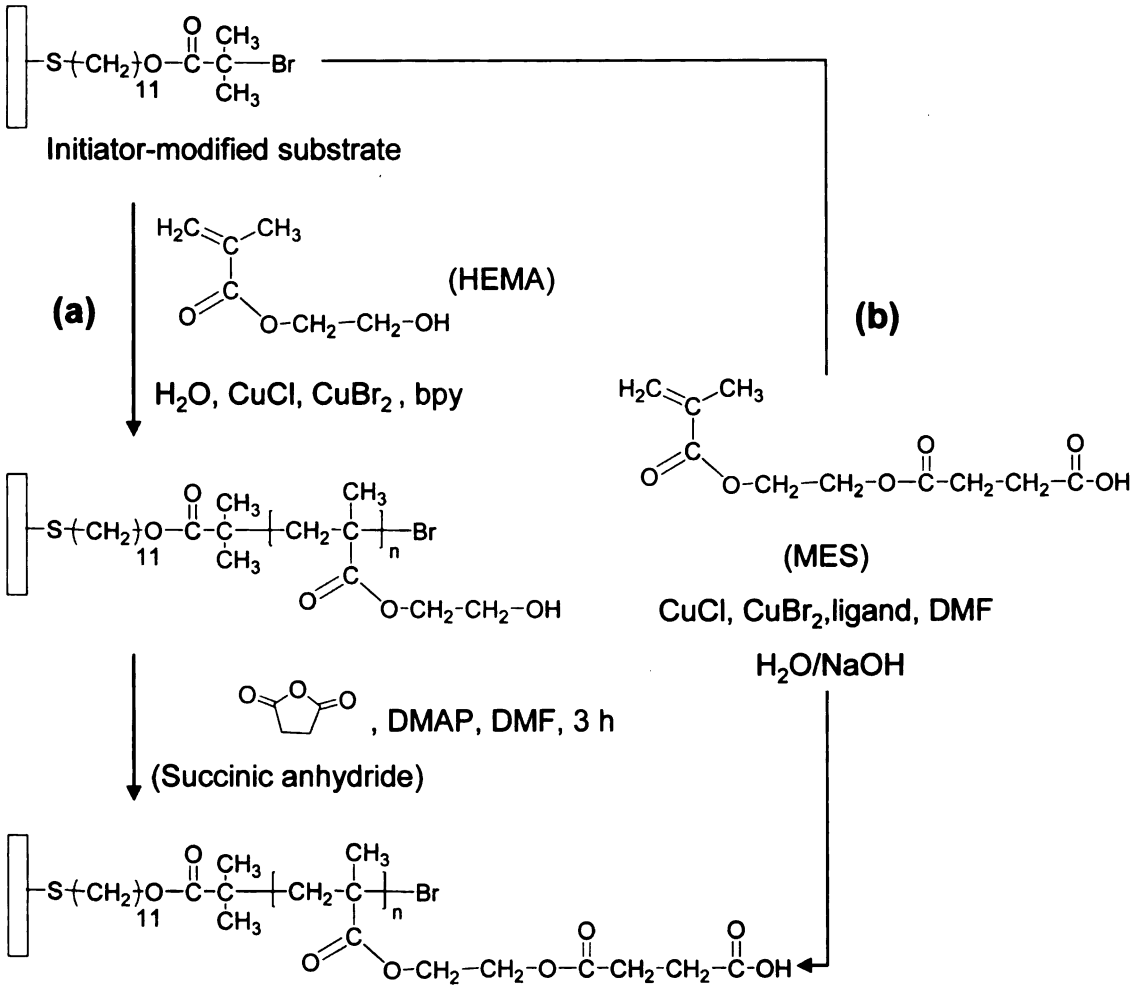

Scheme 5.1. Polymerization of **(a)** HEMA or **(b)** MES from initiator immobilized on a gold substrate. Derivatization of the poly(HEMA) with succinic anhydride gives brushes with the same composition as poly(MES).

There are a number of other methods for synthesizing poly(carboxylic acid) brushes because they have potential applications in cell adhesion and growth,[1,2] immobilization of biomacromolecules,[3-5] synthesis of shell-crosslinked micelles,[6,7] and entrapment of nanoparticles and catalysts.[8] Synthesis of polyacid brushes frequently includes surface-initiated anionic polymerization[9-13] or ATRP[14-18] of an ester-containing monomer and subsequent hydrolysis. For instance, Boyes *et al.* synthesized polyacid

brushes through growth and hydrolysis of poly(*tert*-butyl acrylate) and poly(methacrylate) films.[16] Unfortunately, these strategies require multiple steps including harsh acidic conditions for deprotection. Techniques such as photopolymerization are capable of directly forming acrylic acid (AA)[19,20] and methacrylic acid (MAA) films,[21] however the use of irradiation or high temperatures for initiation might be incompatible with opaque or temperature-sensitive substrates. Additionally, conventional free radical techniques lead to extensive polymerization in solution and require exhaustive rinsing to remove physisorbed polymers. The use of controlled polymerization methods can potentially overcome these limitations.[22,23] Among the strategies for controlled polymerization, ATRP is attractive due to its mild reaction conditions (room temperature in many cases), tolerance to impurities, and use of readily available catalysts, initiators and monomers.[24-26] Perhaps most importantly, surface-initiated ATRP results in minimal solution polymerization and allows control over polymer thickness by variation of polymerization time. Thus, ATRP is attractive for creating films in complex geometries such as the pores of membranes and for tailoring film architectures to maximize protein adsorption.

Here, we describe the rapid synthesis of carboxylic acid-containing polymer brushes using surface-initiated ATRP of an acidic monomer, MES. The combination of this monomer and highly active ATRP catalysts, e.g., Cu(I) complexed with 1,1,4,7,10,10-hexamethyltriethylenetetramine (HMTETA), allows rapid formation of polyacid brushes from a surface. ATRP from initiators immobilized on Au-coated Si wafers yields films with an ellipsometric thickness of 120 nm in less than 15 min. To the

best of our knowledge, this is the first example of direct ATRP of protonated acidic monomers that is capable of yielding such thick films.

Several papers reported growth of polymer brushes via surface-initiated ATRP of acid monomers in aqueous solution, but most polymerization rates and/or thicknesses were low.[27-31] Using ATRP from immobilized initiators, Sankhe *et al.* polymerized itaconic acid and MAA from Au, but film growth ceased after the formation of 10 nm-thick coatings.[32] The addition of salt to polymerization solutions allowed more controlled growth of poly(itaconic acid) and poly(MAA) films, but the growth rates were only 0.2 nm/h and 1 nm/h, respectively.[33] Other groups used a similar strategy to grow ~40 nm-thick poly(AA) brushes.[31,34] Tugulu and coworkers reported that direct, aqueous polymerization of sodium methacrylate from initiators on Si can yield 300 nm thick poly(MAA) in 3 h.[35] Using the same conditions, we tried growing poly(MAA) brushes from Au surfaces that were modified by immersion in a solution containing a disulfide initiator, $(BrC(CH_3)_2COO(CH_2)_{11}S)_2$. These polymerizations yielded inhomogeneous films that were visibly rough and not smooth enough for ellipsometric characterization. Similar results occurred on Si modified with initiators. In contrast, the polymerization of MES in its protonated form provides visibly homogeneous films, and ellipsometry of these films yields data that are characteristic of smooth coatings.

As mentioned in prior chapters, polyacid films are attractive as protein binders[3,20,36-38] for applications such as protein purification by affinity adsorption,[36,39-41] immunoassays,[42] enzymatic reactions,[3] and analyses with antibody arrays.[43-46] In these applications, the formation of thick polymer brushes is vital for achieving high binding capacities. This chapter also shows that a 55 nm-thick poly(MES) film absorbs the

equivalent of ~70 monolayers (14.4±0.3 $\mu g/cm^2$) of lysozyme, and derivatization of poly(MES) with metal-ion complexes allows binding of large amounts of protein via metal-affinity interactions. The binding capacities are similar to those of poly(AA) brushes prepared by polymerization of *tert*-butyl acrylate and subsequent hydrolysis, but the poly(MES) synthesis is a one-step, aqueous process.

5.2. Experimental section

5.2.1. Materials

11-mercaptoundecanol (97%), DMF (anhydrous, 99.8%), 2-bromoisobutyryl bromide (98%), CuBr (99.999%), $CuBr_2$ (99%), bpy (99%), 1,1,4,7,10,10-hexamethyltriethylenetetramine (HMTETA), 1,4,8,11-tetraaza-1,4,8,11-tetramethylcyclotetradecane (Me_4Cyclam), 4,4′-dinonyl-2,2′-bipyridyl (dnNbpy), EDC, NHS, 4-(bromomethyl)benzoic acid (97%), column packing for removing hydroquinone and monomethyl ether hydroquinone (MEHQ, cat. no. 311332), TWEEN-20 surfactant, BSA and lysozyme were used as received from Sigma-Aldrich. $CuSO_4 \cdot 5H_2O$ (CCI), NaOH (Spectrum), NaH_2PO_4 (CCI), Na_2HPO_4 (Aldrich) and aminobutyl NTA (Fluka) were also used without purification. HEMA (Aldrich, 97%, inhibited with 300 ppm hydroquinone monomethyl ether) was purified by passing it through a column of activated basic alumina (Aldrich). In most cases, MES (Aldrich, inhibited with 750 ppm MEHQ), MAA (Aldrich, 99%, inhibited with 250 ppm MEHQ), AA (Aldrich, 99%, inhibited with 200 ppm MEHQ) were used as received, but where noted, the inhibitor was removed by passing the monomer through a column of inhibitor removal packing. The disulfide initiator, $(BrC(CH_3)_2COO(CH_2)_{11}S)_2$,[47] and tris[2-(dimethylamino)ethyl]amine (Me_6TREN)[48] were synthesized as described previously.

Buffers were prepared using analytical grade chemicals and deionized water (Milli-Q, 18.2 MΩ cm).

5.2.2. Polymerization of MES on Au substrates

Au-coated wafers (200 nm of sputtered Au on 20 nm of sputtered Cr on Si wafers) were cleaned with UV-ozone for 15 min, immersed in a 1 mM ethanolic solution of the disulfide initiator, $(BrC(CH_3)_2COO(CH_2)_{11}S)_2$, for 24 h, rinsed sequentially with ethanol and water, and dried under a stream of N_2. These initiator-modified substrates were then transferred to a N_2-filled glove bag where polymerization was carried out at ambient temperature.

To prepare most polymerization solutions, 10 mL of a mixture of neat monomer and 1 M aqueous NaOH (1:1, v/v) was first degassed with three freeze-pump-thaw cycles. A 1 mL solution of DMF containing CuBr, $CuBr_2$ and ligands was similarly degassed, and in a N_2-filled glove bag, this solution of catalyst was mixed with the monomer/NaOH solution. Finally, the initiator-coated substrate was immersed in the polymerization solution, and after the desired time, the coated wafers were removed from the glove bag, immediately sonicated in DMF for 10 min, rinsed sequentially with ethanol and water, and dried under a stream of N_2. Final concentrations of the different catalysts in the various polymerization solutions were: CuBr (2 mM), $CuBr_2$ (1 mM), HMTETA (6 mM); CuBr (2 mM), $CuBr_2$ (1 mM), Me_4Cyclam (2 mM), dnNbpy (1 mM); and CuBr (2 mM), $CuBr_2$ (1 mM), Me_6TREN (6 mM).[14,49] In a few cases, we halved the concentrations of HMTETA and Me_6TREN ligands and achieved similar film thicknesses.[14,50] For the system containing bpy, the concentrations were CuBr (0.55 mM), $CuBr_2$ (0.16 mM) and bpy (1.56 mM). The use of a bpy system containing 6 mM

bpy, 2 mM CuBr, and 1 mM $CuBr_2$ resulted in very thin (< 25 nm) films after 2 h of polymerization. The pH of the polymerization solutions was ~5.0.

When examining polymerization rates as a function of the amount of NaOH added to the polymerization solution, the monomer and catalyst concentrations were kept constant. For these studies, neat monomer, aqueous solutions of 1 M and 5 M NaOH, deionized water, and catalyst solution containing CuBr, $CuBr_2$, and HMTETA in DMF were degassed separately with three freeze-pump-thaw cycles and transferred to a N_2-filled glove bag. Solutions were prepared by mixing 5 mL of MES with varying amounts of NaOH solution and water in order to achieve the desired molar ratios of NaOH to MES. The total volume in each case was 10 mL. One milliliter of degassed catalyst solution was then mixed with the polymerization solution, and the initiator-coated films were immersed in this solution for 2 h. The polymer-coated wafers were removed from the glove bag, immediately sonicated in DMF for 10 min, rinsed sequentially with ethanol and water, and dried under a stream of N_2.

5.2.3. Derivatization of carboxylic acid groups and protein immobilization

The carboxylic acid groups of poly(MES) were activated by immersing the films in a solution containing NHS (0.1 M) and EDC (0.1 M) in water for 30 min, and the films were rinsed sequentially with water and ethanol (20 mL each) and dried with N_2. The NHS-modified films were immersed for 1 h in an aqueous solution of aminobutyl NTA (0.1 M, pH 10.2), rinsed with 20 mL of water and dried with N_2. Finally, the NTA-Cu^{2+} complex was formed by immersing the coated wafer in 50 mM $CuSO_4$ for 2 h, rinsing the substrate sequentially with water and ethanol (20 mL each) and drying with N_2. To immobilize BSA, the poly(MES)-NTA-Cu^{2+} films were immersed in a solution of 1.0

mg/mL BSA in phosphate buffer (20 mM, pH 7.2) for 18 h. The films were then rinsed with 20 mL washing buffer (phosphate buffer containing 150 mM NaCl and 0.1% Tween-20, pH 7.2) followed by 20 mL of phosphate buffer and 20 mL ethanol. Films were dried under a stream of N_2.

For lysozyme-binding studies, poly(MES) wafers were immersed in a 1 mg/mL solution of lysozyme in phosphate buffer for 3 h. The films were then rinsed with 20 mL of washing buffer followed by 20 mL of phosphate buffer and 20 mL of ethanol. Films were dried under a stream of N_2. Before characterizing the poly(MES)-NTA-Cu^{2+} and poly(MES)-NTA-Cu^{2+}-protein films by reflectance FTIR spectroscopy and ellipsometry, the films were immersed in phosphate buffer for 15 min followed by rinsing with 20 mL ethanol and drying under a stream of N_2

5.2.4. Quantification of protein binding

To quantify the amount of protein bound to poly(MES) brushes on Au-coated Si wafers, the method mentioned in Chapter 2 was employed. Briefly, a calibration curve was obtained by plotting the ellipsometric thickness of spin-coated BSA or lysozyme films against the reflectance FTIR absorbance of their amide I band (for more details refer to page 60). The amide absorbance of lysozyme or BSA adsorbed to poly(MES) or poly(MES)-NTA-Cu^{2+} films was then compared to the calibration curve to obtain the thickness added due to protein adsorption. These results were confirmed by ellipsometric studies.

5.2.5. Kinetics of solution polymerization of MES, MAA and HEMA

Solution polymerizations of MES and MAA were performed using 4-(bromomethyl)benzoic acid as the initiator.[30] For these studies, neat monomer (with or

without inhibitor), 1 M aqueous NaOH, and catalyst solution in DMF were degassed separately using three freeze-pump-thaw cycles and transferred to a N_2-filled glove bag. Initiator (20 mM) was dissolved in 1 mL of 1 M NaOH. In another vial, neat monomer (5 mL) was mixed with 4 mL of 1 M NaOH, and 1 mL of degassed catalyst solution containing CuBr (2 mM), $CuBr_2$ (1 mM), and HMTETA (6 mM) in DMF was added. The initiator and monomer solutions were mixed together, and a 0.5-mL aliquot of this mixture was transferred to an NMR tube containing 50 μL of D_2O. (Before adding the polymerization solution, the NMR tube was purged with N_2 for 30 min and then kept in a N_2-filled glove bag for at least 3 h to remove oxygen). The time difference between the start of polymerization and the start of NMR data acquisition was 8 min.

5.2.6. Instrumentation

^1H NMR Spectra were collected on a Varian Inova-300 spectrometer, and reflectance FTIR spectra of films on Au-coated wafers were obtained with a Nicolet Magna-IR 560 spectrophotometer containing a PIKE grazing angle (80°) accessory. A UV/ozone-cleaned Au-coated wafer was used to obtain a background spectrum. Film thicknesses were determined using a rotating analyzer ellipsometer (model M-44; J.A. Woollam) at an incident angle of 75°, assuming a film refractive index of 1.5. Ellipsometric measurements were performed on at least three spots on a film.

5.3. Results and Discussion

5.3.1. Kinetics of surface-initiated MES polymerization

Scheme 5.2. outlines the synthesis of poly(MES) brushes on Au-coated Si wafers and the derivatization of these brushes with metal-ion complexes that bind proteins.

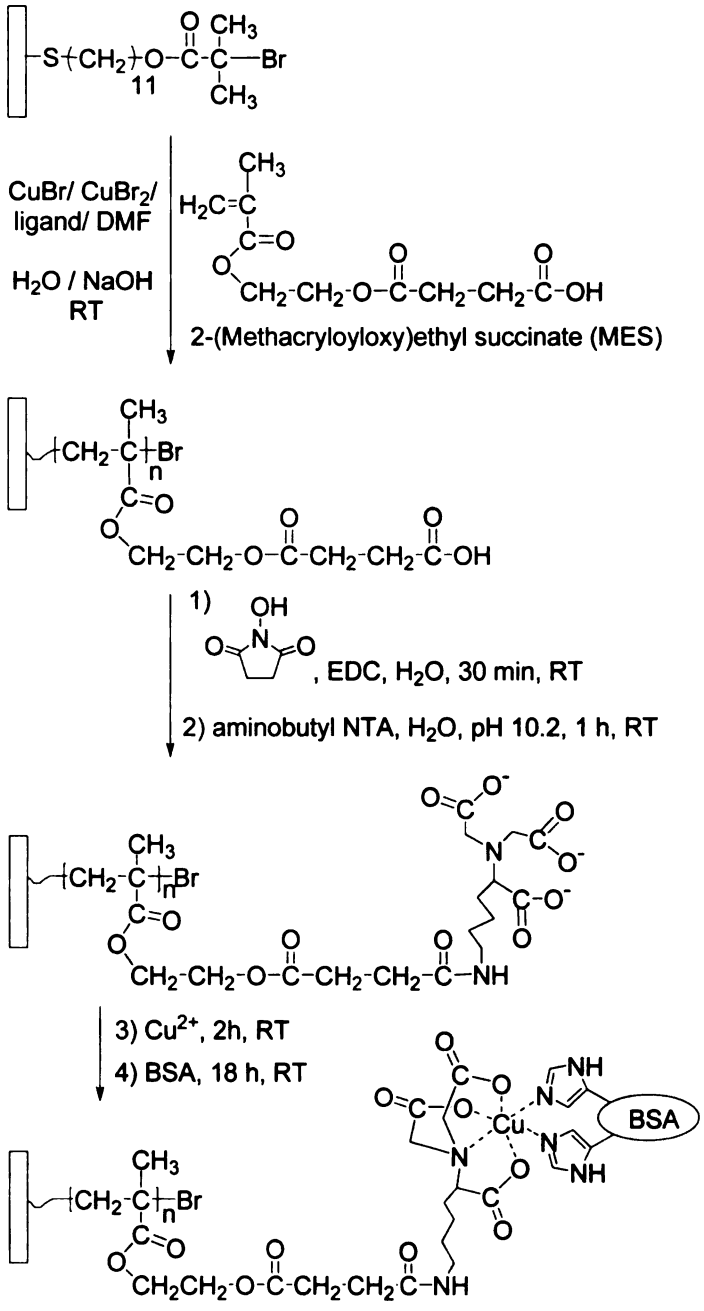

Scheme 5.2. Synthesis of protein-binding poly(MES) brushes on Au surfaces.

Growth and modification of poly(MES) brushes on Au- coated Si wafers were characterized with reflectance FTIR spectroscopy using a clean wafer as background **(Figure 5.1.)**. The peak at ~1740 cm^{-1} in **spectrum (a)** is assigned to the ester carbonyl

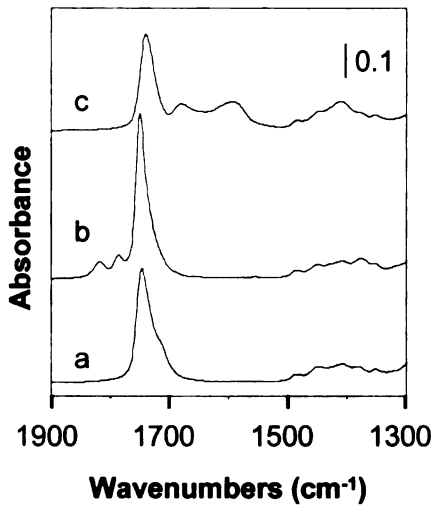

Figure 5.1. Reflectance FTIR spectra of a poly(MES) brush on a Au-coated Si wafer (**a**) before and after the following sequential steps: (**b**) activation with EDC/NHS; (**c**) reaction with aminobutyl NTA.

groups of poly (MES). Exposing the film to a 0.1 M mixture of EDC and NHS in water converted —COOH groups to succinimidyl esters. Formation of the succinimide ester resulted in new peaks at 1817 and 1786 cm^{-1} **(Figure 5.1., spectrum b)**, and an increase in the absorbance around 1753 cm^{-1}. Subsequently, the EDC/NHS-activated poly(MES) was allowed to react with aminobutyl-NTA. This reaction resulted in a loss of the absorbances due to the active ester, and a shifting of the peak at 1753 cm^{-1} back to 1740 cm^{-1} **(Figure 5.1., spectrum c)**. The new absorbance at 1680 cm^{-1} suggests NTA immobilization, as it likely results from a combination of absorbance due to the carboxylate groups of NTA and amide bonds formed between poly(MES) and NTA. The broad peak around 1600 cm^{-1} could be due to carboxylate groups from either NTA or hydrolyzed active esters. After immersion of NTA-derivatized poly(MES) films in 0.1 M $CuSO_4$, there was no dramatic change in the IR spectrum.

We examined the kinetics of room-temperature, surface-initiated MES polymerization using several catalyst systems **(Figure 5.2.)**. Usually, ATRP maintains a low concentration of active radicals to provide control over molecular mass and polydispersities, and the rate of ATRP is low. However, the use of HMTETA or Me_4Cyclam/dnNbpy as ligands for the Cu catalyst systems yields unusually rapid film growth and high film thicknesses. The decline in film growth rate with time for these

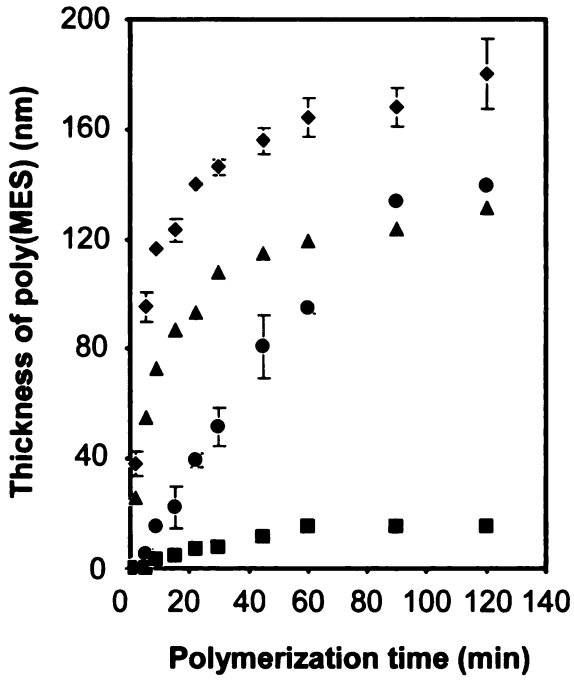

Figure 5.2. Evolution of ellipsometric thickness with time for surface-initiated polymerization of MES using HMTETA (diamonds); Me_4Cyclam)/dnNbpy (triangles); Me_6TREN (circles) and bpy (squares) catalyst systems. The room-temperature, aqueous polymerizations occurred on Au-coated Si, and each point represents a different film. The diamonds and circles show the average of 3 independent runs, and the error bars correspond to the standard deviation.

systems suggests a relatively high radical concentration that leads to rapid polymerization as well as some termination. Compared to HMTETA and Me_4Cyclam/dnNbpy catalyst systems, polymerizations using Me_6TREN as the Cu ligand were more controlled, as evidenced by a nearly linear increase in thickness with time for the first hour of polymerization. Even with the Me_6TREN catalyst system, however, the brush thickness was >120 nm after 90 min of polymerization. In contrast, polymerizations using bpy as the catalyst ligand yielded <25 nm-thick poly(MES) films. As proposed by Matyjaszewski,[51] multidentate ligands like Me_4Cyclam, Me_6TREN and HMTETA may complex the cupric species more efficiently than bpy, shifting the equilibrium towards the Cu(II) species and providing a higher radical concentration and faster polymerization than bpy-Cu catalysis. Previous studies demonstrated that Me_4Cyclam, Me_6TREN and HMTETA Cu complexes are highly active catalysts for solution ATRP at ambient temperature,[52,53] however Me_6TREN provides better control over polymerizations due to a higher deactivation rate.[51,53,54]

5.3.2. Comparison of ATRP of MES, MAA and AA

To determine whether the high rates of film growth are partly due to the relatively high reactivity of MES, we grew films of poly(AA) and poly(MAA) using the CuBr/$CuBr_2$/HMTETA catalyst system. After 2 h of polymerization, poly(AA) and poly(MAA) brush thicknesses were <15 nm and 60 nm, respectively, while the poly(MES) thickness was >170 nm. Notably the rates of polymerization of MES and HEMA are similar **(Figure 5.3.)**, suggesting that the methacrylates have an inherently faster polymerization rate than methacrylic and acrylic acid. Unfortunately, methyl

methacrylate and ethyl methacrylate are not soluble in water, so we could not investigate the polymerization of these monomers under similar conditions.

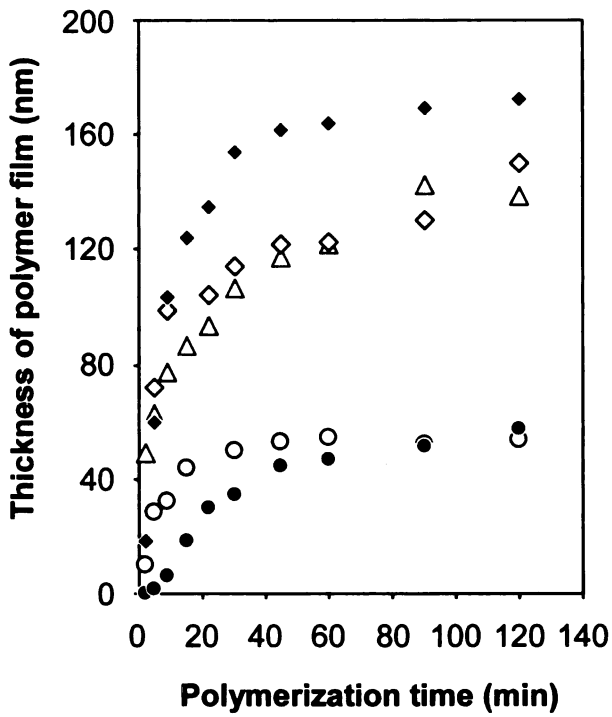

Figure 5.3. Evolution of ellipsometric film thickness with time for surface-initiated polymerization of **(a)** MES inhibited with 750 ppm of MEHQ (filled diamonds) **(b)** MES without inhibitor (hollow diamonds) **(c)** HEMA without inhibitor (hollow triangles) **(d)** MAA inhibited with 250 ppm of MEHQ (filled circles) and **(e)** MAA without inhibitor (hollow circles). Polymerizations were performed at room temperature on initiator-modified Au substrates in aqueous solutions using $CuBr/CuBr_2$/HMTETA as a catalyst. Each point represents a different film. Polymerization of MES or MAA occurred in 10 mL of a mixture of neat monomer and 1 M aqueous NaOH (1:1, v/v) whereas for HEMA, polymerization took place in 1:1, v/v monomer and deionized water.

We should note that during most polymerizations of MES and MAA, the inhibitor (MEHQ) was still present. As shown in **Figure 5.3.**, the initial rate of MAA polymerization increased in the absence of inhibitor, but film growth stopped after 30 min so the overall MAA film thickness (<60 nm) was the same as that obtained in the presence of inhibitor. MES, on the other hand, gave films that were ~15% thicker when polymerized in the presence of inhibitor. Lower initial radical concentrations in the presence of inhibitor could lead to less termination and thicker films with MES. In any case, in the presence or absence of inhibitor, poly(MES) films are much thicker than poly(MAA) films.

To test whether the observed kinetic behavior during film growth is specific to surface-initiated polymerization, we examined solution-phase ATRP of MES and MAA under similar conditions. **Figure 5.4.** shows that both in the presence and absence of inhibitor, MES polymerizes much more rapidly than MAA. Polymerization of inhibitor-free MAA resulted in only 4.2% conversion to poly(MAA) (**Figure 5.4.**, hollow circles), and no detectable MAA polymerization occurred in the presence of inhibitor (**Figure 5.4.**, filled circles). In contrast, polymerization of inhibitor-free MES reached >99.5% conversion in about 7 h. Thus, the faster growth of poly(MES) than poly(MAA) from surfaces is likely a direct result of the different reactivities of the two monomers.

Interestingly, unlike polymerization from a surface, the solution phase polymerization of MES is faster without inhibitor. This difference between solution and surface polymerization of MES presumably occurs because there are many more initiators in solution than on the substrate, so termination by radical recombination is less

important in solution. Additionally, radicals are likely in closer proximity on the surface than in solution.[26]

Figure 5.5. and **Figure 5.6.** show the NMR spectra of the polymerization solutions for MES and MAA polymerization respectively.

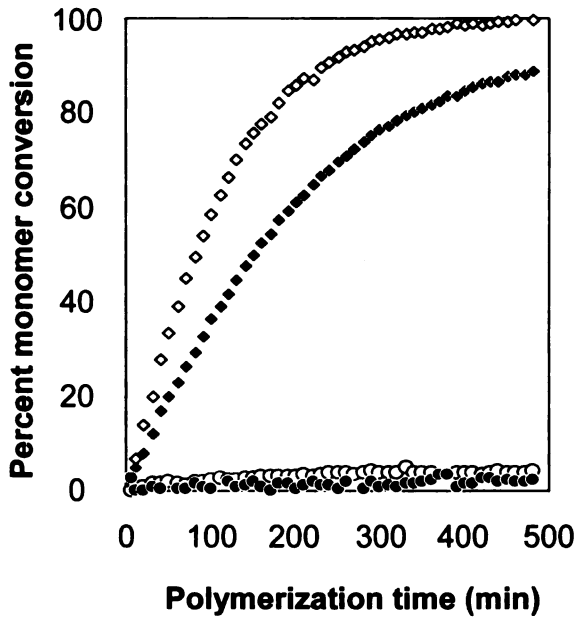

Figure 5.4. Percent monomer conversion as a function of time for solution polymerization of MES without inhibitor (hollow diamonds), MES inhibited with 750 ppm of MEHQ (filled diamonds), MAA without inhibitor (hollow circles), and MAA inhibited with 250 ppm of MEHQ (filled circles). Polymerizations were studied using NMR at room temperature.

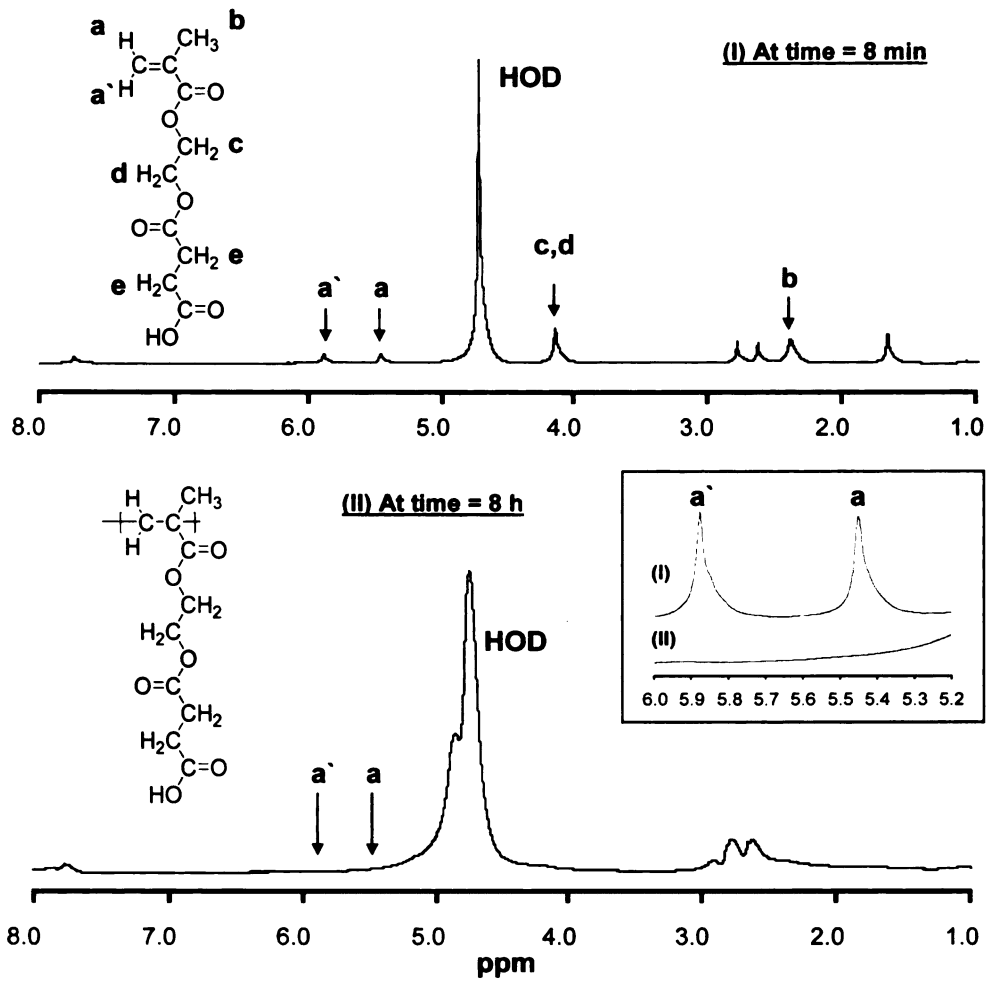

Figure 5.5. ^{1}H NMR spectra of an MES polymerization solution 8 min (I, top) and 8 h (II, bottom) after the addition of initiator. The polymerization solution contained neat MES (without inhibitor), 1 M NaOH in H_2O, and CuBr, $CuBr_2$, and HMTETA in DMF. The sodium salt of α-bromo-*p*-toluic acid was used as the initiator. 0.5 mL of polymerization solution and 50 μL D_2O were added to the NMR tube. The inset contains an expanded view of the region of the spectrum containing peaks due to the alkene protons.

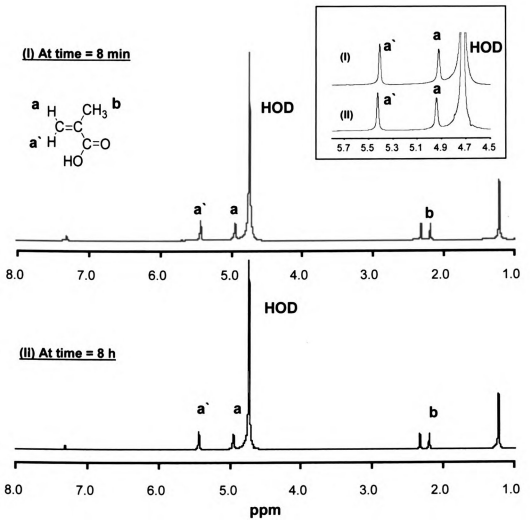

Figure 5.6. ^{1}H NMR spectra of an MAA polymerization solution 8 min (I, top), and 8 h (II, bottom) after the addition of initiator. The polymerization solution contained neat MAA (without inhibitor), 1 M NaOH in H_2O, and CuBr, $CuBr_2$, and HMTETA in DMF. The sodium salt of α-bromo-*p*-toluic acid was used as the initiator. 0.5 mL of polymerization solution and 50 μL D_2O were added to the NMR tube. The inset contains an expanded view of the region of the spectrum containing peaks due to the alkene protons.

5.3.3. Effect of NaOH on MES polymerization

We also examined film growth as a function of the amount of NaOH added to the polymerization solution. **Figure 5.7.** shows that film thicknesses are highest when most of the MES in solution is in the protonated form (little NaOH is added), but even with a 1:1 ratio of NaOH to MES, films with thicknesses >100 nm can form. Thus, both

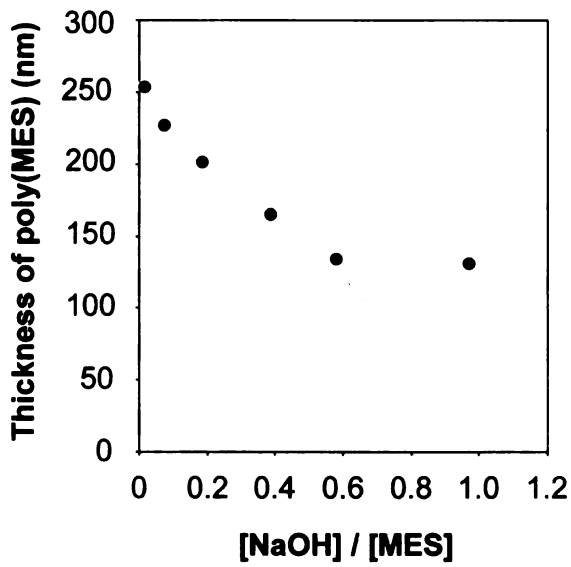

Figure 5.7. Thickness of poly(MES) brushes as a function of the molar ratio of NaOH to MES added to the polymerization solution. The brushes were grown using a 2 h, room temperature polymerization with a CuBr/$CuBr_2$/HMTETA catalyst system.

protonated and deprotonated MES can polymerize, but the protonated form polymerizes faster. This is in agreement with some previous reports that showed that the rate of polymerization of acidic monomers decreases with increasing pH.[55,56] The decrease in rate at high pH presumably occurs because the electrostatic repulsion between growing chains and monomers decreases the rate at which monomers can reach confined radicals.

At NaOH to MES ratios <0.08, the polymerization solution is turbid, and when no NaOH is added, the solution consists of two phases, the denser of which contains MES and most of the catalyst, as discerned by its blue color. Even two-phase polymerizations, when no NaOH is added to the reaction mixture, give film thicknesses similar to those obtained when adding small amounts of NaOH to the solution. (The substrate sits in the MES-rich phase during polymerization.) However, some water in the MES phase is necessary for rapid brush growth,[57] as polymerization from a solution containing only monomer and catalyst gives film thicknesses of 25 nm after 2 h of polymerization.

5.3.4. Protein binding to poly(MES) brushes and their derivatives

To demonstrate the utility of poly(MES) brushes, we examined their ability to bind proteins. Initially, we immersed poly(MES) films on Au-coated Si in 1 mg/mL solutions of lysozyme in 20 mM phosphate buffer (pH 7.2) for 3 h. After removal of the film from solution and rinsing, reflectance FTIR spectroscopy allowed determination of the amount of bound lysozyme using a procedure we developed previously[4] (for more details refer to page no. 60). Briefly, we prepared a linear calibration curve of ellipsometric thickness versus reflectance FTIR amide absorbance (1670 cm^{-1}) for spin-coated lysozyme films on Au-coated Si wafers. Using the calibration curve and the FTIR spectra that reveal immobilized lysozyme (e.g., **Figure 5.8.**c), we calculated protein binding capacity with the assumption that the lysozyme film has a density of 1 g/cm^3. Remarkably, a 55 nm poly(MES) film binds 14.4±0.3 μg lysozyme/cm^2, which is equivalent to ~70 monolayers of lysozyme in the brushes (assuming a monolayer thickness of 2 nm).[58] Ellipsometric measurements also show that the film thickness increases from 55 nm to 205 nm after lysozyme adsorption. This binding capacity is

higher than the 38 monolayers of lysozyme reported to bind to sulfonated poly(glycidyl methacrylate) coatings,[36] and is comparable to the ~80 lysozyme monolayers found to bind to poly(AA) brushes prepared by hydrolysis of poly(*tert*-butyl acrylate).[4]

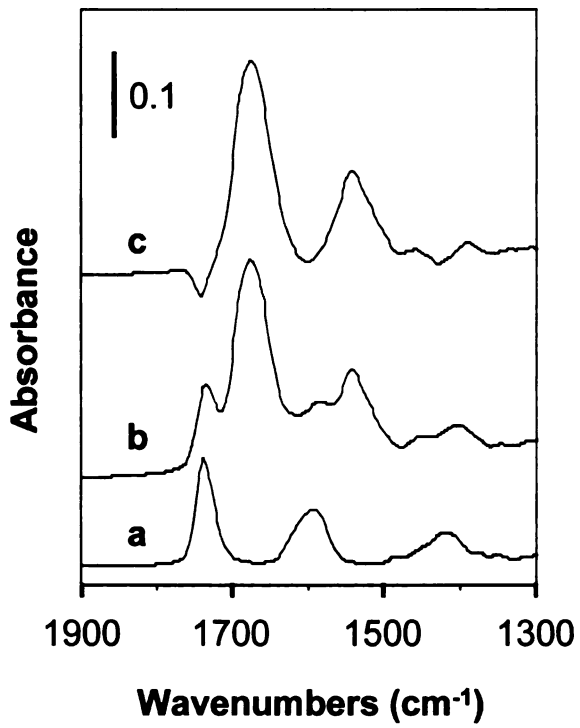

Figure 5.8. Reflectance FTIR spectra of a **(a)** poly(MES) film **(b)** poly (MES)-lysozyme film and **(c)** immobilized lysozyme, which was obtained by subtracting **(a)** from **(b)**. The 55 nm thick poly(MES) film was immersed in 1.0 mg/mL lysozyme solution for 3 h and then rinsed with buffers and ethanol.

Building on these promising results, we investigated the adsorption of BSA in poly(MES) brushes modified with NTA-Cu^{2+} complexes **(Scheme 5.2.)**. This adsorption occurs through a metal-affinity interaction between BSA and the Cu(II) complex. We immersed poly(MES)-NTA-Cu^{2+} films overnight in a solution containing 1 mg/mL BSA and then thoroughly rinsed these films with buffers and solvent. As seen in **Figure 5.9.**, 55 nm and 85 nm poly(MES) films derivatized with NTA-Cu^{2+} had BSA binding capacities of 6.8 and 7.2 $\mu g/cm^2$, respectively, which is equivalent to 17 and 18 monolayers of BSA in poly(MES) brushes (assuming a monolayer thickness of 4 nm).[59] These high binding capacities and the fact that BSA binding initially increases with brush thickness suggest that binding occurs both at the film-solution interface and inside the brushes. However steric hindrance to binding may result in the plateau in adsorption capacity at thicknesses >60 nm **(Figure 5.9.)**. The poly(MES) binding

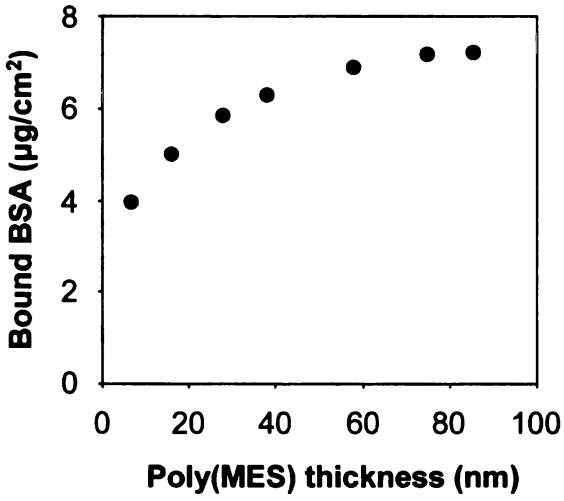

Figure 5.9. BSA binding capacity as a function of poly(MES) film thickness. The poly(MES) films were derivatized with NTA-Cu^{2+} complexes, and the amount of bound BSA was determined using reflectance FTIR spectroscopy.

capacity is similar to that reported previously for poly(AA), but the poly(MES) can be synthesized in a rapid, one-step procedure.[4]

5.4. Conclusions

Surface-initiated aqueous ATRP enables rapid growth of poly(MES) brushes under gentle conditions that should allow formation of films on a wide range of substrates. Both on a surface and in solution, polymerization of MES occurs much faster than polymerization of MAA, presumably because methacrylates are more reactive than MAA or AA. HEMA, another water-soluble methacrylate, shows brush growth rates similar to those of MES. Moreover, poly(MES) brushes and their derivatives are capable of binding many monolayers of BSA as well as lysozyme.

5.5. References:

(1) Singh, N.; Cui, X.; Boland, T.; Husson, S. M. *Biomaterials* **2007**, *28*, 763-771.

(2) Ghosh, P.; Amirpour, M. L.; Lackowski, W. M.; Pishko, M. V.; Crooks, R. M. *Angewandte Chemie International Edition* **1999**, *38*, 1592-1595.

(3) Cullen, S. P.; Liu, X.; Mandel, I. C.; Himpsel, F. J.; Gopalan, P. *Langmuir* **2008**, *24*, 913-920.

(4) Dai, J.; Bao, Z.; Sun, L.; Hong, S. U.; Baker, G. L.; Bruening, M. L. *Langmuir* **2006**, *22*, 4274-4281.

(5) Tsarevsky, N. V.; Braunecker, W. A.; Vacca, A.; Gans, P.; Matyjaszewski, K. *Macromolecular Symposium* **2007**, *248*, 60-70.

(6) Bütün, V.; Lowe, A. B.; Billingham, N. C.; Armes, S. P. *Journal of the American Chemical Society* **1999**, *121*, 4288-4289.

(7) Zhang, Q.; Remsen, E. E.; Wooley, K. L. *Journal of the American Chemical Society* **2000**, *122*, 3642-3651.

(8) Xu, J.; Bhattacharyya, D. *Industrial & Engineering Chemistry Research* **2007**, *46*, 2348-2359.

(9) Balastre, M.; Li, F.; Schorr, P.; Yang, J. C.; Mays, J. W.; Tirrell, M. V. *Macromolecules* **2002**, *35*, 9480-9486.

(10) Mykytiuk, J.; Armes, S. P.; Billingham, N. C. *Polymer Bulletin* **1992**, *29*, 139-145.

(11) Zhang, H.; Rühe, J. *Macromolecular Rapid Communications* **2003**, *24*, 576-579.

(12) Haddleton, D. M.; Crossman, M. C.; Dana, B. H.; Duncalf, D. J.; Heming, A. M.; Kukulj, D.; Shooter, A. J. *Macromolecules* **1999**, *32*, 2110-2119.

(13) Rannard, S. P.; Billingham, N. C.; Armes, S. P.; Mykytiuk, J. *European Polymer Journal* **1993**, *29*, 407-414.

(14) Bao, Z.; Bruening, M. L.; Baker, G. L. *Journal of the American Chemical Society* **2006**, *128*, 9056-9060.

(15) Matyjaszewski, K.; Miller, P. J.; Shukla, N.; Immaraporn, B.; Gelman, A.; Luokala, B. B.; Siclovan, T. M.; Kickelbick, G.; Vallant, T.; Hoffmann, H.; Pakula, T. *Macromolecules* **1999**, *32*, 8716-8724.

(16) Boyes, S. G.; Akgun, B.; Brittain, W. J.; Foster, M. D. *Macromolecules* **2003**, *36*, 9539-9548.

(17) Treat, N. D.; Ayres, N.; Boyes, S. G.; Brittain, W. J. *Macromolecules* **2006**, *39*, 26-29.

(18) Biesalski, M.; Rühe, J. *Macromolecules* **2003**, *36*, 1222-1227.

(19) Hu, S.; Ren, X.; Bachman, M.; Sims, C. E.; Li, G. P.; Allbritton, N. L. *Analytical Chemistry* **2004**, *76*, 1865-1870.

(20) Ulbricht, M.; Yang, H. *Chemistry of Materials* **2005**, *17*, 2622-2631.

(21) Rahane, S. B.; Floyd, J. A.; Metters, A. T.; Kilbey, S. M., II *Advanced Functional Materials* **2008**, *18*, 1232-1240.

(22) Matyjaszewski, K. Overview: fundamentals of controlled living radical polymerization, *ACS Symposium Series* **1998**, *685*, 2-30.

(23) Matyjaszewski, K. Comparison and classification of controlled/living radical polymerizations, *ACS Symposium Series* **2000**, *768*, 2-26.

(24) Chung, I.-D.; Britt, P.; Xie, D.; Harth, E.; Mays, J. *Chemical Communications* **2005**, 1046-1048.

(25) Tsarevsky, N. V.; Pintauer, T.; Matyjaszewski, K. *Macromolecules* **2004**, *37*, 9768-9778.

(26) Kim, J.-B.; Huang, W.; Miller, M. D.; Baker, G. L.; Bruening, M. L. *Journal of Polymer Science Part A: Polymer Chemistry* **2003**, *41*, 386-394.

(27) Keoshkerian, B.; Georges, M. K.; Boils-Boissier, D. *Macromolecules* **1995**, *28*, 6381-6382.

(28) Vo, C.-D.; Iddon, P. D.; Armes, S. P. *Polymer* **2007**, *48*, 1193-1202.

(29) Ashford, E. J.; Naldi, V.; O'Dell, R.; Billingham, N. C.; Armes, S. P. *Chemical Communications* **1999**, 1285-1286.

(30) Wang, X. S.; Jackson, R. A.; Armes, S. P. *Macromolecules* **2000**, *33*, 255-257.

(31) Singh, N.; Wang, J.; Ulbricht, M.; Wickramasinghe, S. R.; Husson, S. M. *Journal of Membrane Science* **2008**, *309*, 64-72.

(32) Sankhe, A. Y.; Husson, S. M.; Kilbey, S. M., II *Macromolecules* **2006**, *39*, 1376-1383.

(33) Sankhe, A. Y.; Husson, S. M.; Kilbey, S. M., II *Journal of Polymer Science Part A: Polymer Chemistry* **2007**, *45*, 566-575.

(34) Dong, R.; Krishnan, S.; Baird, B. A.; Lindau, M.; Ober, C. K. *Biomacromolecules* **2007**, *8*, 3082-3092.

(35) Tugulu, S.; Barbey, R.; Harms, M.; Fricke, M.; Volkmer, D.; Rossi, A.; Klok, H.-A. *Macromolecules* **2007**, *40*, 168-177.

(36) Kawai, T.; Saito, K.; Lee, W. *Journal of Chromatography B: Analytical Technologies in the Biomedical and Life Sciences* **2003**, *790*, 131-142.

(37) Singh, N.; Husson, S. M.; Zdyrko, B.; Luzinov, I. *Journal of Membrane Science* **2005**, *262*, 81-90.

(38) Kurosawa, S.; Aizawa, H.; Talib, Z. A.; Atthoff, B.; Hilborn, J. *Biosensors and Bioelectronics* **2004**, *20*, 1165-1176.

(39) Jain, P.; Sun, L.; Dai, J. H.; Baker, G. L.; Bruening, M. L. *Biomacromolecules* **2007**, *8*, 3102-3107.

(40) Roper, D. K.; Lightfoot, E. N. *Journal of Chromatography A* **1995**, *702*, 3-26.

(41) Lee, W. C.; Lee, K. H. *Analytical Biochemistry* **2004**, *324*, 1-10.

(42) Arenkov, P.; Kukhtin, A.; Gemmell, A.; Voloshchuk, S.; Chupeeva, V.; Mirzabekov, A. *Analytical Biochemistry* **2000**, *278*, 123-131.

(43) MacBeath, G.; Schreiber, S. L. *Science* **2000**, *289*, 1760-1763.

(44) Phizicky, E.; Bastiaens, P. I. H.; Zhu, H.; Snyder, M.; Fields, S. *Nature* **2003**, *422*, 208-215.

(45) Zhu, H.; Bilgin, M.; Bangham, R.; Hall, D.; Casamayor, A.; Bertone, P.; Lan, N.; Jansen, R.; Bidlingmaier, S.; Houfek, T.; Mitchell, T.; Miller, P.; Dean, R. A.; Gerstein, M.; Snyder, M. *Science* **2001**, *293*, 2101-2105.

(46) Dai, J. H.; Baker, G. L.; Bruening, M. L. *Analytical Chemistry* **2006**, *78*, 135-140.

(47) Shah, R. R.; Merreceyes, D.; Husemann, M.; Rees, I.; Abbott, N. L.; Hawker, C. J.; Hedrick, J. L. *Macromolecules* **2000**, *33*, 597-605.

(48) Ciampoli.M; Nardi, N. *Inorganic Chemistry* **1966**, *5*, 1150.

(49) Huang, W. X.; Kim, J. B.; Bruening, M. L.; Baker, G. L. *Macromolecules* **2002**, *35*, 1175-1179.

(50) Zheng, Y.; Michigan State University, 2007; Vol. Ph.D. Dissertation.

(51) Matyjaszewski, K. *Current Organic Chemistry* **2002**, *6*, 67-82.

(52) Pintauer, T.; Matyjaszewski, K. *Coordination Chemistry Reviews* **2005**, *249*, 1155-1184.

(53) Tsarevsky, N. V.; Matyjaszewski, K. *Journal of Polymer Science Part A: Polymer Chemistry* **2006**, *44*, 5098-5112.

(54) Xia, J. H.; Gaynor, S. G.; Matyjaszewski, K. *Macromolecules* **1998**, *31*, 5958-5959.

(55) Niwa, M.; Date, M.; Higashi, N. *Macromolecules* **1996**, *29*, 3681-3685.

(56) Matyjaszewski, K.; Xia, J. H. *Chemical Reviews* **2001**, *101*, 2921-2990.

(57) Wang, X.-S.; Lascelles, S. F.; Jackson, R. A.; Armes, S. P. *Chemical Communications* **1999**, 1817-1818.

(58) Tsuneda, S.; Shinano, H.; Saito, K.; Furusaki, S.; Sugo, T. *Biotechnology Progress* **1994**, *10*, 76-81.

(59) Carter, D. C.; He, X. M.; Munson, S. H.; Twigg, P. D.; Gernert, K. M.; Broom, M. B.; Miller, T. Y. *Science* **1989**, *244*, 1195-1198.

Chapter 6

His-tagged protein purification with high capacity affinity membranes containing functionalized poly(MES) brushes

6.1. Introduction

Chapter 3 demonstrates the use of polymer brush-modified nylon membranes for purification of His-tagged proteins from cell extracts. Unfortunately, nylon membranes modified with poly(HEMA)-NTA-Ni^{2+} brushes have a relatively low protein binding capacity (25 mg protein/cm^3 of membrane), perhaps because the organic solvents employed in the brush synthesis and derivatization partially damage the membrane structure. To avoid the use of organic solvents, we created a completely aqueous procedure for growth of polymer brushes inside polymeric membranes (chapter 4). However, despite the successful polymerization of HEMA with aqueous initiation from surfaces, the creation of protein-binding brushes requires conversion of hydroxyl groups in poly(HEMA) to carboxylic acid moieties, and this involves reaction of poly(HEMA) with succinic anhydride in an organic solvent that may damage the membrane. To overcome this problem, we developed the surface-initiated aqueous ATRP of an acidic monomer, MES, as a rapid, one-step route to polyacid brushes (see chapter 5 for details). This procedure avoids the need to react the brush with succinic anhydride in an organic solvent. Also, poly(MES) brushes and their derivatives exhibit high protein-binding capacities. Thus, modification of polymeric membranes with poly(MES) should allow for high-capacity purification of His-tagged proteins directly from a cell extract. This chapter describes the growth, derivatization, and characterization of poly(MES) brushes

inside porous nylon membranes, and the use of these modified membranes as protein absorbers. Protein breakthrough curves show remarkable HisU, BSA and lysozyme binding capacities of 85, 80 ± 2 and 118 ± 8 mg protein per cm^3 of membrane, respectively. (The lysozyme binds to poly(MES) via ion-exchange interactions, whereas BSA binds to poly(MES)-NTA-Cu^{2+} via affinity interactions). Most importantly, the poly(MES)-NTA-Ni^{2+}-modified membranes allow isolation of His-tagged CRALBP directly from a cell extract.

6.2. Experimental section

6.2.1. Materials

Hydroxylated (LoProdyne® LP) nylon membranes with 1.2 and 5.0 μm-diameter surface pores were obtained from Pall Corporation; nylon microfiltration membranes (non-hydroxylated, 1.2 μm) were received from GE Water & Process Technologies; and regenerated cellulose membranes (RC 60, 1.0 μm) were purchased from Whatman. All membranes were cut into 25 mm diameter discs prior to modification or use. 2-Bromoisobutyryl bromide (98%), CuBr (99.999%), $CuBr_2$ (99%), MES (Aldrich, inhibited with 750 ppm MEHQ), EDC, NHS, EDTA, imidazole (99%), TWEEN-20 surfactant, lysozyme, and BSA were used as received from Sigma Aldrich. Me_6TREN (ATRP Solutions), $CuSO_4 \cdot 5H_2O$ (CCI), $NiSO_4 \cdot 5H_2O$ (Columbus Chemical), NaH_2PO_4 (CCI), Na_2HPO_4 (Aldrich), aminobutyl NTA (Fluka), NaOH (Spectrum), and Coomassie protein assay reagent (Pierce) were also used without purification. Tetrahydrofuran (THF, Jade Scientific Inc., anhydrous, 99%) was distilled and stored over molecular sieves. Trichlorosilane initiator (11-(2-bromo-2-methyl)propionyloxy)undecyltrichlorosilane) was synthesized according to a literature

procedure.[1] Buffers were prepared using analytical grade chemicals and deionized (Milli-Q, 18.2 MΩ cm) water.

6.2.2. Initiator attachment in porous polymer membranes

6.2.2.-a. Initiator attachment in hydroxylated (LoProdyne® LP) nylon membranes

A LoProdyne® LP nylon membrane was cleaned with UV/ozone (Boekel model 135500) for 10 min, and placed inside a home-built Teflon cell. Initiator attachment occurred by circulating 1 mM trichlorosilane initiator in 20 mL of anhydrous THF through the membrane for 2 h at a flow rate of 3 mL/min, followed by subsequent rinsing with 20 mL of ethanol at the same flow rate.

6.2.2.-b. Initiator attachment in non-hydroxylated nylon membranes

Prior to modification with initiator, the surface amide groups in the non-hydroxylated nylon membranes (GE Water & Process Technologies) were activated according to a procedure described by Xu and coworkers.[2] Briefly, 30 membranes were immersed for 12 h in a 60 °C solution containing 50 mL formaldehyde and 1 mL of 85% (w/v) phosphoric acid. This resulted in conversion of the nylon membrane surface to N-methylol polyamide (or nylon-OH) **(Scheme 6.1.(a))**. After the reaction, the activated membranes were washed with copious amounts of water and dried overnight under vacuum. Initiator attachment in these membranes occurred as described above by circulating 1 mM trichlorosilane initiator in 20 mL of anhydrous THF through the membrane for 2 h and rinsing with 20 mL of ethanol **(Scheme 6.1.(b))**.

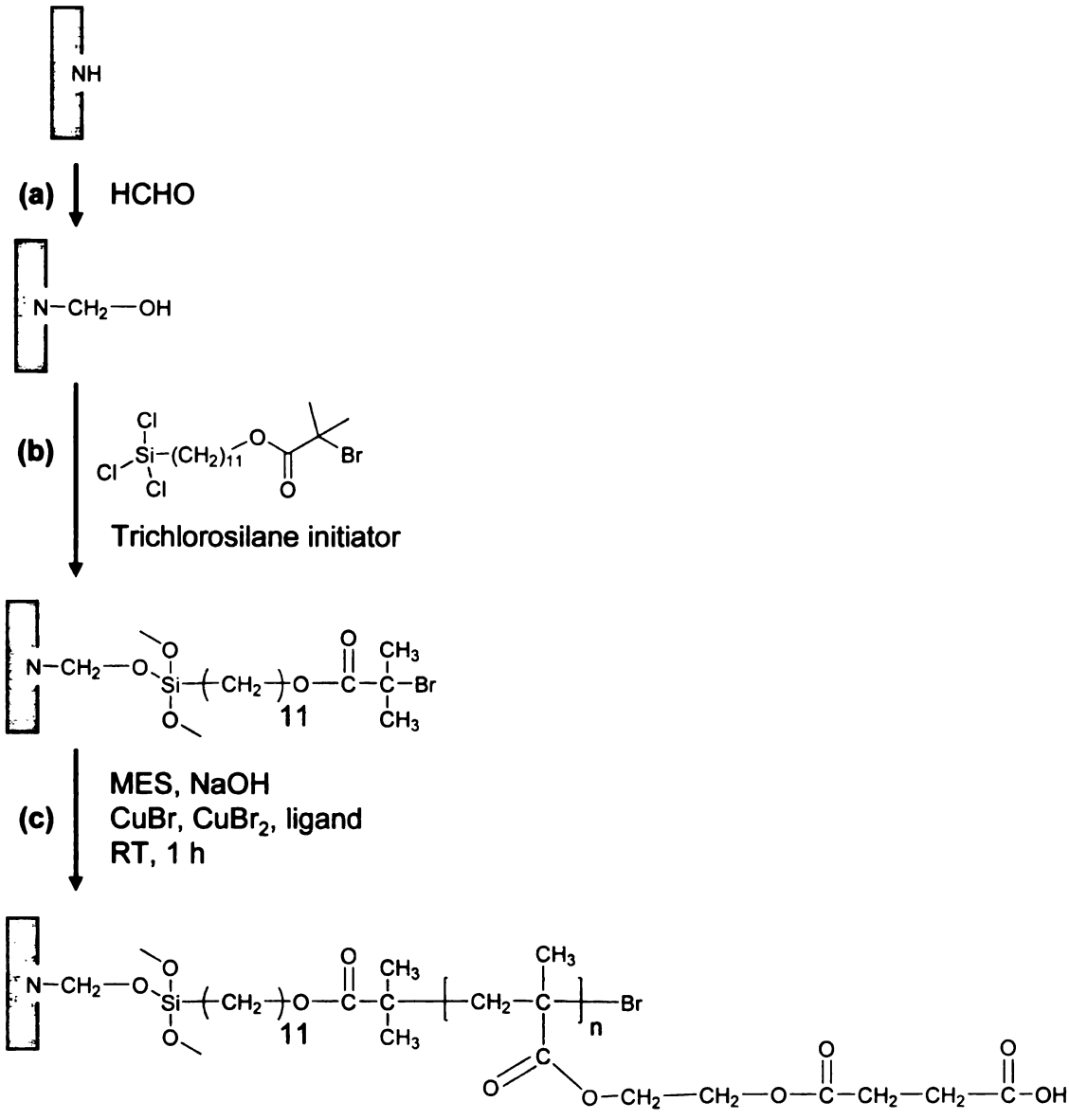

Scheme 6.1. Schematic illustration of **(a)** activation of the amide groups in a nylon membrane to introduce hydroxyl functionalities **(b)** trichlorosilane initiator immobilization on the hydroxylated membrane and **(c)** polymerization of MES from initiator-modified membrane.

6.2.3. Polymerization of MES in porous nylon membranes

To prepare polymerization solutions, 10 mL of a mixture of neat MES monomer and 1 M aqueous NaOH (1:1, v/v) was first degassed with three freeze-pump-thaw cycles. A 1 mL solution of DMF containing CuBr (2mM), $CuBr_2$ (1 mM), and Me_6TREN (6 mM)[3-5] was similarly degassed, and in a N_2-filled glove bag, this solution of catalyst was mixed with the monomer/NaOH solution. Polymerization of MES occurred in the glove bag by circulating this solution through the initiator-modified membrane at a flow rate of 0.9 mL/min **(Scheme 6.1.(c))**. *Unless mentioned otherwise, the polymerization time was 1 h.* After polymerization, the membrane was cleaned by passing ethanol (20 mL) followed by 20 mL of deionized water (Milli-Q, 18.2 MΩ cm, 20 mL) through the membrane at a flow rate of 1-2 mL/min. (Acetone should not be used with nylon membrane as it partially damages the membrane structure).

6.2.4. Poly(MES) derivatization and protein binding

Chapter 5 describes the derivatization procedure, which is shown in **Scheme 5.2.** Briefly, the carboxylic acid groups of poly(MES) were activated by circulating an aqueous solution containing NHS (0.1 M) and EDC (0.1 M) through a poly(MES)-modified nylon membrane for 1 h. This was followed by rinsing sequentially with 20 mL of deionized water and 20 mL of ethanol through the membrane. An aqueous solution of aminobutyl NTA (0.1 M, pH 10.2) was then flowed through the NHS-modified membranes for 1 h, and the membrane was subsequently rinsed with 20 mL of water. Finally, the NTA-Cu^{2+} (or Ni^{2+}) complex was formed by circulating aqueous 0.1 M $CuSO_4$ (or $NiSO_4$) through the membrane for 2 h followed by rinsing with water followed by ethanol (20 mL each). The membrane was dried with N_2 prior to protein binding.

To study lysozyme binding, a solution of lysozyme (1 mg/mL) in 20 mM phosphate buffer (pH 7.2) was pumped through the poly(MES)-modified membrane using a peristaltic pump (flow rate ~ 1 mL/min), and the permeate was collected for analysis at specific time intervals. Subsequently, the membrane was rinsed with 20 mL of pH 7.2 washing buffer I (20 mM phosphate buffer containing 0.1% Tween-20 surfactant and 0.15 M NaCl) followed by 20 mL of phosphate buffer. The protein was then eluted using 5-10 mL of 20 mM phosphate buffer (pH 7.2) containing 1 M potassium thiocyanate.

For BSA binding, a membrane modified with poly(MES)-NTA-Cu^{2+} was used. A solution of 1 mg/mL BSA in 20 mM phosphate buffer (pH 7.2) was pumped through the poly(MES)-NTA-Cu^{2+}-modified membrane using a peristaltic pump at various flow rates (section **6.3.2.-c.)**, and the permeate was collected for analysis at specific time intervals. Subsequently, the membrane was rinsed with 20 mL of pH 7.2 washing buffer I followed by 20 mL of phosphate buffer. The protein was then eluted using 5-10 mL of a solution containing 20 mM sodium phosphate, 0.5 M NaCl, and 0.5 M imidazole at pH 7.2. Cu^{2+} was later eluted using a 50 mM EDTA solution (pH 7.2), and the poly(MES)-NTA film was recharged with Cu^{2+} prior to reuse.

Prior to purification of His-tagged CRALBP (36 kD) that was over-expressed in *E. coli*, the cells were lysed with sonication and centrifuged at 4 °C (Dr. James Geiger kindly provided the cell extracts.) Supernatant (1.25 mL) was added to 3.75 mL of 20 mM, pH 7.2 phosphate buffer that contained 10 mM imidazole and 300 mM NaCl. This solution was pumped through the poly(MES)-NTA-Ni^{2+} modified nylon membrane in an amicon 8010 cell at a pressure less than 6.9×10^3 Pascal (1 psig) at room temperature. The

flow rate was 1.2 mL of extract/min. Subsequently, the membrane was rinsed with 20 mL of washing buffer I followed by 20 mL of washing buffer II (pH 7.2, 20 mM phosphate buffer containing 45 mM imidazole and 0.15 M NaCl), and protein was eluted using a pH 7.2 solution containing 20 mM sodium phosphate, 0.5 M NaCl, and 0.5 M imidazole at pH 7.2.

In CRALBP purification with the spin-trap column, 1.25 mL of cell-free extract containing over-expressed His-tagged CRALBP was added to 3.75 mL of 20 mM phosphate buffer (pH 7.2) that contained 10 mM imidazole and 300 mM NaCl. The solution was loaded onto the spin-trap column (in 500 μL fractions, 10 times) and the column was centrifuged. This was followed by rinsing with 20 mL pH 7.2 washing buffer I and with 20 mL pH 7.2 washing buffer II. The protein was then eluted using a 600 μL solution containing 20 mM sodium phosphate, 0.5 M NaCl, and 0.5 M imidazole at pH 7.2.

6.2.5. Characterization of brush growth and derivatization

Film growth on polymer membranes was verified using attenuated total reflectance (ATR) FTIR spectroscopy (Perkin Elmer Spectrum One Instrument, air background) as well as field-emission scanning electron microscopy (FESEM, Hitachi S-4700II equipped with an EDAX Phoenix energy dispersive X-ray spectrometer system, acceleration voltage of 15V).

6.2.6. Protein quantification

To determine the amount of protein eluted from the modified membrane, 50 μL of permeate was added to 2.95 mL of a solution of Coomassie reagent, and the mixture was shaken a few times and allowed to react for 5 min at room temperature. The UV/vis absorbance spectra of these solutions were then obtained with a Perkin-Elmer UV/Vis (model Lambda 40) spectrophotometer. A calibration curve for the absorbance of lysozyme, BSA and HisU at 595 nm was prepared using a series of protein solutions (concentration range of 100 μg to 1 mg of protein per mL) that were mixed with Coomassie reagent in a 50 μL to 2.95 mL ratio. All spectra were measured against a Coomassie reagent background.

6.2.7. Determination of protein purity by SDS-PAGE

The protein solutions were analyzed by SDS-PAGE with a 16% cross-linked separating gel and a 4% cross-linked stacking gel (acrylamide). Protein bands were visualized using standard silver staining[6] or coomassie blue staining[7] procedures.

6.3. Results and discussion

6.3.1. Characterization of poly(MES)-derivatized membranes

To form brush-modified membranes, poly(MES) was grown from ATRP initiators that were immobilized via silanization within the porous polymer membrane (**Scheme 6.1.b.**). The brushes were derivatized as shown in chapter 5, **Scheme 5.2.**, with reactant solutions being circulated through the membrane using a peristaltic pump. **Figure 6.1.** shows the ATR-FTIR spectra of a nylon membrane (a) before and after (b) polymerization of MES, (c) subsequent reaction with NHS/EDC, and (d) derivatization with aminobutyl NTA. The IR-spectrum of the bare nylon membrane contains dominant

amide I and amide II peaks at 1630 and 1533 cm^{-1}, respectively **(Figure 6.1., spectrum (a))**. The growth of poly(MES) is evident by the appearance of a small carbonyl peak at 1723 cm^{-1} **(Figure 6.1., spectrum (b))**. Passing a mixture of EDC and NHS in water through the membrane converted –COOH groups to succinimidyl esters. Peaks due to the succinimide ester appeared at 1810 and 1779 cm^{-1} **(Figure 6.1., spectrum (c))**. Subsequently, the EDC/NHS-activated poly(MES) was allowed to react with aminobutyl-NTA. This reaction resulted in a loss of the absorbance due to the succinimide ester, **(Figure 6.1., spectrum (d))**.

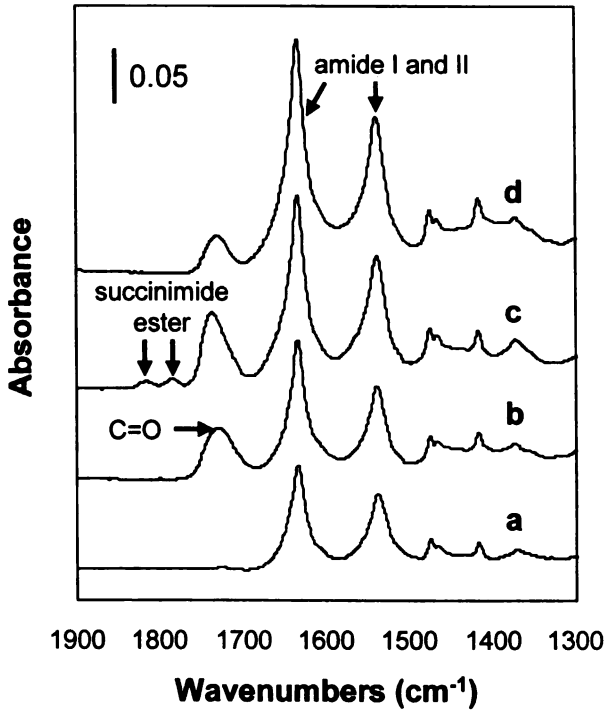

Figure 6.1. ATR-FTIR spectra of a hydroxyl functionalized nylon membrane before (**a**) and after the following sequential steps: (**b**) formation of poly(MES) brushes inside the membrane; (**c**) activation with EDC/NHS; (**d**) reaction with aminobutyl NTA.

Using a constant pressure of 6.9×10^4 Pascal (10 psig), we also monitored the changes in pure water flux through the membrane before and after each derivatization step. A bare nylon membrane with a 1.2 μm nominal filtration cut off shows a pure water flux of 71 ± 7 mL/cm^2 min, but after modification with poly(MES), the flux drops to 14 ± 3 mL/cm^2 min presumably due to the resistance to the flow of water by highly swollen poly(MES) brushes. Derivatization of poly(MES) with NHS gives an increase in water flux to 56 ± 2 mL/cm^2 min, which is consistent with a decreased brush swelling after formation of the succinimide ester. The hydrophilicity of the brushes increases after immobilization of aminobutyl NTA, and the water flux decreases to 0.38 ± 0.22 mL/cm^2 min. In addition to being hydrophilic, the swollen poly(MES)-NTA brushes have a higher molecular mass than poly(MES), which may also lead to decline in permeability. Finally after immobilization of Cu^{2+} or Ni^{2+}, the flux increases to 8.6 ± 3 mL/cm^2 min indicating that the metal ion immobilization decreases the swelling of polymer brushes. Nevertheless, the flux through poly(MES)-NTA-Cu^{2+} or poly(MES)-NTA-Ni^{2+} membrane is only 12% of that through a bare nylon membrane, suggesting that the modified polymer swells in water and occupies a significant fraction of the membrane volume. If flow in these spongy membranes could be decreased by the Hagen-Poiseuille law where the flow rate at a constant pressure is proportional to the pore radius to the fourth power, the 88% drop in flux relative to a bare membrane would correspond to a 40% drop in pore radius.

SEM images also corroborate the growth of poly(MES)-NTA-Cu^{2+} brushes in the polymer membranes. The image of a pristine membrane **(Figure 6.2.(a))** contains many open pores, whereas modified pores **(Figure 6.2.(b))** appear much less open, presumably because they are covered with a polymer film.

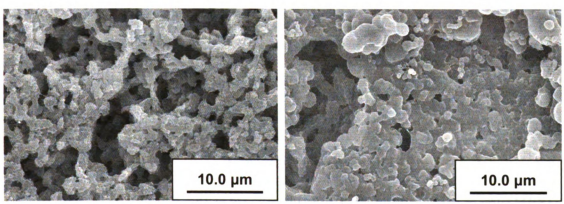

Figure 6.2. SEM images of **(a)** a bare nylon membrane with a 1.2 μm nominal filtration cutoff and **(b)** a similar membrane modified with a poly(MES)-NTA-Cu^{2+} film.

6.3.2. Protein binding to polymer brush-modified membranes

6.3.2.-a. Protein binding capacity in nylon membranes with two different pore sizes

We first studied lysozyme binding to poly(MES) brushes in nylon membranes (LoProdyne® LP) with nominal pore sizes of 1.2 μm and 5.0 μm. In this case, binding to the poly(MES) brushes occurs via ion-exchange interactions. Solutions containing 1 mg/mL of lysozyme in pH 7.2 phosphate buffer were pumped through the membrane, and permeate aliquots were analyzed using a Bradford assay. **Figure 6.3.** shows the breakthrough curves for lysozyme binding to poly(MES)-modified nylon membranes with different pore sizes. The lysozyme binding capacities, as determined by integration

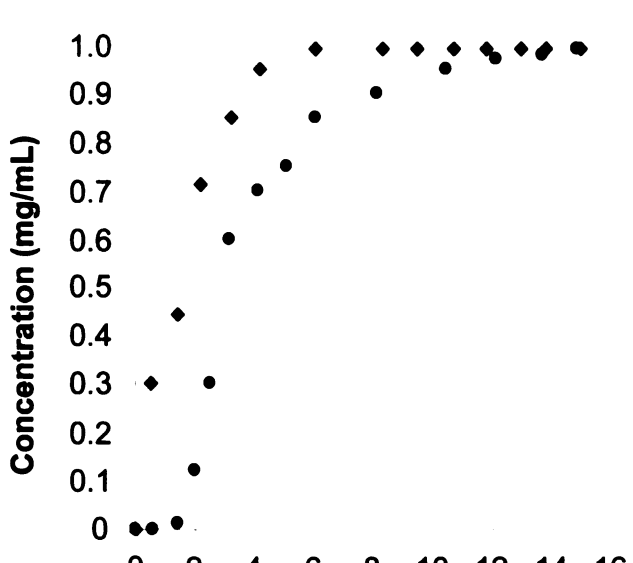

Figure 6.3. Breakthrough curves for absorption of 1 mg/mL lysozyme in poly(MES)-modified nylon membranes with 1.2 μm (circles) and 5.0 μm (diamonds) nominal filtration cutoffs. The permeate flow rates through the 1.2 μm and 5.0 μm membranes were 1.0 mL/min and 1.1 mL/min respectively.

of the differences between the feed concentrations and the permeate concentrations in the breakthrough curves, are 110 mg/cm^3 and 45 mg/cm^3 for nylon membranes with 1.2 μm and 5 μm nominal cutoffs, respectively.

After obtaining the breakthrough curves for lysozyme, the poly(MES)-modified membranes were washed with 20 mL I buffer followed by 20 mL phosphate buffer, and the protein was eluted in 5-10 mL of 20 mM phosphate buffer (pH 7.2) containing 1 M potassium thiocyanate. Analysis of the eluent (using a Bradford assay) showed a lysozyme binding capacity of 118 ± 8 mg/cm^3 and 51 ± 5 mg/cm^3 for 1.2 μm and 5 μm membranes respectively. These values agree well with capacities determined from

breakthrough curves and suggest that essentially all of the lysozyme was eluted from the membrane.

To examine BSA binding, we derivatized the 1.2 μm and 5.0 μm nylon-poly(MES) membranes with NTA-Cu^{2+} complexes as described in section **6.2.4.** and pumped a 1 mg/mL solution of BSA in pH 7.2 phosphate buffer through the membranes. The BSA presumably binds to the brushes via interaction between histidine residues in the protein and the Cu^{2+} complexes in the polymer brush. Analyses of permeate aliquots gave the breakthrough curves in **Figure 6.4.**, and these curves imply BSA binding

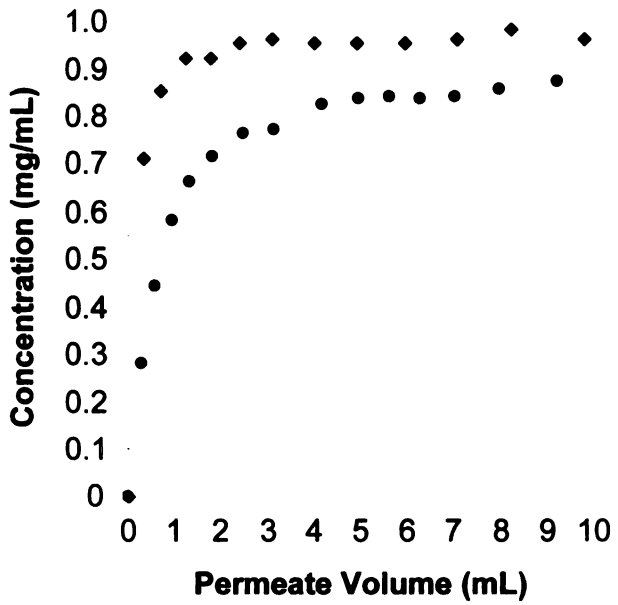

Figure 6.4. Breakthrough curve for absorption of BSA in nominal 1.2 μm (circles) and 5.0 μm (diamonds) nylon membranes modified with poly(MES)-NTA-Cu^{2+} brushes. The flow rates of the 1 mg/mL BSA solution through the 1.2 μm and 5.0 μm membranes were 1.1 mL/min and 0.98 mL/min, respectively.

capacities of 65 mg/cm^3 and 20 mg/cm^3 for 1.2 μm and 5 μm nominal pore-sized nylon membranes, respectively. After obtaining the breakthrough curves, the poly(MES)-NTA-Cu^{2+}-BSA membranes were washed with 20 mL washing buffer I followed by 20 mL phosphate buffer, and the bound BSA was eluted with 5-10 mL of EDTA. Analyses of the eluents using a Bradford assay showed BSA binding capacities of 80 ± 2 mg/cm^3 and 24 ± 4 mg/cm^3 for 1.2 μm and 5 μm membranes respectively. The 20% higher capacities obtained with eluent analysis rather than breakthrough curves likely reflect the higher accuracy inherent in analyzing single eluent solutions rather than multiple solutions for breakthrough curves. The breakthrough curve analysis also involves of the difference between two similar concentrations as the membrane becomes saturated, which is inherently imprecise.

Both the lysozyme and BSA binding capacities indicate that 5 μm membranes have lower protein binding capacities than 1.2 μm membranes. This is not surprising given the more open pore structure of a 5 μm membrane relative to a 1.2 μm membrane **(Figure 6.5.)**. The 5 μm membranes likely have a lower amount of polymer brush per membrane volume and, hence, a lower binding capacity per membrane volume. Smaller volume fractions of brushes in the larger membrane pores are also consistent with the decreases in pure water flux after growth of the poly(MES). At constant pressure ($6.9x10^3$ Pa), water flux through a 5.0 μm membrane modified with poly(MES) is ~35% of the flux through a pristine membrane (flux decreased from 99 ± 7 mL/cm^2 min to 35 ± 0.6 mL/cm^2 min after modification with poly(MES)), whereas as discussed in section **6.3.1.**, water flux through a 1.2 μm membranes modified with poly(MES) is only 20% of that through an unmodified membrane.

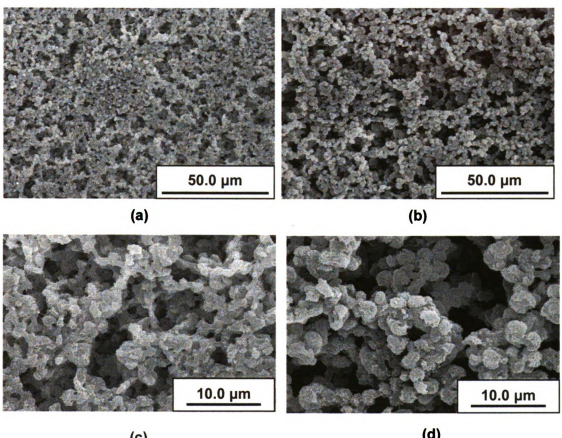

Figure 6.5. SEM images of pristine nylon membranes with **[(a), (c)]** 1.2 µm nominal filtration cutoffs, and **[(b), (d)]** 5.0 µm nominal filtration cutoffs.

6.3.2.-b. Protein binding capacity as a function of polymerization time

Using both breakthrough curves and eluent analysis, we also examined how the lysozyme binding capacity varied with the time employed in MES polymerization in 1.2 μm nylon membranes. **Figure 6.6.** shows that the lysozyme binding capacity increases with increasing MES polymerization times up to 1 h of polymerization and then decrease with longer reaction times. The longer polymerization times should result in thicker polymer brushes (see **Figure 5.2.** in chapter 5), so the initial increase in protein binding with polymerization time most likely results from more protein binding sites in thicker brushes.[8] However increasing the polymerization time beyond 1 h leads to decreased

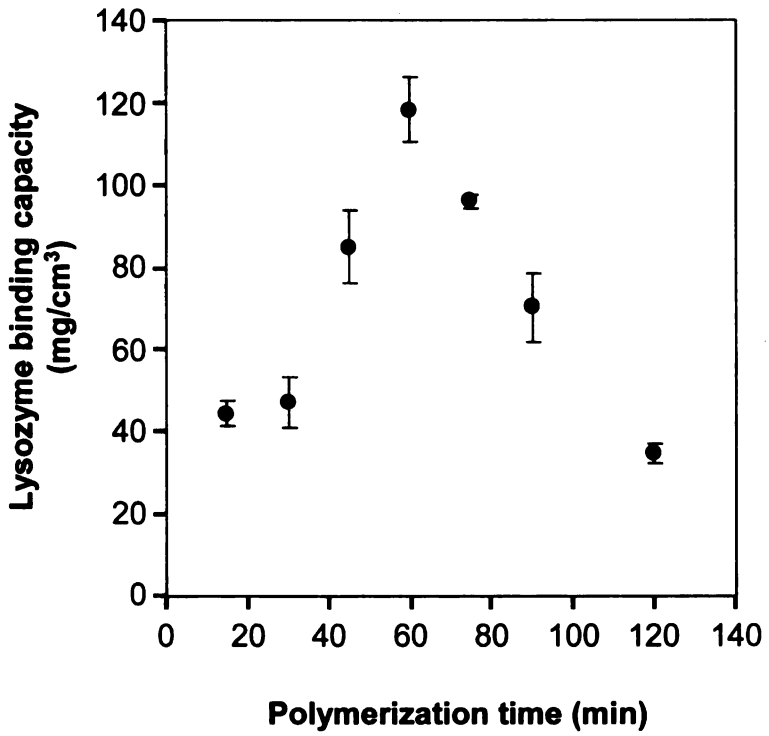

Figure 6.6. Lysozyme binding capacity as a function of MES polymerization time. Each point represents a different membrane and shows an average of three independent runs. The error bars correspond to the standard deviation.

protein binding, which may occur because the polymer brush is so thick and crowded that the interior of the brush is no longer accessible for protein binding.[8] Longer brushes may also block some pores to decrease binding capacity. Nevertheless, a 1 h polymerization yields membranes with a lysozyme binding capacity of 118 ± 8 mg/cm^3. This capacity is 2 to 4-fold higher than the binding capacities of commercial ion-exchange membranes.[9-11]

6.3.2.-c. Protein binding capacity as a function of flow rate

One of the potential advantages of membrane absorbers over column-based separations with nanoporous resins is that convection through membrane pores should minimize diffusion limitations and lead to rapid binding and short purification times. However, if slow diffusion into polymer brushes or slow binding kinetics limit the rate of binding, this advantage may be negated. Slow diffusion into brushes is likely to be more problematic for larger proteins, so we examined protein binding as a function of flow rate for BSA absorption in a membrane containing poly(MES)-NTA-Cu^{2+} brushes. **Figure 6.7.** shows the breakthrough curves for this system at three different flow rates (0.3 mL/min, 0.8 mL/min, 1.1 mL/min). Within the limits of experimental error, the protein binding capacity is independent of flow rate over this range (capacity is ~ 60 mg/cm^3). These results are in agreement with the findings of Knudsen and coworkers, who reported that the dynamic capacity of cation-exchange membranes for antibody purification remained constant even for a 50-fold increase in flow rate.[12] Moreover, increasing the flow rate does not lead to earlier protein breakthrough, although admittedly breakthrough is relatively rapid at all three flow rates. Thus, poly(MES)-NTA-Cu^{2+} modified membranes can be used at a flow rate of 1 mL/min without compromising the protein binding capacity.

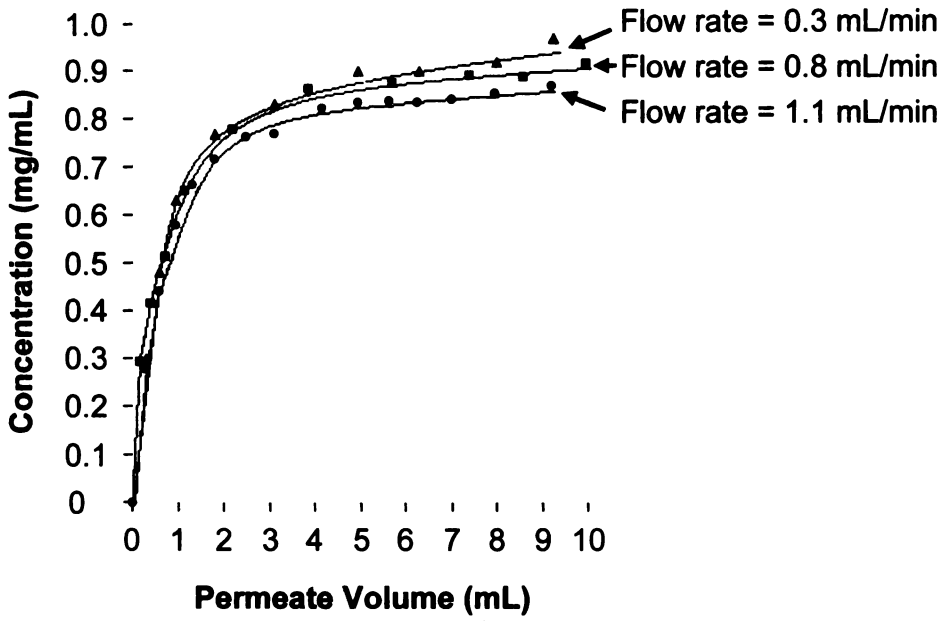

Figure 6.7. Breakthrough curves for absorption of 1 mg/mL BSA in poly(MES)-NTA-Cu^{2+}-modifed nylon membranes (1.2 μm nominal filtration cutoff) at flow rates of 0.3 mL/min (triangles), 0.8 mL/min (squares), and 1.1 mL/min (circles). Curves are added to guide the eye.

6.3.2.-d. Protein binding in membranes with different compositions

To test whether the high protein binding capacity is specific to LoProdyne® LP nylon membranes, we also studied other nylon and regenerated cellulose membranes modified with polymer brushes. Nylon membranes from GE Water & Process Technologies (nominal pore sizes of 1.2 and 5.0 μm) were hydroxylated as described in section **6.2.2.-b** prior to initiator attachment via the resulting hydroxyl groups and subsequent polymerization of MES. Poly(MES)-modified GE membranes showed lysozyme binding capacities of 122 mg/cm^3 and 50 mg/cm^3 for 1.2 μm and 5 μm membranes respectively. After modification with NTA-Cu^{2+}, the BSA binding capacities

were 82 mg/cm^3 and 23 mg/cm^3 for 1.2 μm and 5 μm membranes, respectively. Thus, the protein binding capacities with these membranes are comparable to those obtained with LoProdyne® LP nylon membranes (see section **6.3.2.-a.)**.

In the case of regenerated cellulose, the membranes were initially modified either by reaction with the trichlorosilane initiator (as described above) or using a method described by Singh and coworkers[13] in which 2-bromoisobutyryl bromide reacts with hydroxyl groups. With either method, the membranes showed excessive swelling and shrinking that resulted in cracking. Thus we were unable to examine protein binding to these materials.

6.3.3. HisU binding to poly(MES)-NTA-Ni^{2+} brushes in membranes

Polyhistidine is the most common affinity tag for protein purification,[14,15] and one of the most important goals of this work is the development of polymeric membranes with a high capacity for binding of His-tagged proteins. HisU served as the model protein for determining the binding capacities for His-tagged proteins because it is readily available in high purity. **Figure 6.8.** shows the breakthrough curve for HisU absorption in a nylon (1.2 μm nominal pore size) membrane modified with poly(MES)-NTA-Ni^{2+}. Integration of the differences between the feed concentration and the permeate concentrations in the breakthrough curve gives a binding capacities of 60 mg/cm^3. After measuring the breakthrough curve of HisU, the poly(MES)-NTA-Ni^{2+}-HisU membrane was washed with 20 mL washing buffer I followed by 20 mL phosphate buffer, and HisU was eluted with 5-10 mL elution buffer containing 0.5 M imidazole. Analysis of the eluent using a Bradford assay showed a binding capacity of 85 mg of HisU per cm^3 membrane. The uncertainty in the amount of binding determined from the breakthrough

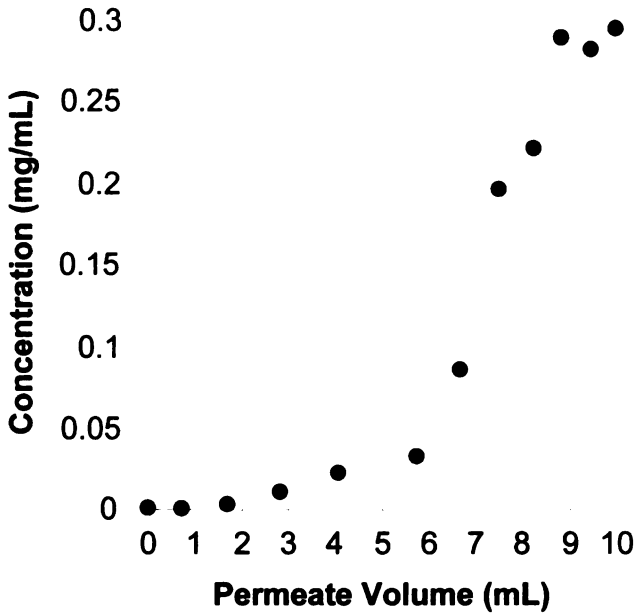

Figure 6.8. HisU breakthrough curve during passage of a 0.3 mg/mL HisU solution through a poly(MES)-NTA-Ni^{2+}-modifed nylon membranes (Loprodyne 1.2 μm nominal filtration cutoff). The permeate flow rate through the membrane was 0.34 mL/min.

curve likely explains that the binding capacity is 25% higher when determined with eluent rather than breakthrough analysis. Nonetheless, the binding capacity of the membrane is as high as 85 mg HisU/cm^3 of membrane, which is at least 6-fold greater than that for affinity membranes reported in the literature.[16-19] The capacity is also higher than that of commercial IMAC resins (maximum reported capacity of 50 mg/mL resin),[20] but we need to test the binding capacity for high molecular weight His-tagged proteins as well.

6.3.4. Purification of His-Tagged CRALBP from cell extracts

The above results show excellent binding of His-tagged proteins by membranes modified with poly(MES)-NTA-Ni^{2+}, but they do not demonstrate whether the

membranes can isolate His-tagged protein from cell extracts. As discussed in chapter 3, nylon membranes modified with poly(HEMA)-NTA-Ni^{2+} brushes are promising for purification of His-tagged proteins directly from a cell extract, but in that case binding capacities were low, presumably because organic solvents damaged the membrane. With improved aqueous syntheses, we examined the performance of nylon membranes modified with poly(MES)-NTA-Ni^{2+} in the purification of His-tagged CRALBP (36 kD) that was over-expressed in *E. coli*. **Figure 6.9.** shows the gel electropherograms of the cell extract **(gels (a) and (b), lane 1)** and the eluent from the membrane **(gel (a), lane 2)**. The eluent contains remarkably pure protein. Unfortunately, we cannot establish the protein binding capacity or elution efficiency in this case because the concentration of

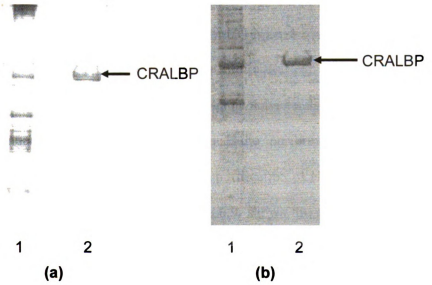

Figure 6.9. SDS-PAGE analysis (coomassie blue staining) of an extract from *E. coli* containing over-expressed His-tagged CRALBP **(gels (a) and (b), lane 1)** and CRALBP purified from the cell extracts using a poly(MES)-NTA-Ni^{2+}-modified membrane **(gel (a), lane 2)** and a spin-trap column **(gel (b), lane 3)**.

CRALBP in the cell extract is unknown.

The goal of this research is to develop affinity membranes for purification of His-tagged proteins in order to overcome limitations in column-based protein separations. To compare the performance of poly(MES)-NTA-Ni^{2+}-modified nylon membrane with commercial spin-trap columns (for details on spin-trap columns refer to chapter 3), His-tagged CRALBP was purified using both systems. The electropherogram of the eluent from a spin-trap column **(Figure 6.9. gel (b), lane 2)** shows high protein purity similar to that obtained with membrane purification. However, membrane-based purification included only 6 min for loading, 5 min for washing, and 2-3 min for elution. Thus purification of His-tagged proteins can be achieved in less than 15 min. On the other hand, spin-trap systems are small scale "columns" with a maximum loading of 600 μL. Thus purification of 5-10 mL of cell extract requires several loading cycles, which increases the time and labor required for the separation. Another advantage of the membrane-based separation is a high capacity (2.9 mg protein/membrane) compared to a spin-trap column (750 μg/column). Hence, these membranes are attractive for rapid, selective purification of His-tagged proteins.

Future studies will focus on reusability of the membranes and comparison of membrane-based purification with relatively large scale Ni-NTA column in terms of purity, protein binding capacity and time of purification.

6.4. Conclusions

This work demonstrates that growth of poly(MES)-NTA-Ni^{2+} brushes inside porous nylon supports yields high-capacity membranes that can selectively purify His-tagged proteins directly from cell extracts. Brush-modified membranes show a binding

capacity of 118 ± 8 mg lysozyme/cm^3 of membrane and 85 mg HisU/cm^3 of membrane along with minimal non-specific adsorption. Lysozyme binding capacity increases with polymerization times up to 1 h and then decreases at longer polymerization times, suggesting that if brushes are too long, binding sites become inaccessible.

Gel electrophoresis results indicate that membranes modified with poly(MES)-NTA-Ni^{2+} can effectively isolate His-tagged CRALBP from a cell-lysate. Importantly these membranes have a pure water flux of 8.6 ± 3 mL/cm^2 min at 6.9 x 10^4 Pascal (10 psig) and support a flow rate of 1.2 mL diluted cell extract/min at a pressure less than 6.9 X 10^3 Pascal (1 psig). Moreover, the purity of the His-tagged protein is comparable to that obtained with commercial spin-trap columns. The membranes have potential advantages over spin-trap and other columns in terms of time and ease of purification as well as binding capacity. Hence, these modified membranes are attractive for high-capacity, selective purification of His-tagged proteins.

6.5. References:

(1) Ciampoli.M; Nardi, N. *Inorganic Chemistry* **1966**, *5*, 1150.

(2) Xu, F. J.; Zhao, J. P.; Kang, E. T.; Neoh, K. G.; Li, J. *Langmuir* **2007**, *23*, 8585-8592.

(3) Jain, P.; Dai, J. H.; Baker, G. L.; Bruening, M. L. *Macromolecules* **2008**, *41*, 8413-8417.

(4) Bao, Z.; Bruening, M. L.; Baker, G. L. *Journal of the American Chemical Society* **2006**, *128*, 9056-9060.

(5) Huang, W. X.; Kim, J. B.; Bruening, M. L.; Baker, G. L. *Macromolecules* **2002**, *35*, 1175-1179.

(6) Wray, W.; Boulikas, T.; Wray, V. P.; Hancock, R. *Analytical Biochemistry* **1981**, *118*, 197-203.

(7) Bertolini, M. J.; Tankersley, D. L.; Schroeder, D. D. *Analytical Biochemistry* **1976**, *71*, 6-13.

(8) Bhut, B. V.; Husson, S. M. *Journal of Membrane Science* **2009**, *337*, 215-223.

(9) Zhao, B.; Brittain, W. J. *Macromolecules* **2000**, *33*, 342-348.

(10) Juang, A.; Scherman, O. A.; Grubbs, R. H.; Lewis, N. S. *Langmuir* **2001**, *17*, 1321-1323.

(11) Wang, J.; Dismer, F.; Hubbuch, J.; Ulbricht, M. *Journal of Membrane Science* **2008**, *320*, 456-467.

(12) Knudsen, H. L.; Fahrner, R. L.; Xu, Y.; Norling, L. A.; Blank, G. S. *Journal of Chromatography A* **2001**, *907*, 145-154.

(13) Singh, N.; Wang, J.; Ulbricht, M.; Wickramasinghe, S. R.; Husson, S. M. *Journal of Membrane Science* **2008**, *309*, 64-72.

(14) Groll, J.; Haubensak, W.; Ameringer, T.; Moeller, M. *Langmuir* **2005**, *21*, 3076-3083.

(15) Gaberc-Porekar, V.; Menart, V. *Chemical Engineering & Technology* **2005**, *28*, 1306-1314.

(16) Kawakita, H.; Masunaga, H.; Nomura, K.; Uezu, K.; Akiba, I.; Tsuneda, S. *Journal of Porous Materials* **2007**, *14*, 387-391.

(17) Nova, C. J. M.; Paolucci-Jeanjean, D.; Belleville, M. P.; Barboiu, M.; Rivallin, M.; Rios, G. *Journal of Membrane Science* **2008**, *321*, 81-89.

(18) Ma, Z. W.; Masaya, K.; Ramakrishna, S. *Journal of Membrane Science* **2006**, *282*, 237-244.

(19) Bayramoglu, G.; Celik, G.; Arica, M. Y. *Colloids and Surfaces a-Physicochemical and Engineering Aspects* **2006**, *287*, 75-85.

(20) Ionov, L.; Stamm, M.; Diez, S. *Nano Letters* **2005**, *5*, 1910-1914.

Chapter 7

Summary and future work

7.1. Research summary

The research described in this dissertation aims at developing polymer brush-modified affinity membranes for high-capacity protein binding as well as rapid and selective purification of His-tagged proteins. In Chapter 2, I discussed growth of poly(HEMA) brushes inside porous alumina membranes and subsequent functionalization of the poly(HEMA) with NTA-Ni^{2+} complexes for rapid, highly selective purification of His-tagged proteins. Gel electrophoresis revealed that the purity of HisU eluted from these materials is >99%, even when the initial solution contains 10% bovine serum or a 20-fold excess of BSA. Moreover, the binding capacity of the membrane is at least 5-fold greater than that for membranes reported in the literature.[1-3] Separations can be completely performed in 30 min or less and membranes are fully reusable. Unfortunately, purification of His-tagged proteins using porous alumina membranes is limited to relatively simple solutions and low flow rates because of a limited pore size. Polymeric membranes, on the other hand, can have larger pore sizes than porous alumina, which should allow rapid purification with more complex solutions. In Chapter 3, we demonstrated the use of porous nylon membranes modified with poly(HEMA)-NTA-Ni^{2+} brushes for selective purification of His-tagged CRALBP directly from a cell lysate. The resulting CRALBP has a purity that is at least as good as that obtained with Ni^{2+} columns. Unfortunately, nylon membranes modified with poly(HEMA)-NTA-Ni^{2+} brushes have a relatively low protein binding capacity (25 mg protein/cm^3 of the membrane), perhaps because the organic solvents employed in the

brush synthesis and derivatization partially damage the membrane structure. To avoid the use of organic solvents that may dissolve or corrupt porous substrates, we developed a completely aqueous procedure for growth of polymer brushes inside polymeric membranes. In Chapter 4, we discussed the use of aqueous layer-by-layer adsorption of polyelectrolyte macroinitiators and subsequent aqueous ATRP from these immobilized initiators for successful growth of poly(HEMA) brushes on polymeric substrates.

Despite the growth of poly(HEMA) brushes with aqueous initiation, the creation of protein-binding brushes requires conversion of hydroxyl groups in poly(HEMA) to carboxylic acid moieties, which involves reaction of poly(HEMA) with succinic anhydride in an organic solvent for several hours. In Chapter 5, we demonstrated that surface-initiated aqueous ATRP of an acidic monomer, MES, allows a rapid, one-step synthesis of polyacid brushes that avoids the need to react the brush with succinic anhydride in an organic solvent. Also, poly(MES) brushes and their derivatives exhibit high protein-binding capacities. FTIR spectroscopy and ellipsometry studies showed that poly(MES) brushes are can bind the equivalent of many monolayers of BSA as well as lysozyme.

In Chapter 6, we described the formation of protein absorbers through the growth and derivatization of poly(MES) brushes inside porous nylon membranes. These membranes exhibit protein binding capacities of 80 ± 2 and 118 ± 8 mg protein per cm^3 of the membrane for BSA and lysozyme, respectively. Finally, we showed that the poly(MES)-NTA-Ni^{2+}-modified membranes can selectively and rapidly purify His-tagged CRALBP directly from a cell extract.

7.2. Future work

A limitation to our current method for creating protein-absorbing nylon membranes is that the initiator attachment requires THF, which makes it difficult to extend the procedure to other polymer membranes. Many polymer membrane materials such as polysulfone and polyethersulfone (PES) are incompatible with the organic solvents used for initiator attachment. Thus, for such substrates organic solvents should be completely avoided in the brush synthesis to preserve the pore structure of the membrane. To overcome this problem, we propose the use of aqueous layer-by-layer adsorption of polyelectrolyte macroinitiators and subsequent aqueous ATRP from these

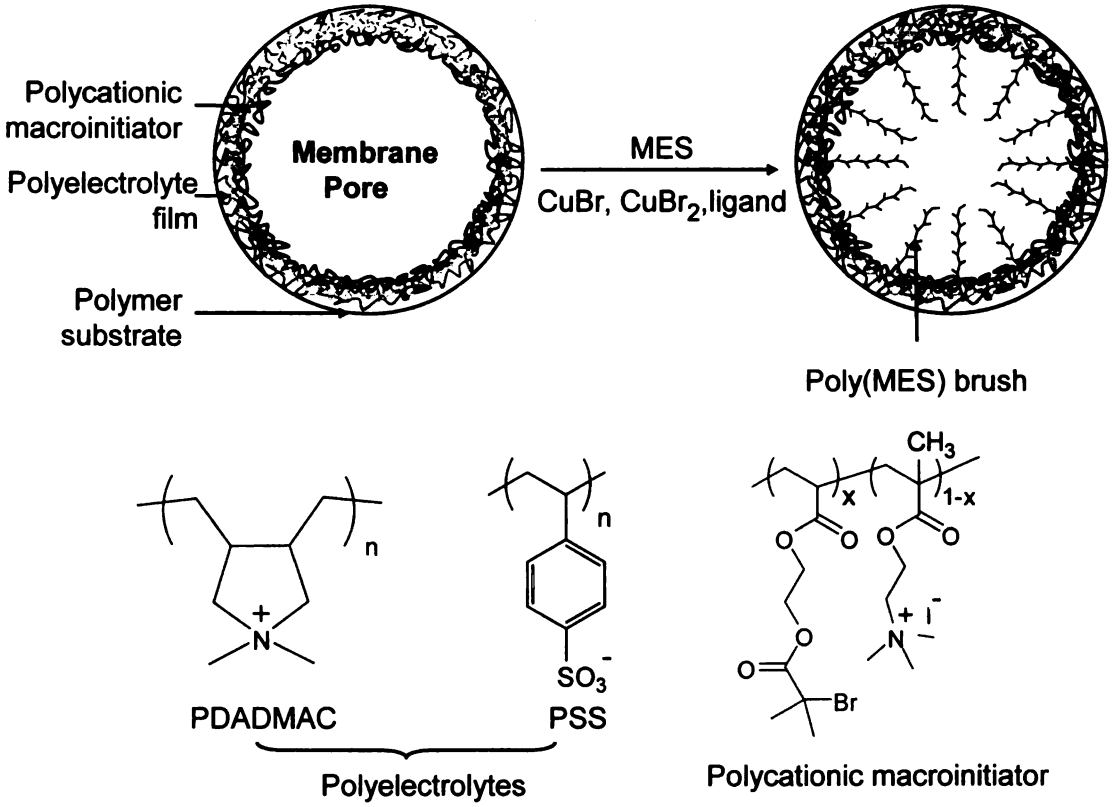

Scheme 7.1. Schematic illustration of growth of poly(MES) brushes by ATRP from macroinitiators adsorbed in a membrane pore.

immobilized initiators for growth of poly(MES) brushes **(Scheme 7.1)**. We have successfully used this method for aqueous growth of poly(HEMA) brushes in PES membranes (described in Chapter 4), however, we still need to study polymerization of MES using the macroinitiator.

Chapter 6 shows that poly(MES)-NTA-Ni^{2+}-modified nylon membrane are promising for rapid, high-capacity purification of His-tagged CRALBP directly from a cell extract. However to generalize this work, it is important to test the performance of these membranes for purification of a variety of overexpressed His-tagged proteins. Future studies should also determine the reusability and elution efficiency of these membranes. To examine the elution efficiency, we propose spiking a cell extract (devoid of over-expressed His-tagged protein) with a known amount of HisU. Purification of this solution using our modified membranes should provide information about the HisU binding capacity as well as elution efficiency.

Chapters 3 and 6 showed that the membrane-based purification is comparable to isolation with conventional IMAC resins in terms of purity. To establish the utility of the membranes, we need to further compare membrane-based purification with IMAC resins in terms of time and ease of purification. Moreover, a challenge with traditional IMAC chromatography is that certain recombinant proteins are contaminated, even after purification. For example, it is difficult to purify proteins like small nuclear RNA activating protein complex (SNAPc),[4-6] mannose 6-phosphate glycoprotein,[7] and GroEL-GroES chaperonin complex[8] using a single-step chromatographic separation. In such cases, highly abundant or "sticky" proteins are present along with the recombinant protein.[8] The binding of sticky proteins to IMAC columns occurs due to affinity for the

resin material or the presence of surface clusters of histidine residues that bind to metal complexes. For example, metal-binding lipocalin,[9] glucosamine-6-phosphate synthase,[10] and peptidoylproline cis-trans isomerase[11] have high affinity for metal-binding sites and are often co-purified with His-tagged proteins during IMAC. On the other hand, proteins like Hsp60 are more likely to bind to the sepharose of typical resins through hydrophobic interactions.[8] In fact in certain cases, the level of Hsp60 is higher than that of recombinant protein.[8] It is important to compare the performance of membranes with the IMAC columns for purification of these proteins. We expect that proteins that bind to the resin will be less abundant in the membrane-purified solutions whereas the proteins binding to Ni^{2+} should be contaminants with both membranes and columns.

In chapter 6, we showed that a poly(MES)-NTA-Ni^{2+} membrane can bind 85 mg of HisU per cm^3 of the membrane, which is equivalent to ~2.9 mg of protein per membrane (assuming a membrane thickness of 110 μm **(Figure 3.2 (b))** and a membrane diameter of 2 cm). Also, the flow rate for cell extract containing over-expressed CRALBP was 1.2 mL/min at a pressure less than 6.9×10^3 Pascal (1 psig). Based on these results, we expect that purification of up to 2.9 mg protein can be achieved rapidly using a 'membrane-based syringe filter' **(Figure 7.1.(a))**. A poly(MES)-NTA-Ni^{2+}-modified membrane can be placed in the membrane holder attached to a syringe **(Figure 7.1.(b))**, and the cell extract, washing, and elution solutions can be sequentially passed through the membrane. The advantage of using this system over conventional small-scale columns would be time and ease of purification. Moreover a membrane-based syringe filter would have a 4-fold higher protein binding capacity than a commercial spin trap column (2.9 mg protein/membrane vs. 750 μg protein/column).

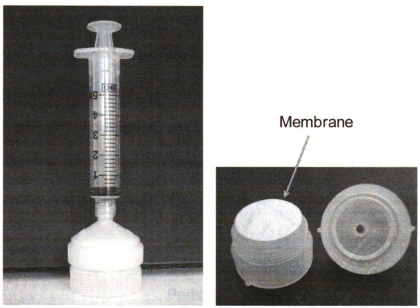

(a) **(b)**

Figure 7.1. **(a)** Syringe filter with a disposable syringe and **(b)** a membrane in the holder.

To purify more than 2.9 mg of protein, we can stack several poly(MES)-NTA-Ni^{2+} membranes in a holder and pass the cell extract through the stack of membranes **(Figure 7.2.)**. This should increase the amount of protein binding, but it might increase the time of purification or the applied pressure. In this case, we will need to optimize the binding capacity and time of purification as a function of applied pressure.

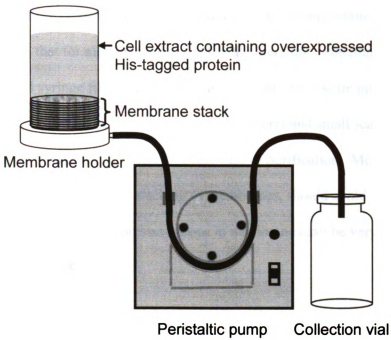

Figure 7.2. Purification of His-tagged protein from a cell extract using a stack of poly(MES)-NTA-Ni^{2+} membranes.

7.3 Potential Impact

Protein purification is vital in biomedical research and the development and manufacture of therapeutic peptides and proteins. Typical purifications involve a series of steps, the most important of which frequently relies on affinity binding. Unfortunately, affinity methods often present a bottleneck in the purification process because of slow diffusion of proteins into the pores of chromatographic gels. Protein-absorbing membranes can overcome this challenge because convective flow through membrane pores provides rapid mass transport to binding sites. The research described in this dissertation shows that porous polymer membranes modified with poly(MES)-NTA-Ni^{2+} brushes allows rapid and highly selective purification of His-tagged proteins with separations achieved in 15 min or less. Moreover the membranes coated with polymer

brushes have binding capacity as high as 85 mg HisU/cm^3 of membrane, which is several folds greater than that for membranes reported in the literature. Potentially, the 'membrane-based syringe filters' are promising for rapid, small scale purification of His-tagged proteins and should be advantageous over conventional small scale purification columns in terms of binding capacity, time and ease of purification. Moreover, scale-up of membrane separations through stacking of membranes, should avoid the challenges of packing large columns, and the pressure drops in membranes can be very low compared to a column-based separation.

7.4. References:

(1) Sun, L.; Dai, J. H.; Baker, G. L.; Bruening, M. L. *Chemistry of Materials* **2006**, *18*, 4033-4039.

(2) Ulbricht, M.; Yang, H. *Chemistry of Materials* **2005**, *17*, 2622-2631.

(3) Kawakita, H.; Masunaga, H.; Nomura, K.; Uezu, K.; Akiba, I.; Tsuneda, S. *Journal of Porous Materials* **2007**, *14*, 387-391.

(4) Lai, H. T.; Kang, Y. S.; Stumph, W. E. *FEBS Letters* **2008**, *582*, 3734-3738.

(5) Emran, F.; Florens, L.; Ma, B. C.; Swanson, S. K.; Washburn, M. P.; Hernandez, N. *Gene* **2006**, *377*, 96-108.

(6) Hanzlowsky, A.; Jelencic, B.; Jawdekar, G.; Hinkley, C. S.; Geiger, J. H.; Henry, R. W. *Protein Expression and Purification* **2006**, *48*, 215-223.

(7) Sleat, D. E.; Della Valle, M. C.; Zheng, H.; Moore, D. F.; Lobel, P. *Journal of Proteome Research* **2008**, *7*, 3010-3021.

(8) Bolanos-Garcia, V. M.; Davies, O. R. *Biochimica Et Biophysica Acta-General Subjects* **2006**, *1760*, 1304-1313.

(9) David, G.; Blondeau, K.; Schiltz, M.; Penel, S.; Lewit-Bentley, A. *Journal of Biological Chemistry* **2003**, *278*, 43728-43735.

(10) Obmolova, G.; Badet-Denisot, M. A.; Badet, B.; Teplyakov, A. *Journal of Molecular Biology* **1994**, *242*, 703-705.

(11) Hottenrott, S.; Schumann, T.; Pluckthun, A.; Fischer, G.; Rahfeld, J. U. *Journal of Biological Chemistry* **1997**, *272*, 15697-15701.